

High-order accurate entropy stable discontinuous Galerkin schemes using artificial viscosity

Thèse de Master
présentée le 20 janvier 2023
à la Faculté des sciences de base
laboratoire Computational Mathematics and Simulation Science
École polytechnique fédérale de Lausanne
pour l'obtention d'un Master ès Sciences
par
Louis Jaugey

Encadrement :

Prof. Jan S. Hesthaven, directeur de thèse
Prof. Gregor Gassner, expert externe
Dr. Junming Duan, superviseur

Lausanne, EPFL, 2023



Acknowledgements

I would like to thank Professor Jan S. Hesthaven for giving me the opportunity to do this master project in the MCSS lab.

The help and expertise of Dr. Junming Duan was absolutely essential for this project. He has always been patient and available to answer my questions. This project would not have been possible without him and I thank him for this.

The advice of Dr. Emmanuel Lanti and Dr. Nicolas Richart from SCITAS helped me improve the efficiency of my code and I thank both of them for sparing me a lot of time.

Finally, I thank my friends and family for the support, the laughs as well as their patience with me.

Lausanne, January 20, 2023

Abstract

Systems of hyperbolic conservation laws are widely used in the scientific and engineering fields, including the shallow water equations of oceanography, the Euler equations of aerodynamics, and the MHD equations of plasma physics. This thesis is concerned with solving such systems using the discontinuous Galerkin (DG) method, which has the advantages of geometric flexibility, high-order accuracy, conservation of physical properties, and parallel efficiency.

It is known that the weak solutions of the quasi-linear hyperbolic conservation laws may not be unique. The entropy condition is therefore an important tool to single out the physically relevant solution among all the weak solutions. Thus it is of great significance to construct entropy stable (ES) DG schemes satisfying discrete entropy conditions, which also improve the stability of the DG schemes. However, the discrete entropy conditions are generally not enough to suppress unphysical oscillations near discontinuities, so that researchers usually adopt other techniques, such as nonlinear limiters or sub-cells finite volume. This work is devoted to further stabilizing the ES DG schemes using artificial viscosity.

Chapter 1 introduces the basic definition of the system of conservation laws (CLs), their weak formulation, entropy conditions, and reviews the important literature in the field of entropy stable numerical methods.

Then the details about numerical schemes including time discretization, finite volume method and standard DG schemes are described in Chapter 2. Then the ES DG schemes are presented with the help of the summation-by-parts operators. Finally the ES DG schemes with artificial viscosity is constructed upon the ES DG schemes. The artificial viscosity term is built on the entropy variables so that the overall scheme still satisfies the discrete entropy conditions. Two different artificial viscosity models are considered to choose the magnitude of the viscosity. Various conservation laws are described in Chapter 3 on which our schemes is tested. The physical flux, entropy pair, entropy conservative/stable flux are detailed in this part.

The results are presented and discussed in Chapter 4. The choice of the artificial coefficients is studied and some benchmark tests are used to show the effectiveness of our method.

Contents

Acknowledgements	i
Abstract	iii
List of Figures	vii
List of Tables	xi
1 Introduction	1
1.1 System of conservation laws	1
1.2 Weak formulation	1
1.3 Entropy conditions	2
1.4 Entropy stable schemes	2
2 Numerical schemes	3
2.1 Time discretization	3
2.2 Finite volume method (FVM)	3
2.3 Discontinuous Galerkin (DG) method	4
2.3.1 DG space	5
2.3.2 Legendre-Gauss-Lobatto (LGL) quadrature	5
2.3.3 DG scheme	6
2.4 Numerical fluxes	7
2.4.1 EC flux	7
2.4.2 ES flux	8
2.4.3 Lax-Friedrichs flux	8
2.5 Entropy conservative/stable DG scheme	8
2.6 Artificial viscosity	10
2.6.1 Dilation-based (DB) viscosity	10
2.6.2 Entropy-based (EB) viscosity	11
2.7 2D ES-DG scheme	12
3 Physical problems	15
3.1 1D advection equation	15
3.2 1D Burgers' equation	16
3.3 1D Euler equations	16

Contents

3.4	2D advection equation	18
3.5	2D Euler equations	18
4	Numerical results and discussions	21
4.1	1D advection equation	21
4.2	1D Burgers' equation	27
4.3	1D Euler equations	34
4.3.1	Sod's shock tube	34
4.4	2D Euler equations	46
4.4.1	Isentropic vortex convection	46
4.4.2	2D Riemann problem 1	51
4.4.3	2D Riemann problem 2	53
4.4.4	2D Riemann problem 3	55
5	Conclusion	57
	Bibliography	60

List of Figures

2.1	Illustration of Runge's phenomena and its mitigation thanks to LGL quadrature using 11 quadrature points. On the left: equidistant quadrature points. On the right: LGL quadrature points.	5
4.1	Initial (left) and final (right) solutions for the 1D smooth test using advection equation.	22
4.2	Convergence test on smooth advection equation for P^1 , P^2 and P^4 elements, without artificial viscosity.	23
4.3	Convergence test on smooth advection equation for P^1 , P^2 and P^4 elements, with dilation based artificial viscosity.	24
4.4	Convergence test on smooth advection equation for P^1 , P^2 and P^4 elements, with entropy based artificial viscosity.	26
4.5	Solution (left) and entropy evolution (right) for Burgers' equation using P^1 and no artificial viscosity.	28
4.6	Solution (left) and entropy evolution (right) for Burgers' equation using P^1 and dilation based viscosity.	28
4.7	Solution (left) and entropy evolution (right) for Burgers' equation using P^1 and entropy based viscosity.	29
4.8	Dilation based (left) and entropy based (right) viscosity for Burgers' equation using P^1 elements.	29
4.9	Solution (left) and entropy evolution (right) for Burgers' equation using P^2 and no artificial viscosity.	30
4.10	Solution (left) and entropy evolution (right) for Burgers' equation using P^2 and dilation based viscosity.	31
4.11	Solution (left) and entropy evolution (right) for Burgers' equation using P^2 and entropy based viscosity.	31
4.12	Dilation based (left) and entropy based (right) viscosity for Burger's equation using P^2 elements.	32
4.13	Solution (left) and entropy evolution (right) for Burgers' equation using P^4 and no artificial viscosity.	32
4.14	Solution (left) and entropy evolution (right) for Burgers' equation using P^4 and dilation based viscosity.	33

List of Figures

4.15 Solution (left) and entropy evolution (right) for Burgers' equation using P^4 and entropy based viscosity.	33
4.16 Dilation based (left) and entropy based (right) viscosity for Burger's equation using P^4 elements.	34
4.17 Solutions of ρ , ρu , P and entropy evolution for Euler equations using P^1 elements and no viscosity.	35
4.18 Solutions of ρ , ρu , P and entropy evolution for Euler equations using P^1 elements and with DB viscosity.	36
4.19 Solutions of ρ , ρu , P and entropy evolution for Euler equations using P^1 elements and EB viscosity.	37
4.20 DB (left) and EB (right) viscosity for Sod's test using P^1 elements.	38
4.21 Solutions of ρ , ρu , P and entropy evolution for Euler equations using P^2 elements and no viscosity.	39
4.22 Solutions of ρ , ρu , P and entropy evolution for Euler equations using P^2 elements and with DB viscosity.	40
4.23 Solutions of ρ , ρu , P and entropy evolution for Euler equations using P^2 elements and EB viscosity.	41
4.24 DB (left) and EB (right) viscosity for Sod's test using P^2 elements.	42
4.25 Solutions of ρ , ρu , P and entropy evolution for Euler equations using P^4 elements and no viscosity.	43
4.26 Solutions of ρ , ρu , P and entropy evolution for Euler equations using P^4 elements and with DB viscosity.	44
4.27 Solutions of ρ , ρu , P and entropy evolution for Euler equations using P^4 elements and EB viscosity.	45
4.28 DB (left) and EB (right) viscosity for Sod's test using P^4 elements.	46
4.29 Density at the initial (left) and final (right) time for the isentropic vortex test.	47
4.30 Convergence test on the isentropic vortex for P^1 elements. Left: without artificial viscosity. Right: with dilation based viscosity.	48
4.31 Convergence test on the isentropic vortex for P^2 elements. Left: without artificial viscosity. Right: with dilation based viscosity.	49
4.32 Convergence test on the isentropic vortex for P^4 elements. Left: without artificial viscosity. Right: with dilation based viscosity.	50
4.33 Results obtained without artificial viscosity, for P^1 (left) and P^2 (right) elements on the first 2D Riemann problem.	51
4.34 Results obtained with DB viscosity and P^1 elements on the first 2D Riemann problem. Density with dilation based viscosity and the corresponding artificial viscosity at the final time.	52
4.35 Results obtained with DB viscosity and P^2 elements on the first 2D Riemann problem. Density with dilation based viscosity and the corresponding artificial viscosity at the final time.	52
4.36 Results obtained without artificial viscosity, for P^1 (left) and P^2 (right) elements on the second 2D Riemann problem.	53

List of Figures

4.37 Results obtained with DB viscosity and P^1 elements on the second 2D Riemann problem. Density with dilation based viscosity and the corresponding artificial viscosity at the final time.	54
4.38 Results obtained with DB viscosity and P^2 elements on the second 2D Riemann problem. Density with dilation based viscosity and the corresponding artificial viscosity at the final time.	54
4.39 Results obtained without artificial viscosity, for P^1 (left) and P^2 (right) elements on the third 2D Riemann problem.	55
4.40 Results obtained with DB viscosity and P^1 elements on the third 2D Riemann problem. Density with dilation based viscosity and the corresponding artificial viscosity at the final time.	56
4.41 Results obtained with DB viscosity and P^2 elements on the third 2D Riemann problem. Density with dilation based viscosity and the corresponding artificial viscosity at the final time.	56

List of Tables

4.1	Convergence test on smooth advection equation for P^1 elements, without artificial viscosity	22
4.2	Convergence test on smooth advection equation for P^2 elements, without artificial viscosity	22
4.3	Convergence test on smooth advection equation for P^4 elements, without artificial viscosity	23
4.4	Convergence test on smooth advection equation for P^1 elements, with dilation based viscosity	25
4.5	Convergence test on smooth advection equation for P^2 elements, with dilation based viscosity	25
4.6	Convergence test on smooth advection equation for P^4 elements, with dilation based viscosity	25
4.7	Convergence test on smooth advection equation for P^1 elements, with entropy based viscosity	26
4.8	Convergence test on smooth advection equation for P^2 elements, with entropy based viscosity	27
4.9	Convergence test on smooth advection equation for P^4 elements, with entropy based viscosity	27
4.10	Convergence test on the isentropic vortex for P^1 elements, without artificial viscosity	47
4.11	Convergence test on the isentropic vortex for P^1 elements, with dilation based viscosity	48
4.12	Convergence test on the isentropic vortex for P^2 elements, without artificial viscosity	49
4.13	Convergence test on the isentropic vortex for P^2 elements, with dilation based viscosity	49
4.14	Convergence test on the isentropic vortex for P^4 elements, without artificial viscosity	50
4.15	Convergence test on the isentropic vortex for P^4 elements, with dilation based viscosity	50

1 Introduction

Many governing equations in physics can be expressed in conservative form, which describes the (local) evolution of a (globally) conserved quantity according to its flux. In general, there can be a set of conserved quantities, leading to a system of conservation laws (CLs). The description of such systems presented below is inspired from Fjordholm et al. (2012).

1.1 System of conservation laws

Consider n conserved quantities $\mathbf{u}(\mathbf{x}, t) : \Omega \times \mathbb{R}^+ \rightarrow \mathbb{R}^n$, $\Omega \subset \mathbb{R}^d$ with d the spatial dimension and their fluxes in each spatial direction $\mathbf{f}_j(\mathbf{u}) : \mathbb{R}^n \rightarrow \mathbb{R}^n$, $j = 1, \dots, d$. The system of CLs is described by

$$\frac{\partial \mathbf{u}}{\partial t} + \sum_{j=1}^d \frac{\partial \mathbf{f}_j(\mathbf{u})}{\partial x_j} = 0. \quad (1.1)$$

To simplify notations, let us first consider systems of CLs in 1D, i.e. $\Omega = [a, b] \subset \mathbb{R}$. This reduces the system of equations to

$$\frac{\partial \mathbf{u}}{\partial t} + \frac{\partial \mathbf{f}(\mathbf{u})}{\partial x} = 0. \quad (1.2)$$

We can verify that the total quantity $\mathbf{U}(t) = \int_{\Omega} \mathbf{u}(x, t) dx$, is governed by the flux at the boundary of the domain:

$$\frac{\partial \mathbf{U}(t)}{\partial t} = \int_{\Omega} \frac{\partial \mathbf{u}}{\partial t} dx = - \int_{\Omega} \frac{\partial \mathbf{f}(\mathbf{u})}{\partial x} dx = \mathbf{f}(\mathbf{u})|_a - \mathbf{f}(\mathbf{u})|_b.$$

The total quantity is therefore conserved with periodic boundary conditions or zero-flux boundary conditions.

1.2 Weak formulation

The main difficulty when approximating CLs is that the solution might contain discontinuities such as shocks which cannot be described by the strong formulation. The weak solution can be obtained by multiplying the CLs with a smooth and compactly supported test function

Chapter 1. Introduction

$\phi(x, t) \in C_c(\mathbb{R} \times \mathbb{R}^+)$ and then integrate it by part:

$$\begin{aligned} 0 &= \int_0^\infty \int_\Omega \partial_t \mathbf{u} \phi + \partial_x \mathbf{f}(\mathbf{u}) \phi \, dx dt \\ &= \int_\Omega \left(\mathbf{u} \phi \Big|_{t=0}^{t \rightarrow \infty} - \int_0^\infty \mathbf{u} \partial_t \phi \, dt \right) dx + \int_0^\infty \left(\mathbf{f}(\mathbf{u}) \phi \Big|_{x=a}^{x=b} - \int_\Omega \mathbf{f}(\mathbf{u}) \partial_x \phi \, dx \right) dt \\ &= - \int_0^\infty \int_\Omega \mathbf{u} \partial_t \phi + \mathbf{f}(\mathbf{u}) \partial_x \phi \, dx dt - \int_\Omega \mathbf{u}_0 \phi(x, 0) dx = 0. \end{aligned}$$

Therefore, \mathbf{u} is a weak solution if

$$\int_0^\infty \int_\Omega \mathbf{u} \partial_t \phi + \mathbf{f}(\mathbf{u}) \partial_x \phi \, dx dt + \int_\Omega \mathbf{u}_0 \phi(x, 0) dx = 0. \quad (1.3)$$

1.3 Entropy conditions

There might be infinitely many solutions to the weak formulation of the problem but only one of them is physical. Some criteria are therefore required to select the correct one. A crucial condition is given by the so-called entropy condition. Consider a convex function $E : \mathbb{R}^n \rightarrow \mathbb{R}$ and corresponding function $Q : \mathbb{R}^n \rightarrow \mathbb{R}$ such that $(\partial Q / \partial \mathbf{u})^T = \mathbf{v}^T \partial \mathbf{f} / \partial \mathbf{u}$, where $\mathbf{v} = \partial E / \partial \mathbf{u}$. The functions E , Q and \mathbf{v} are called entropy, entropy flux and entropy variable, respectively. Multiplying Equation (1.2) by \mathbf{v}^T , it is easy to see that, for smooth solutions, one gets

$$\underbrace{\left(\frac{\partial E}{\partial \mathbf{u}} \right)^T \frac{\partial \mathbf{u}}{\partial t}}_{\partial E / \partial t} + \underbrace{\mathbf{v}^T \frac{\partial \mathbf{f}}{\partial \mathbf{u}} \frac{\partial \mathbf{u}}{\partial x}}_{(\partial Q / \partial \mathbf{u})^T} = \frac{\partial E}{\partial t} + \frac{\partial Q}{\partial x} = 0. \quad (1.4)$$

This property is called *entropy conservation* or EC. This is however only true for smooth solutions. When the solution is discontinuous, entropy must be dissipated at discontinuities. This means that we have the following entropy inequality

$$\frac{\partial E}{\partial t} + \frac{\partial Q}{\partial x} \leq 0, \quad (1.5)$$

in the sense of distribution. This property is called *entropy stability* or ES.

1.4 Entropy stable schemes

The entropy stability is a generalization of the L^2 -energy bound in the linear case. It is important to construct high-order accurate entropy conservative (EC) or ES schemes which satisfy discrete entropy conditions, which can give a kind of nonlinear stability to the numerical schemes. The second-order ES schemes were established by Tadmor (1987) and the high-order version was constructed by Fjordholm et al. (2012). With the help of the summation-by-parts operators, the ES DG schemes were developed in Gassner (2013); Carpenter et al. (2014) and then on simplex meshes in Chen and Shu (2017). We refer readers to the review paper Gassner and Winters (2021) and references therein.

2 Numerical schemes

Schemes used to approximate solutions to CLs must satisfy a discrete version of conservation as this will guarantee that they capture the correct shock speed (Hesthaven (2018)). They must also dissipate entropy at shocks to avoid unphysical oscillations.

2.1 Time discretization

Consider the semi-discrete schemes:

$$\frac{\partial \mathbf{u}_i(t)}{\partial t} = \mathbf{L}(\mathbf{u}_i(t)), \quad (2.1)$$

where \mathbf{L} is an (high-order) approximation of $-\partial \mathbf{f} / \partial x$.

In this work, the third order SSP-RK3 scheme is used for time integration. It is defined as

$$\begin{aligned} \mathbf{u}^{(1)} &= \mathbf{u}^n + \Delta t \mathbf{L}(\mathbf{u}^n) \\ \mathbf{u}^{(2)} &= \frac{3}{4} \mathbf{u}^n + \frac{1}{4} \mathbf{u}^{(1)} + \frac{\Delta t}{4} \mathbf{L}(\mathbf{u}^{(1)}) \\ \mathbf{u}^{n+1} &= \frac{1}{3} \mathbf{u}^n + \frac{2}{3} \mathbf{u}^{(2)} + \frac{2\Delta t}{3} \mathbf{L}(\mathbf{u}^{(2)}), \end{aligned} \quad (2.2)$$

where \mathbf{u}^n is the numerical approximation of \mathbf{u} at t^n .

2.2 Finite volume method (FVM)

This method (described in e.g. Ciarlet et al. (1990)) approximates the average value of \mathbf{u} in a cell $\bar{\mathbf{u}} = \frac{1}{\Delta x_i} \int_{x_{i-\frac{1}{2}}}^{x_{i+\frac{1}{2}}} \mathbf{u} dx$, where $\Delta x_i = x_{i+\frac{1}{2}} - x_{i-\frac{1}{2}}$. Integrating Equation (1.2) over the i -th cell

Chapter 2. Numerical schemes

gives

$$\begin{aligned} \frac{\partial}{\partial t} \int_{x_{i-\frac{1}{2}}}^{x_{i+\frac{1}{2}}} \mathbf{u} \, dx &= - \int_{x_{i-\frac{1}{2}}}^{x_{i+\frac{1}{2}}} \frac{\partial \mathbf{f}(\mathbf{u})}{\partial x} \, dx \iff \\ \Delta x_i \frac{\partial \bar{\mathbf{u}}_i}{\partial t} &= -\mathbf{f}(\mathbf{u}) \Big|_{x_{i-\frac{1}{2}}}^{x_{i+\frac{1}{2}}} = -(\mathbf{f}(\mathbf{u}_{i+\frac{1}{2}}) - \mathbf{f}(\mathbf{u}_{i-\frac{1}{2}})). \end{aligned} \quad (2.3)$$

This is an exact expression but $\mathbf{f}(\mathbf{u}_{i+\frac{1}{2}})$ is unclear due to the piecewise constant approximation. A numerical approximation of $\mathbf{f}(\mathbf{u}_{i+\frac{1}{2}})$, known as the numerical flux, is introduced and denoted by $\mathbf{F}_{i+\frac{1}{2}}$. The scheme can be written as

$$\frac{\partial \bar{\mathbf{u}}_i(t)}{\partial t} = -\frac{1}{\Delta x} (\mathbf{F}_{i-\frac{1}{2}}(t) - \mathbf{F}_{i+\frac{1}{2}}(t)). \quad (2.4)$$

Summing Equation (2.4) over i shows that the conservative property is satisfied in the discrete sense:

$$\sum_{i=1}^N \frac{\partial \mathbf{u}_i}{\partial t} = -\frac{1}{\Delta x} \sum_{i=1}^N (\mathbf{F}_{i+\frac{1}{2}}(t) - \mathbf{F}_{i-\frac{1}{2}}(t)) = -\frac{1}{\Delta x} (\mathbf{F}_{N+\frac{1}{2}}(t) - \mathbf{F}_{\frac{1}{2}}(t)),$$

which is equal to 0 with periodic boundary conditions or zero-flux boundary conditions.

This scheme can be of any order by using a high-order approximation of the flux $\mathbf{f}(\mathbf{u}_{i+\frac{1}{2}}(t))$. The main strategy to get these approximations is to reconstruct the value of \mathbf{u} at the boundaries of the cell with a combination of $\{\bar{\mathbf{u}}_{i-p}, \dots, \bar{\mathbf{u}}_{i+q}\}$, $p, q \in \mathbb{N}$. Typical combinations are the one used in the (weighted) essentially non-oscillating or (W)ENO schemes which use multiple polynomial reconstructions and chooses the best one (or weights them in the case of WENO) based on the smoothness of the result. More details can be found in Shu (2020). The reconstructed values on the left and the right of $x_{i+\frac{1}{2}}$, namely $\mathbf{u}_{i+\frac{1}{2}}^-$ and $\mathbf{u}_{i+\frac{1}{2}}^+$, are then combined in a two point numerical flux $\mathbf{F}_{i+\frac{1}{2}} = \mathbf{F}(\mathbf{u}_{i+\frac{1}{2}}^-, \mathbf{u}_{i+\frac{1}{2}}^+)$, which is consistent with the physical flux \mathbf{f} , i.e. $\mathbf{F}(\mathbf{u}, \mathbf{u}) = \mathbf{f}(\mathbf{u})$. Numerical fluxes will be discussed in Section 2.4.

2.3 Discontinuous Galerkin (DG) method

The general strategy of DG methods is to split the spatial domain in $N \in \mathbb{N}$ subsets (called cells) and approximate the solution in each of them with a polynomial of degree $k \in \mathbb{N}$. Different from the FVM, the DG method achieves high-order accuracy by using more degrees of freedom in each cell rather than the reconstruction, i.e. polynomial approximation instead of piecewise constant approximation. Cells contain $k+1$ quadrature points $\{\xi_j\}_{j=0}^k$ and a unique polynomial of degree k can therefore be defined within each cell. Quadrature points are associated with quadrature weights $\{\omega_j\}_{j=0}^k$ which allows to define usual operations on the interpolating polynomials (see Section 2.3.2). The mathematical descriptions presented here are inspired from Chen and Shu (2017).

2.3.1 DG space

The DG space of polynomials of degree k is

$$\mathbf{V}_h^k = \{\boldsymbol{\phi} \in [L^2(\Omega)]^n : \boldsymbol{\phi}|_{I_i} \in [\mathbb{P}^k(I_i)]^n, 1 \leq i \leq N\}. \quad (2.5)$$

Note that, as opposed to the traditional Galerkin method (finite element method), $\boldsymbol{\phi}$ is not required to be continuous across the cell interfaces.

2.3.2 Legendre-Gauss-Lobatto (LGL) quadrature

The LGL quadrature points and weights are defined with Legendre polynomials \mathcal{P}_k as described in Johansson and Mezzarobba (2018). Taking the reference element $[-1, 1]$, the $k + 1$ quadrature points $\{\xi_j\}_{j=0}^k$ are defined as the i -th root of $\mathcal{P}_k(x)$ such that $-1 = \xi_0 \leq \xi_1 \leq \dots \leq \xi_k = 1$. The weights are given by

$$\omega_i = \frac{2}{(1 - \xi_i^2)(\mathcal{P}'_k(\xi_i))^2}.$$

The implementation is adapted from Winckel (2004). The advantage of these quadrature points is that it mitigates Runge's phenomena, which usually appears with equally spaced quadrature points, as shown in Figure 2.1. The fact that it contains the end points is also convenient to construct the ES-DG schemes based on the summation-by-parts property (Equation (2.8)).

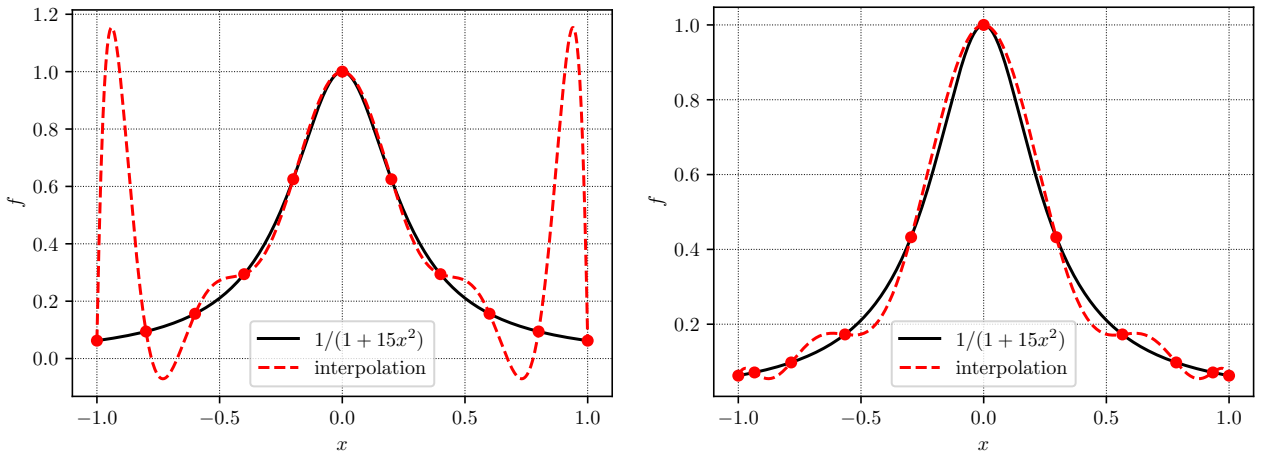


Figure 2.1: Illustration of Runge's phenomena and its mitigation thanks to LGL quadrature using 11 quadrature points. On the left: equidistant quadrature points. On the right: LGL quadrature points.

The transformation from the reference cell $[-1, 1]$ to a generic one $[a, b] \subset \mathbb{R}$ is obtained with $x_j = \frac{1}{2}((a+b) + (b-a)\xi_j)$.

Chapter 2. Numerical schemes

Interpolation The numerical solution is interpolated using Lagrangian polynomials defined by

$$L_j(\xi) = \prod_{\substack{l=0 \\ l \neq j}}^k \frac{\xi - \xi_l}{\xi_j - \xi_l}. \quad (2.6)$$

Note that $L_j(\xi_l) = \delta_{jl}$. Its derivative is given by

$$L'_j(\xi) = \sum_{\substack{l=0 \\ l \neq j}}^k \frac{1}{\xi_j - \xi_l} \prod_{\substack{k=0 \\ k \neq j, l}}^k \frac{\xi - \xi_k}{\xi_j - \xi_k}. \quad (2.7)$$

It is useful to define the following matrices:

- Difference matrix $D_{jl} = L'_l(\xi_j)$
- Mass matrix $M_{jl} = \omega_j \delta_{jl}$
- Stiffness matrix $S_{jl} = \langle L_j, L'_l \rangle = \int_{-1}^1 L_j(\xi) L'_l(\xi) d\xi = \sum_{m=0}^k \omega_m L_j(\xi_m) L'_l(\xi_m)$
- Boundary matrix $B = \text{diag}(-1, 0, \dots, 0, 1)$

Note that we have $S = MD$. These matrices allow to compute numerical approximations of continuous operations. In particular, for some function $f : [-1, 1] \rightarrow \mathbb{R}$, the mass matrix and the difference matrix can be seen as discrete integration and derivation operations respectively. This is particularly useful to define a discrete version of integral by part, known as summation-by-parts (SBP):

$$MD + D^T M = S + S^T = B. \quad (2.8)$$

2.3.3 DG scheme

To simplify notation, only scalar CL are considered here. By multiplying Equation (1.2) with any test function $\phi \in V_h^k$ and integrating on the cell I_i , one gets

$$\frac{\Delta x}{2} \int_{I_i} \frac{\partial u}{\partial t} \phi dx = \int_{I_i} f(u) \frac{\partial \phi}{\partial x} dx - f_{i+\frac{1}{2}} \phi(x_{i+\frac{1}{2}}^-) + f_{i-\frac{1}{2}} \phi(x_{i-\frac{1}{2}}^+). \quad (2.9)$$

The $(\vec{\cdot})$ notation is used to represent the values of a function at each quadrature points of a given cell I_i , e.g. $\vec{g} = (g(x_{i,0}), \dots, g(x_{i,k}))^T$ for $x_{i,l} \in I_i$, $l = 0, \dots, k$. The integral in Equation (2.9) can be approximated using the $k+1$ points of a cell (omitting subscript i):

$$\frac{\Delta x}{2} \vec{\phi}^T M \frac{\partial \vec{u}}{\partial t} = (D\vec{\phi})^T M \vec{f} - \phi B \vec{f}_*, \quad (2.10)$$

where $\vec{f}_* = (F_{i-\frac{1}{2}}, 0, \dots, 0, F_{i+\frac{1}{2}})^T$. Using the SBP property and the fact that ϕ can be arbitrary, we get

$$\frac{\Delta x}{2} M \frac{\partial \vec{u}}{\partial t} = D^T M \vec{f} - B \vec{f}_* = (B - MD) \vec{f} - B \vec{f}_*. \quad (2.11)$$

Multiplying by M^{-1} leads to the semi-discrete nodal DG scheme:

$$\frac{\Delta x}{2} \frac{\partial \vec{u}}{\partial t} = -D \vec{f} + M^{-1} B(\vec{f} - \vec{f}_*) . \quad (2.12)$$

This scheme does not satisfy any entropy condition but it can be modified to make it EC or ES (Chen and Shu (2017)).

2.4 Numerical fluxes

Before presenting the EC/ES DG schemes, it is useful to define some numerical fluxes and in particular EC and ES fluxes, noted $\tilde{\mathbf{F}}$ and \mathbf{F} respectively. The EC/ES property of a flux is directly linked to the numerical entropy condition of their corresponding DG scheme that will be exposed later in Section 2.5. The chosen numerical flux must be consistent with \mathbf{f} . There are many possible choices for it and some of them are introduced below.

2.4.1 EC flux

Although an EC flux does not dissipate entropy, it is still interesting to construct such flux. Indeed, continuous solutions do not require entropy dissipation (see Section 1.3) and an EC flux is sufficient in such case. Furthermore, it can serve as a building block for an ES flux so the EC flux is described first.

Numerical entropy conservation Entropy conservative scheme satisfy a semi-discrete version of Equation (1.4) (Tadmor (1987)):

$$\frac{\partial E(\mathbf{u}_i(t))}{\partial t} = -\frac{1}{\Delta x} \left(\tilde{Q}_{i+\frac{1}{2}}(t) - \tilde{Q}_{i-\frac{1}{2}}(t) \right), \quad (2.13)$$

for some numerical entropy flux $\tilde{Q}_{i+\frac{1}{2}}$, consistent with Q . To simplify the notation, it is useful to define the jump function $[\cdot]$ and the average $\{\cdot\}$ between a left and a right state $(\cdot)_L$ and $(\cdot)_R$.

$$[\cdot] = (\cdot)_R - (\cdot)_L, \quad \{\cdot\} = \frac{1}{2}((\cdot)_L + (\cdot)_R).$$

The entropy potential¹ is defined as $\psi(\mathbf{u}) := \mathbf{v}^T(\mathbf{u})\mathbf{f}(\mathbf{u}) - Q(\mathbf{u})$. The following theorem (from Tadmor (1987)) is useful to find EC fluxes.

Theorem 1. *If a consistent numerical flux $\tilde{\mathbf{F}}(\mathbf{u}_L, \mathbf{u}_R)$ satisfies*

$$[\mathbf{v}]^T \tilde{\mathbf{F}} = [\psi], \quad (2.14)$$

then the scheme defined in Equation (2.19) with numerical flux $\tilde{\mathbf{F}}$ is entropy conservative.

¹It is called a potential because $\frac{\partial \psi}{\partial \mathbf{v}} = \mathbf{f}(\mathbf{u}) + \mathbf{v}^T \frac{\partial \mathbf{f}}{\partial \mathbf{u}} \frac{\partial \mathbf{u}}{\partial \mathbf{v}} - \left(\frac{\partial Q}{\partial \mathbf{u}} \right)^T \frac{\partial \mathbf{u}}{\partial \mathbf{v}} = \mathbf{f}(\mathbf{u})$

Chapter 2. Numerical schemes

Furthermore, solutions computed with such scheme satisfy Equation (2.13) with the numerical entropy flux

$$\tilde{Q} = \{\{\mathbf{v}\}\}^T \tilde{\mathbf{F}} - \{\{\psi\}\}. \quad (2.15)$$

Although a general solution exists for Equation (2.14), it is usually hard to compute, except in specific situations. The expression of $\tilde{\mathbf{F}}(\mathbf{u}_L, \mathbf{u}_R)$ will be given later for each CL studied.

2.4.2 ES flux

As explained before, EC flux is generally not sufficient since it does not dissipate entropy. However, one can devise an ES flux from a given EC flux.

Numerical entropy stability ES scheme satisfy the semi-discrete version of Equation (1.5) (Tadmor (1987)):

$$\frac{\partial E(\mathbf{u}_i(t))}{\partial t} + \frac{1}{\Delta x} \left(\hat{Q}_{i+\frac{1}{2}}(t) - \hat{Q}_{i-\frac{1}{2}}(t) \right) \leq 0. \quad (2.16)$$

An ES flux can be created from an EC flux by adding a diffusion term:

$$\mathbf{F}_{i+\frac{1}{2}} = \tilde{\mathbf{F}}_{i+\frac{1}{2}} - \frac{1}{2} D_{i+\frac{1}{2}} \llbracket \mathbf{v} \rrbracket_{i+\frac{1}{2}}, \quad (2.17)$$

where D is called the diffusion matrix. There are many possibilities to choose this matrix and some of them are exposed in Tadmor (1987); Fjordholm et al. (2012).

2.4.3 Lax-Friedrichs flux

A popular choice of numerical flux is the local Lax-Friedrichs flux, defined as

$$\mathbf{F}(\mathbf{u}_L, \mathbf{u}_R) = \mathbf{f}(\mathbf{u}_L) + \mathbf{f}(\mathbf{u}_R) - \frac{\alpha}{2} (\mathbf{u}_R - \mathbf{u}_L), \quad (2.18)$$

where $\alpha = \max(\lambda_{\max}(\mathbf{u}_L), \lambda_{\max}(\mathbf{u}_R))$, if $\lambda_{\max}(\mathbf{u})$ represents the maximal eigen value of the Jacobian matrix $\partial \mathbf{f} / \partial \mathbf{u}$. The Lax-Friedrichs flux is consistent with \mathbf{f} as well as entropy stable.

2.5 Entropy conservative/stable DG scheme

The EC/ES DG scheme is very similar to the one given in Equation (2.12) and is formulated for each quadrature point of a single cell:

$$\frac{\Delta x}{2} \frac{d\mathbf{u}_l}{dt} = -2 \sum_{r=0}^k D_{lr} \tilde{\mathbf{F}}(\mathbf{u}_l, \mathbf{u}_r) + \frac{\tau_l}{\omega_l} (\mathbf{f}_l - \mathbf{f}_{*,l}), \quad (2.19)$$

where $\tau_j = -\delta_{0,j} + \delta_{k,j}$. Note that setting $\tilde{\mathbf{F}}(\mathbf{u}_L, \mathbf{u}_R) = \frac{1}{2}(\mathbf{f}(\mathbf{u}_L) + \mathbf{f}(\mathbf{u}_R))$ would give back the scheme from Equation (2.12), though it is not EC or ES in general.

Theorem 2. *If $\tilde{\mathbf{F}}(\mathbf{u}_L, \mathbf{u}_R)$ is consistent, symmetric and EC in the sense of Equation (2.14), then the scheme described by Equation (2.19) is entropy conservative within a single element.*

Proof:

$$\frac{d}{dt} \left(\sum_{j=0}^k \frac{\Delta x}{2} \omega_j E_j \right) = \sum_{j=0}^k \frac{\Delta x}{2} \omega_j \mathbf{v}_j^T \frac{d\mathbf{u}_j}{dt} = \sum_{j=0}^k \tau_j \mathbf{v}_j^T (\mathbf{f}_j - \mathbf{f}_{*,j}) - 2 \sum_{j=0}^k \sum_{l=0}^k S_{jl} \mathbf{v}_j^T \tilde{\mathbf{F}}(u_j, u_l).$$

By the SBP property, we have

$$\begin{aligned} \sum_{j=0}^k \sum_{l=0}^k S_{jl} \mathbf{v}_j^T \tilde{\mathbf{F}}(\mathbf{u}_j, \mathbf{u}_l) &= \sum_{j=0}^k \sum_{l=0}^k (B_{jl} + S_{jl} - S_{lj}) \mathbf{v}_j^T \tilde{\mathbf{F}}(u_j, u_l) = \\ \sum_{j=0}^k \tau_j \mathbf{v}_j^T \mathbf{f}_j + \sum_{j=0}^k \sum_{l=0}^k S_{jl} (\mathbf{v}_j - \mathbf{v}_l)^T \tilde{\mathbf{F}}(\mathbf{u}_j, \mathbf{u}_l) &= \\ \sum_{j=0}^k \tau_j \mathbf{v}_j^T \mathbf{f}_j + \sum_{j=0}^k \sum_{l=0}^k S_{jl} (\psi_j - \psi_l) &= \sum_{j=0}^k \tau_j (\mathbf{v}_j^T \mathbf{f}_j - \psi_j). \end{aligned}$$

Therefore

$$\frac{d}{dt} \left(\sum_{j=0}^k \frac{\Delta x}{2} \omega_j E_j \right) = \sum_{j=0}^k \tau_j (\psi_j - \mathbf{v}_j^T \mathbf{f}_{*,j}) = (\psi_k - \mathbf{v}_k^T \mathbf{f}_{*,k}) - (\psi_0 - \mathbf{v}_0^T \mathbf{f}_{*,0}). \quad (2.20)$$

Only boundary terms remain so the scheme is indeed locally EC.

Theorem 3. *If \mathbf{F} is entropy stable, then the scheme described by Equation (2.19) is entropy stable.*

Proof:

According to Equation (2.20), the entropy production rate at the interface is

$$(\psi_i^k - (\mathbf{v}_i^k)^T \mathbf{F}_{i+\frac{1}{2}}) - (\psi_{i+1}^0 - (\mathbf{v}_{i+1}^0)^T \mathbf{F}_{i+\frac{1}{2}}) = (\mathbf{v}_{i+1}^0 - \mathbf{v}_i^k)^T \mathbf{F}(\mathbf{u}_i^k, \mathbf{u}_{i+1}^0) - (\psi_{i+1}^0 - \psi_i^k) \leq 0,$$

since \mathbf{F} is ES. Assuming periodic boundary conditions or zero-entropy flux boundary conditions, then the whole scheme is entropy stable.

Time step size Δt The time step size is adapted at each time step using the CFL condition. It is computed as follows:

$$\Delta t = \frac{CFL}{\beta}, \quad \beta = \max_{\substack{1 \leq i \leq N \\ 0 \leq l \leq k}} \left(\lambda_{\max,i}^l \frac{k^2}{\Delta x} \right), \quad (2.21)$$

where $\lambda_{\max,i}^l$ is the maximal eigen value of the Jacobian matrix $\partial \mathbf{f} / \partial \mathbf{u}$, at the l^{th} quadrature point in the i^{th} cell.

2.6 Artificial viscosity

The idea is to slightly change the original equation to

$$\frac{\partial \mathbf{u}}{\partial t} + \frac{\partial \mathbf{f}(\mathbf{u})}{\partial x} = \nu \frac{\partial^2 \mathbf{u}}{\partial x^2}, \quad (2.22)$$

where the parameter ν is called the artificial viscosity and is typically small. In the limit $\nu \rightarrow 0$, the original equation is recovered.

Although using conserved variables usually works in practice, the proof of the scheme's ES property is not established. The entropy variables \mathbf{v} are used instead,

$$\frac{\partial \mathbf{u}}{\partial t} + \frac{\partial \mathbf{f}(\mathbf{u})}{\partial x} = \nu \frac{\partial^2 \mathbf{v}}{\partial x^2}. \quad (2.23)$$

Defining $\mathbf{q} = \nu(\partial \mathbf{v} / \partial x)$, Equation (2.23) becomes

$$\frac{\partial \mathbf{u}}{\partial t} + \frac{\partial}{\partial x} (\mathbf{f}(\mathbf{u}) - \mathbf{q}) = 0. \quad (2.24)$$

Applying the quadrature rule to \mathbf{q} and $\partial \mathbf{u} / \partial t$, the scheme becomes

$$\begin{aligned} \frac{\partial \mathbf{u}_r}{\partial t} + 2 \sum_{s=1}^k D_{rs} \tilde{\mathbf{F}}(\mathbf{u}_r, \mathbf{u}_s) - \sum_{s=1}^k D_{rs} \mathbf{q}_s &= \frac{\tau_r}{\omega_r} (\mathbf{f}_r - \mathbf{q}_r + \mathbf{q}_{*r} - \mathbf{f}_{*r}) \\ \mathbf{q}_r &= \nu_r \left(\sum_{s=1}^k D_{rs} \mathbf{v}_s + \frac{\tau_r}{\omega_r} (\mathbf{v}_{*r} - \mathbf{v}_r) \right), \end{aligned} \quad (2.25)$$

where $\tilde{\mathbf{g}}_* = (\tilde{\mathbf{g}}_{i-\frac{1}{2}}, 0, \dots, 0, \tilde{\mathbf{g}}_{i+\frac{1}{2}})^T$ with $\tilde{\mathbf{g}}_{i \pm \frac{1}{2}} = [\mathbf{g}]_{i \pm \frac{1}{2}} = \pm(\mathbf{g}_{i \pm \frac{1}{2}}^- - \mathbf{g}_{i \pm \frac{1}{2}}^+)$ (using $\mathbf{g} = \mathbf{v}, \mathbf{q}$).

Note that the artificial viscosity term is considered constant during a time step, regardless of the multiple stages performed by the SSP-RK3 scheme.

The definition of ν is not unique. Intuitively, it should be chosen small on smooth regions and larger close to discontinuities. Two artificial viscosity models are presented below, based on the notions in Yu and Hesthaven (2020).

2.6.1 Dilation-based (DB) viscosity

This model assumes oscillations appear at points where a specific quantity \mathbf{s} varies quickly. For scalar cases, \mathbf{s} is simply the conserved quantity u and for Euler's equations, \mathbf{s} is the speed i.e. $\mathbf{s} = (v_1, v_2)^T$. For the 2D case. The dilation-based viscosity is defined as

$$\nu_\beta = c_\beta |\nabla \cdot \mathbf{s}| (h/P)^2, \quad (2.26)$$

where c_β is an arbitrary constant and $h = (\Delta x_1 \cdots \Delta x_d)^{1/d}$. The factor $|\nabla \cdot \mathbf{s}|$ is computed numerically using the difference matrix. For a specific dimension r , the derivative is computed

at each quadrature point l (along that dimension r):

$$\left(\frac{\partial \vec{s}^r}{\partial x_r} \right)_l = \frac{2}{\Delta x_l} \sum_{m=0}^k D_{l,m} s_m, \quad (2.27)$$

where \vec{s}^r represents the values of \mathbf{s} along direction r , on each quadrature point. In order to limit dissipation, the final viscosity is computed by

$$\nu_{DB} = \min(\nu_\beta, \nu_{\max}), \quad (2.28)$$

where ν_{\max} is defined by

$$\nu_{\max} = c_{\max}(h/P) \max_{\mathbf{x} \in G_K} |\mathbf{f}'(\mathbf{u}(x, t))|, \quad (2.29)$$

where $\max_{\mathbf{x} \in G_K} |\mathbf{f}'(\mathbf{u}(x, t))|$ is the norm of the vector composed of the maximal (in the cell) eigen values in each direction i.e. $((\lambda_{\max}^1)^2 + \dots + (\lambda_{\max}^d)^2)^{1/2}$.

Note that this type of artificial viscosity limits the scheme accuracy to second order because of the h^2 factor in Equation (2.26). The viscosity is defined on each quadrature point in the cell so it can be used directly as it is.

2.6.2 Entropy-based (EB) viscosity

This model relies on the entropy dissipation which occurs at the discontinuities. Recall that the ES condition reads

$$W = \frac{\partial E}{\partial t} + \nabla \cdot \mathbf{Q} \leq 0. \quad (2.30)$$

W can be numerically estimated with the Crank-Nicolson scheme:

$$W \approx \frac{E(\mathbf{u}^n) - E(\mathbf{u}^{n-1})}{\Delta t^{n-1}} + \frac{\nabla \cdot \mathbf{Q}(\mathbf{u}^n) + \nabla \cdot \mathbf{Q}(\mathbf{u}^{n-1})}{2}, \quad (2.31)$$

where $\nabla \cdot \mathbf{Q}$ can be computed with the difference matrix. The entropy based viscosity is computed for i -th cell with

$$\nu_{E,i} = c_E \cdot (h/P) \cdot \max \left((h/P) \max_{\mathbf{x} \in G_K} |W|, \max_{\mathbf{x} \in \partial G_K} |\llbracket \mathbf{Q} \rrbracket| \right) / T, \quad (2.32)$$

where

$$T = \max_{x \in \Omega} \left| E(x, t) - \frac{1}{|\Omega|} \int_{\Omega} E d\Omega \right|. \quad (2.33)$$

Note that $T = 1$ for the situations studied in this work. The final viscosity is chosen as

$$\nu_E = \min(\nu_E, \nu_{\max}), \quad (2.34)$$

where ν_{\max} is given by Equation (2.29). Note that the EB viscosity scales as $\mathcal{O}(h^2(\Delta t^2 + h^k))$ (Zingan et al. (2013)). As it is, the entropy based viscosity give a piece-wise constant viscosity

Chapter 2. Numerical schemes

which could lead to stability issues. The viscosity must therefore be smoothed to get a C_0 function. Here, the viscosity is averaged at cells' interface and the average value are connected by a linear segment. The viscosity is extrapolated from these segments at each cell's quadrature points.

Time step size Δt The value of Δt is adapted at each time step using the CFL condition. It is computed as follow:

$$\Delta t = \frac{CFL}{\beta}, \quad \beta = \max_{\substack{1 \leq i \leq N \\ 0 \leq l \leq k}} \left(\lambda_{\max,i}^l \frac{k^2}{h} + \nu_i^l \frac{k^4}{h^2} \right), \quad (2.35)$$

where $\lambda_{\max,i}^l$ is the maximal eigen value of $\partial \mathbf{f} / \partial \mathbf{u}$ and ν_i^l is the artificial viscosity, each at l^{th} quadrature point in the i^{th} cell.

2.7 2D ES-DG scheme

A system of CLs in 2D can be expressed as follows

$$\frac{\partial \mathbf{u}}{\partial t} + \frac{\partial}{\partial x} \mathbf{f}^1 + \frac{\partial}{\partial y} \mathbf{f}^2 = 0. \quad (2.36)$$

Adding the artificial viscosity term, the equation becomes

$$\frac{\partial \mathbf{u}}{\partial t} + \frac{\partial}{\partial x} (\mathbf{f}^1 - \mathbf{q}^1) + \frac{\partial}{\partial y} (\mathbf{f}^2 - \mathbf{q}^2) = 0, \quad (2.37)$$

where, $\mathbf{q}^1 = \nu(\partial \mathbf{v} / \partial x)$ and $\mathbf{q}^2 = \nu(\partial \mathbf{v} / \partial y)$. The scheme is a tensor product of the 1D scheme:

$$\begin{aligned} \frac{\partial \mathbf{u}_{l,m}}{\partial t} + \frac{4}{\Delta x} \sum_{s=0}^k D_{ms} \mathbf{F}^1(\mathbf{u}_{l,m}, \mathbf{u}_{l,s}) + \frac{4}{\Delta y} \sum_{r=0}^k D_{lr} \mathbf{F}^2(\mathbf{u}_{l,m}, \mathbf{u}_{r,m}) \\ - \frac{2}{\Delta x} \sum_{s=0}^k D_{ms} \mathbf{q}^1_{l,s} - \frac{2}{\Delta y} \sum_{r=0}^k D_{lr} \mathbf{q}^2_{r,m} \\ = \frac{\tau_l}{\omega_l} \frac{2}{\Delta x} (\mathbf{f}_{l,m} - \mathbf{q}^1_{l,m} + \mathbf{q}_{*l,m} - \mathbf{f}_{*l,m}) \\ + \frac{\tau_m}{\omega_m} \frac{2}{\Delta y} (\mathbf{f}_{l,m} - \mathbf{q}^2_{l,m} + \mathbf{q}_{l,*m} - \mathbf{f}_{l,*m}), \end{aligned} \quad (2.38)$$

$$\begin{aligned} \mathbf{q}^1_{l,m} &= \nu_{l,m} \frac{2}{\Delta x} \left(\sum_{s=0}^k D_{ms} \mathbf{v}_{l,s} + \frac{\tau_r}{\omega_r} (\mathbf{v}_{l,*m} - \mathbf{v}_{l,*m}) \right), \\ \mathbf{q}^2_{l,m} &= \nu_{l,m} \frac{2}{\Delta y} \left(\sum_{r=0}^k D_{lr} \mathbf{v}_{r,m} + \frac{\tau_l}{\omega_l} (\mathbf{v}_{*l,m} - \mathbf{v}_{l,m}) \right). \end{aligned}$$

Time step size Δt The time step size is adapted at each time step using the CFL condition. It is computed as follow:

$$\Delta t = \frac{CFL}{\beta}, \quad \beta = \max_{\substack{1 \leq i, j \leq N \\ 0 \leq l, m \leq k}} \left(\frac{1}{2} \left(\frac{\lambda_{\max, i, j}^{1, l, m}}{\Delta x} + \frac{\lambda_{\max, i, j}^{2, l, m}}{\Delta y} \right) k^2 + \nu_{i, j}^{l, m} \frac{k^4}{\Delta x \Delta y} \right), \quad (2.39)$$

where $\lambda_{\max, i, j}^{1, l, m}$ and $\lambda_{\max, i, j}^{2, l, m}$ are the maximal eigen value of the Jacobian matrix associated to \mathbf{f}^1 and \mathbf{f}^2 respectively and $\nu_{i, j}^{l, m}$ is the artificial viscosity, each at quadrature point (l, m) in cell (i, j) .

3 Physical problems

Physical problems studied in this work are presented in this section. The conserved variables and the fluxes are given as well as the entropy variables, entropy function, entropy fluxes and the potential. As a reminder, the entropy function $E(\mathbf{u})$ is a convex function. The entropy variables \mathbf{v} are defined as

$$\mathbf{v} = \frac{\partial E}{\partial \mathbf{u}}. \quad (3.1)$$

The entropy flux Q must satisfy the following condition

$$\left(\frac{\partial Q(\mathbf{u})}{\partial \mathbf{u}} \right)^T = \mathbf{v}^T \frac{\mathbf{f}(\mathbf{u})}{\partial \mathbf{u}}. \quad (3.2)$$

The potential ψ is defined as

$$\psi(\mathbf{u}) = \mathbf{v}^T \mathbf{f}(\mathbf{u}) - Q(\mathbf{u}). \quad (3.3)$$

3.1 1D advection equation

The 1D advection equation is expressed as

$$\frac{\partial u}{\partial t} + c \frac{\partial u}{\partial x} = 0, \quad (3.4)$$

with $c \in \mathbb{R}$. Therefore, $f(u) = cu$. An analytical solution can easily be expressed:

$$u(x, t) = u_0(x - ct), \quad (3.5)$$

where $u_0(x)$ is the initial condition, i.e. $u(x, t = 0) = u_0(x)$. Defining $E(u) = \frac{1}{2}u^2$, one gets $V = u$, $\partial Q/\partial u = cu \rightarrow Q = \frac{1}{2}cu^2$ and $\psi = \frac{1}{2}cu^2$.

Entropy conservative flux We require \tilde{F} to satisfy

$$[V] \tilde{F} = [\psi]. \quad (3.6)$$

Chapter 3. Physical problems

We have $\llbracket V \rrbracket = \llbracket u \rrbracket$ and $\llbracket \psi \rrbracket = \llbracket \frac{1}{2} c u^2 \rrbracket$. Therefore

$$\tilde{F}(u_j, u_l) = \frac{1}{2} c \frac{\llbracket u^2 \rrbracket}{\llbracket u \rrbracket} = \frac{1}{2} c \frac{u_l^2 - u_j^2}{u_l - u_j} = \frac{1}{2} c(u_j + u_l). \quad (3.7)$$

For the numerical tests, c is set to $c = 1$.

3.2 1D Burgers' equation

Burgers' equation is expressed as

$$\frac{\partial u}{\partial t} + u \frac{\partial u}{\partial x} = 0. \quad (3.8)$$

Therefore, $f(u) = \frac{1}{2} u^2$. An analytical solution can be obtained in some situations using the method of characteristics though it will not be detailed here.

Defining $E(u) = \frac{1}{2} u^2$ one gets $V = u$, $\partial Q / \partial u = u^2 \rightarrow Q = \frac{1}{3} u^3$ and $\psi = \frac{1}{6} u^3$.

Entropy conservative flux We require \tilde{F} to satisfy

$$\llbracket V \rrbracket \tilde{F} = \llbracket \psi \rrbracket. \quad (3.9)$$

We have $\llbracket V \rrbracket = \llbracket u \rrbracket$ and $\llbracket \psi \rrbracket = \llbracket \frac{1}{6} u^3 \rrbracket$. Therefore

$$\tilde{F}(u_j, u_l) = \frac{1}{6} \frac{\llbracket u^3 \rrbracket}{\llbracket u \rrbracket} = \frac{1}{6} \frac{u_l^3 - u_j^3}{u_l - u_j} = \frac{1}{6} (u_j^2 + u_j u_l + u_l^2). \quad (3.10)$$

3.3 1D Euler equations

Euler's equations are a simplification of Navier-Stokes equations, where viscosity and thermal conductivity are both zero. This system of equations can be expressed as a system of CL with the variables $\mathbf{u} = (\rho, \rho v, E)^T$ and the flux $\mathbf{f} = (\rho v, \rho v^2 + P, v(E + P))^T$, where, $P = (\gamma - 1)(E - \frac{1}{2} \rho v^2)$ with $\gamma = 7/5$. The entropy function, variables and flux are defined as follow:

$$E = \frac{-\rho s}{\gamma - 1}, \quad \mathbf{V} = \begin{pmatrix} \frac{\gamma - s}{\gamma - 1} - \frac{\rho v^2}{2P} \\ \rho v / P \\ -\rho / P \end{pmatrix}, \quad Q = \frac{-\rho v s}{\gamma - 1},$$

where $s = \log(P) - \gamma \log(\rho)$ and the potential is $\psi = \rho v$.

Entropy conservative flux We require $\tilde{\mathbf{F}}$ to satisfy

$$\llbracket \mathbf{V} \rrbracket^T \tilde{\mathbf{F}} = \llbracket \psi \rrbracket. \quad (3.11)$$

Computations are expressed as function of (ρ, v, β) , where $\beta = \rho/P$. We use the identity $\llbracket ab \rrbracket = \{\{a\}\llbracket b \rrbracket + \{\{b\}\llbracket a \rrbracket\}$ and the log average, defined¹ as:

$$\{\{a\}\}^{ln} = \frac{\llbracket a \rrbracket}{\llbracket \log a \rrbracket}. \quad (3.12)$$

The right hand side of the Equation (3.11) becomes:

$$\llbracket \psi \rrbracket = \llbracket \rho v \rrbracket = \{\{v\}\llbracket \rho \rrbracket + \{\{\rho\}\llbracket v \rrbracket\}.$$

The component of the vector $\llbracket \mathbf{V} \rrbracket$ can be expressed as:

$$\begin{aligned} \llbracket V^1 \rrbracket &= -\frac{1}{\gamma-1} \llbracket s \rrbracket - \frac{1}{2} \llbracket \beta v^2 \rrbracket = \frac{1}{\gamma-1} \llbracket \log(\beta) \rrbracket + \llbracket \log(\rho) \rrbracket - \frac{1}{2} (\{\{\beta\}\} \llbracket v^2 \rrbracket + \{\{v^2\}\} \llbracket \beta \rrbracket) \\ &= \frac{1}{\gamma-1} \frac{\llbracket \beta \rrbracket}{\{\{\beta\}\}^{ln}} + \frac{\llbracket \rho \rrbracket}{\{\{\rho\}\}^{ln}} - \{\{\beta\}\} (\{\{v\}\} \llbracket v \rrbracket - \{\{v^2\}\} \llbracket \beta \rrbracket), \end{aligned}$$

$$\llbracket V^2 \rrbracket = \llbracket \beta v \rrbracket = \{\{\beta\}\} \llbracket v \rrbracket + \{\{v\}\} \llbracket \beta \rrbracket,$$

$$\llbracket V^3 \rrbracket = -\llbracket \beta \rrbracket.$$

Therefore, Equation (3.11) becomes

$$\begin{aligned} \llbracket \mathbf{V} \rrbracket^T \tilde{\mathbf{F}} &= \frac{1}{\{\{\rho\}\}^{ln}} \tilde{F}_1 \llbracket \rho \rrbracket + \{\{\beta\}\} (\tilde{F}_2 - \{\{v\}\} \tilde{F}_1) \llbracket v \rrbracket \\ &\quad + \left[\left(\frac{1}{\gamma-1} \frac{1}{\{\{\beta\}\}^{ln}} - \frac{1}{2} \{\{v^2\}\} \right) \tilde{F}_1 + \{\{v\}\} \tilde{F}_2 - \tilde{F}_3 \right] \llbracket \beta \rrbracket \\ &= \{\{v\}\} \llbracket \rho \rrbracket + \{\{\rho\}\} \llbracket v \rrbracket = \llbracket \rho v \rrbracket = \llbracket \psi \rrbracket. \end{aligned}$$

This yields to a system of 3 equations with 3 unknowns:

$$\bullet \quad \frac{1}{\{\{\rho\}\}^{ln}} \tilde{F}_1 = \{\{v\}\} \implies \tilde{F}_1 = \{\{v\}\} \{\{\rho\}\}^{ln}.$$

$$\bullet \quad \{\{\beta\}\} (\tilde{F}_2 - \{\{v\}\} \tilde{F}_1) = \{\{\rho\}\} \implies \tilde{F}_2 = \frac{\{\{\rho\}\}}{\{\{\beta\}\}} + \{\{v\}\} \tilde{F}_1.$$

$$\bullet \quad \tilde{F}_3 = \left(\frac{1}{\gamma-1} \frac{1}{\{\{\beta\}\}^{ln}} - \frac{1}{2} \{\{v^2\}\} \right) \tilde{F}_1 + \{\{v\}\} \tilde{F}_2.$$

¹This definition may be numerically unstable if a is small. In this case, a Taylor expansion of $\{\{\cdot\}\}^{ln}$ should be used instead.

3.4 2D advection equation

The 2D advection equation is expressed as

$$\frac{\partial u}{\partial t} + c_1 \frac{\partial u}{\partial x} + c_2 \frac{\partial u}{\partial y} = 0. \quad (3.13)$$

Therefore, $f^1(u) = c_1 u$ and $f^2(u) = c_2 u$. As for the 1D case, an analytical solution can easily be expressed:

$$u(x, y, t) = u_0((x - c_1 t) + (y - c_2 t)), \quad (3.14)$$

where $u_0(x, y)$ is the initial condition, i.e. $u(x, y, t = 0) = u_0(x, y)$.

Defining $E(u) = \frac{1}{2} u^2$, one gets $V = u$, $\partial Q_1 / \partial u = c_1 u \rightarrow Q_1 = \frac{1}{2} c_1 u^2 \rightarrow \psi_1 = \frac{1}{2} c_1 u^2$ and $\partial Q_2 / \partial u = c_2 u \rightarrow Q_2 = \frac{1}{2} c_2 u^2 \rightarrow \psi_2 = \frac{1}{2} c_2 u^2$.

Entropy conservative flux Both \tilde{F}^1 and \tilde{F}^2 are similar to the 1D EC flux:

$$\tilde{F}^1(u_l, u_s) = \frac{1}{2} c_1(u_l + u_s), \quad \tilde{F}^2(u_m, u_r) = \frac{1}{2} c_2(u_m + u_r). \quad (3.15)$$

3.5 2D Euler equations

The 2D Euler equations is a system of CL with variable \mathbf{u} and fluxes \mathbf{f}^1 and \mathbf{f}^2 defined as:

$$\mathbf{u} = \begin{pmatrix} \rho \\ \rho v_1 \\ \rho v_2 \\ E \end{pmatrix}, \quad \mathbf{f}^1 = \begin{pmatrix} \rho v_2 \\ \rho v_1^2 + P \\ \rho v_1 v_2 \\ v_1(E + P) \end{pmatrix}, \quad \mathbf{f}^2 = \begin{pmatrix} \rho v_2 \\ \rho v_1 v_2 \\ \rho v_2^2 + P \\ v_2(E + P) \end{pmatrix},$$

where $P = (\gamma - 1)(E - \frac{1}{2}\rho(v_1^2 + v_2^2))$. The entropy function, variables, and fluxes are given by

$$E = \frac{-\rho s}{\gamma - 1}, \quad \mathbf{v} = \begin{pmatrix} \frac{\gamma - s}{\gamma - 1} - \frac{\rho(v_1^2 + v_2^2)}{2P} \\ \rho v_1 / P \\ \rho v_2 / P \\ -\rho / P \end{pmatrix}, \quad Q_1 = \frac{-\rho v_1 s}{\gamma - 1}, \quad Q_2 = \frac{-\rho v_2 s}{\gamma - 1},$$

and the potentials are $\psi_1 = \rho v_1$ and $\psi_2 = \rho v_2$.

Entropy conservative fluxes We require $\tilde{\mathbf{F}}^1$ and $\tilde{\mathbf{F}}^2$ to satisfy $[\![\mathbf{V}]\!]^T \tilde{\mathbf{F}}^1 = [\![\psi_1]\!]$ and $[\![\mathbf{V}]\!]^T \tilde{\mathbf{F}}^2 = [\![\psi_2]\!]$ respectively. Computations are expressed as function of (ρ, v_1, v_2, β) , where $\beta = \rho / P$. The right hand side of both equations become:

1. $[\![\psi_1]\!] = [\![\rho v_1]\!] = \{\{v_1\}\}[\![\rho]\!] + \{\{\rho\}\}[\![v_1]\!]$

$$2. \quad \llbracket \psi_2 \rrbracket = \llbracket \rho v_2 \rrbracket = \{\{\nu_2\}\} \llbracket \rho \rrbracket + \{\{\rho\}\} \llbracket v_2 \rrbracket$$

The entropy variables are defined by $\mathbf{V} = (\frac{\gamma-s}{\gamma-1} - \frac{\beta}{2}(v_1^2 + v_2^2), \beta v_1, \beta v_2, -\beta)^T$. The jump of the entropy variable can therefore be rewritten as:

$$\begin{aligned} \llbracket V^1 \rrbracket &= -\frac{1}{\gamma-1} \llbracket s \rrbracket - \frac{1}{2} \llbracket \beta(v_1^2 + v_2^2) \rrbracket \\ &= \frac{1}{\gamma-1} \llbracket \log(\beta) \rrbracket + \llbracket \log(\rho) \rrbracket - \frac{1}{2} (\{\{\beta\}\} \llbracket v_1^2 + v_2^2 \rrbracket + \{\{v_1^2 + v_2^2\}\} \llbracket \beta \rrbracket) \\ &= \frac{1}{\gamma-1} \frac{\llbracket \beta \rrbracket}{\{\{\beta\}\}^{ln}} + \frac{\llbracket \rho \rrbracket}{\{\{\rho\}\}^{ln}} - \{\{\beta\}\} (\{\{\nu_1\}\} \llbracket v_1 \rrbracket + \{\{\nu_2\}\} \llbracket v_2 \rrbracket - \{\{v_1^2 + v_2^2\}\} \llbracket \beta \rrbracket), \end{aligned}$$

$$\llbracket V^2 \rrbracket = \llbracket \beta v_1 \rrbracket = \{\{\beta\}\} \llbracket v_1 \rrbracket + \{\{\nu_1\}\} \llbracket \beta \rrbracket,$$

$$\llbracket V^3 \rrbracket = \llbracket \beta v_2 \rrbracket = \{\{\beta\}\} \llbracket v_2 \rrbracket + \{\{\nu_2\}\} \llbracket \beta \rrbracket,$$

$$\llbracket V^4 \rrbracket = -\llbracket \beta \rrbracket.$$

The first direction:

$$\begin{aligned} \llbracket V \rrbracket^T \tilde{\mathbf{F}}^1 &= \frac{1}{\{\{\rho\}\}^{ln}} \tilde{F}_1^1 \llbracket \rho \rrbracket + \{\{\beta\}\} (\tilde{F}_2^1 - \{\{\nu_1\}\} \tilde{F}_1^1) \llbracket v_1 \rrbracket + \{\{\beta\}\} (\tilde{F}_3^1 - \llbracket \nu_2 \rrbracket \tilde{F}_1^1) \llbracket v_2 \rrbracket \\ &\quad + \left[\left(\frac{1}{\gamma-1} \frac{1}{\{\{\beta\}\}^{ln}} - \frac{1}{2} \{\{v_1^2 + v_2^2\}\} \right) \tilde{F}_1^1 + \{\{\nu_1\}\} \tilde{F}_2^1 + \{\{\nu_2\}\} \tilde{F}_3^1 - \tilde{F}_4^1 \right] \llbracket \beta \rrbracket \\ &= \{\{\nu_1\}\} \llbracket \rho \rrbracket + \{\{\rho\}\} \llbracket \nu_1 \rrbracket = \llbracket \rho v_1 \rrbracket = \llbracket \psi_1 \rrbracket. \end{aligned}$$

This yields to a system of 4 equations with 4 unknowns:

- $\frac{1}{\{\{\rho\}\}^{ln}} \tilde{F}_1^1 = \{\{\nu_1\}\} \implies \tilde{F}_1^1 = \{\{\nu_1\}\} \{\{\rho\}\}^{ln}$
- $\{\{\beta\}\} (\tilde{F}_2^1 - \{\{\nu_1\}\} \tilde{F}_1^1) = \{\{\rho\}\} \implies \tilde{F}_2^1 = \frac{\{\{\rho\}\}}{\{\{\beta\}\}} + \{\{\nu_1\}\} \tilde{F}_1^1$
- $\{\{\beta\}\} (\tilde{F}_3^1 - \llbracket \nu_2 \rrbracket \tilde{F}_1^1) = 0 \implies \tilde{F}_3^1 = \{\{\nu_2\}\} \tilde{F}_1^1$
- $\tilde{F}_4^1 = \left(\frac{1}{\gamma-1} \frac{1}{\{\{\beta\}\}^{ln}} - \frac{1}{2} \{\{v_1^2 + v_2^2\}\} \right) \tilde{F}_1^1 + \{\{\nu_1\}\} \tilde{F}_2^1 + \{\{\nu_2\}\} \tilde{F}_3^1$

Chapter 3. Physical problems

The second direction:

$$\begin{aligned} \llbracket V \rrbracket^T \tilde{\mathbf{F}}^2 &= \frac{1}{\{\rho\}^{ln}} \tilde{F}_1^2 \llbracket \rho \rrbracket + \{\beta\} (\tilde{F}_2^2 - \{\nu_1\} \tilde{F}_1^2) \llbracket \nu_1 \rrbracket + \{\beta\} (\tilde{F}_3^2 - \llbracket \nu_2 \rrbracket \tilde{F}_1^2) \llbracket \nu_2 \rrbracket \\ &+ \left[\left(\frac{1}{\gamma-1} \frac{1}{\{\beta\}^{ln}} - \frac{1}{2} \{\nu_1^2 + \nu_2^2\} \right) \tilde{F}_1^2 + \{\nu_1\} \tilde{F}_2^2 + \{\nu_2\} \tilde{F}_3^2 - \tilde{F}_4^2 \right] \llbracket \beta \rrbracket \\ &= \{\nu_2\} \llbracket \rho \rrbracket = \llbracket \rho \nu_2 \rrbracket + \{\rho\} \llbracket \nu_2 \rrbracket = \llbracket \psi_2 \rrbracket. \end{aligned}$$

This yields to a system of 4 equations with 4 unknowns:

- $\frac{1}{\{\rho\}^{ln}} \tilde{F}_1^2 = \{\nu_2\} \implies \tilde{F}_1^2 = \{\nu_2\} \{\rho\}^{ln}$
- $\{\beta\} (\tilde{F}_2^2 - \{\nu_1\} \tilde{F}_1^2) = 0 \implies \tilde{F}_{2,2} = \{\nu_1\} \tilde{F}_1^2$
- $\{\beta\} (\tilde{F}_3^2 - \llbracket \nu_2 \rrbracket \tilde{F}_1^2) = \{\rho\} \implies \tilde{F}_3^2 = \frac{\{\rho\}}{\{\beta\}} + \{\nu_2\} \tilde{F}_1^2$
- $\tilde{F}_4^2 = \left(\frac{1}{\gamma-1} \frac{1}{\{\beta\}^{ln}} - \frac{1}{2} \{\nu_1^2 + \nu_2^2\} \right) \tilde{F}_1^2 + \{\nu_1\} \tilde{F}_2^2 + \{\nu_2\} \tilde{F}_3^2$

It is easy to verify² that \tilde{F}_1 and \tilde{F}_2 are consistent with f_1 and f_2 respectively.

²Indeed, setting both sides to the same value, we have $\{\{a\}\} = \{\{a\}\}^{ln} = a$

4 Numerical results and discussions

All the following results are obtained using the Lax-Friedrichs flux as the ES flux, i.e.

$$\mathbf{F}(\mathbf{u}_L, \mathbf{u}_R) = \mathbf{f}(\mathbf{u}_L) + \mathbf{f}(\mathbf{u}_R) - \frac{\alpha}{2}(\mathbf{u}_R - \mathbf{u}_L), \quad (4.1)$$

where $\alpha = \max(\lambda_{\max}(\mathbf{u}_L), \lambda_{\max}(\mathbf{u}_R))$, and $\lambda_{\max}(\mathbf{u})$ represents the maximal eigen value of the Jacobian matrix $\partial\mathbf{f}/\partial\mathbf{u}$.

In the following results, the plotted numerical solutions are the average values inside each cells, both for the 1D and 2D schemes.

4.1 1D advection equation

The advection equation is used to verify the convergence rate of the scheme on a smooth solution.

Smooth test The initial condition is $u(x) = 1 + \sin(2\pi x)$. At the time t , the solution is therefore $u(x, t) = 1 + \sin(2\pi(x - t))$. The value of u at $t = 0$ and at the final time $t_{fin} = 0.2$ is shown in Figure 4.1. The error ϵ is computed by using the numerical solution at quadrature points l within the cell i , with three different norms:

- $L^1 : \epsilon = \frac{\Delta x}{k} \left(\sum_{i=1}^N \sum_{l=1}^k |u_i^l - u(x_i^l)| \right)$
- $L^2 : \epsilon = \left(\frac{\Delta x}{k} \sum_{i=1}^N \sum_{l=1}^k (u_i^l - u(x_i^l))^2 \right)^{1/2}$
- $L^\infty : \epsilon = \max_{1 \leq i \leq N} \max_{1 \leq l \leq k} |u_i^l - u(x_i^l)|$

The number of cell is varied between $N = 10$ and $N = 50$ for all tests. The time step Δt is varied with Δx to match the expected convergence, according to the theoretical time integration order.

Chapter 4. Numerical results and discussions

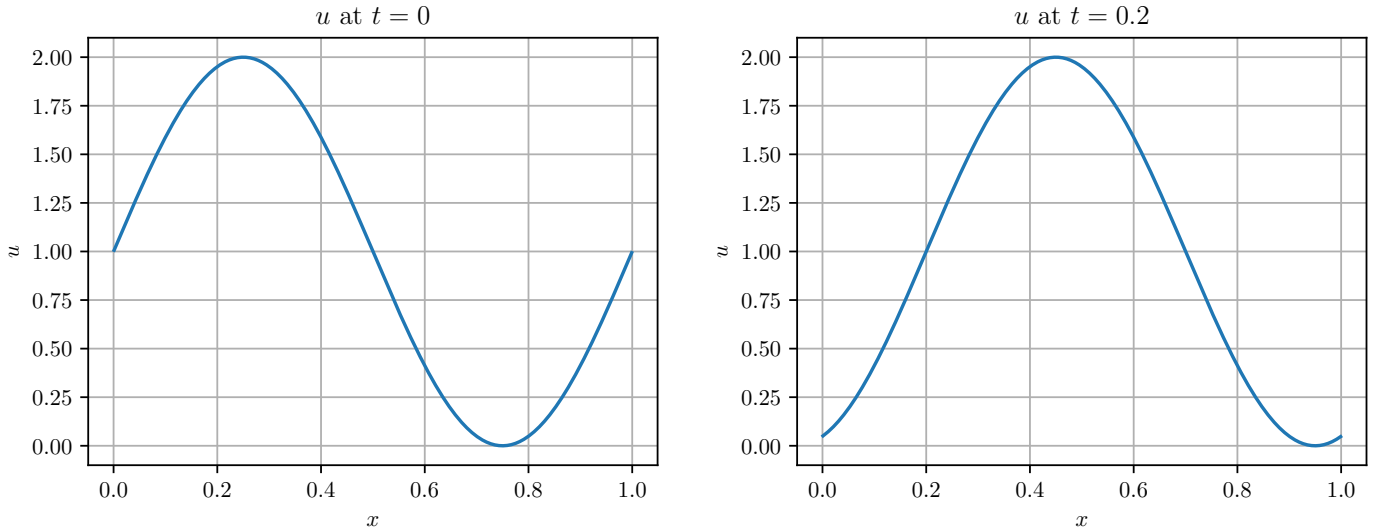


Figure 4.1: Initial (left) and final (right) solutions for the 1D smooth test using advection equation.

Without artificial viscosity The results computed without artificial viscosity are presented in Table 4.1, Table 4.2, Table 4.3 and in Figure 4.2. The time integration is of order 3, therefore $\Delta t = C(\Delta x)^{(k+1)/3}$, with $C = 0.1$.

N	L^1 error	order	L^2 error	order	L^∞ error	order
10	6.663e-02	-	7.631e-02	-	1.176e-01	-
20	1.947e-02	1.77	2.166e-02	1.82	3.223e-02	1.87
30	8.663e-03	2.00	9.750e-03	1.97	1.441e-02	1.99
40	5.058e-03	1.87	5.615e-03	1.92	8.111e-03	2.00
50	3.188e-03	2.07	3.576e-03	2.02	5.196e-03	2.00

Table 4.1: Convergence test on smooth advection equation for P^1 elements, without artificial viscosity.

N	L^1 error	order	L^2 error	order	L^∞ error	order
10	2.860e-03	-	4.168e-03	-	9.484e-03	-
20	3.532e-04	3.02	5.337e-04	2.97	1.251e-03	2.92
30	1.037e-04	3.02	1.593e-04	2.98	3.756e-04	2.97
40	4.358e-05	3.01	6.741e-05	2.99	1.594e-04	2.98
50	2.223e-05	3.02	3.458e-05	2.99	8.186e-05	2.99

Table 4.2: Convergence test on smooth advection equation for P^2 elements, without artificial viscosity.

4.1 1D advection equation

N	L^1 error	order	L^2 error	order	L^∞ error	order
10	2.948e-06	-	5.077e-06	-	1.487e-05	-
20	9.462e-08	4.96	1.589e-07	5.00	4.739e-07	4.97
30	1.243e-08	5.01	2.084e-08	5.01	6.171e-08	5.03
40	2.955e-09	4.99	4.918e-09	5.02	1.454e-08	5.02
50	9.628e-10	5.03	1.610e-09	5.00	4.764e-09	5.00

Table 4.3: Convergence test on smooth advection equation for P^4 elements, without artificial viscosity.

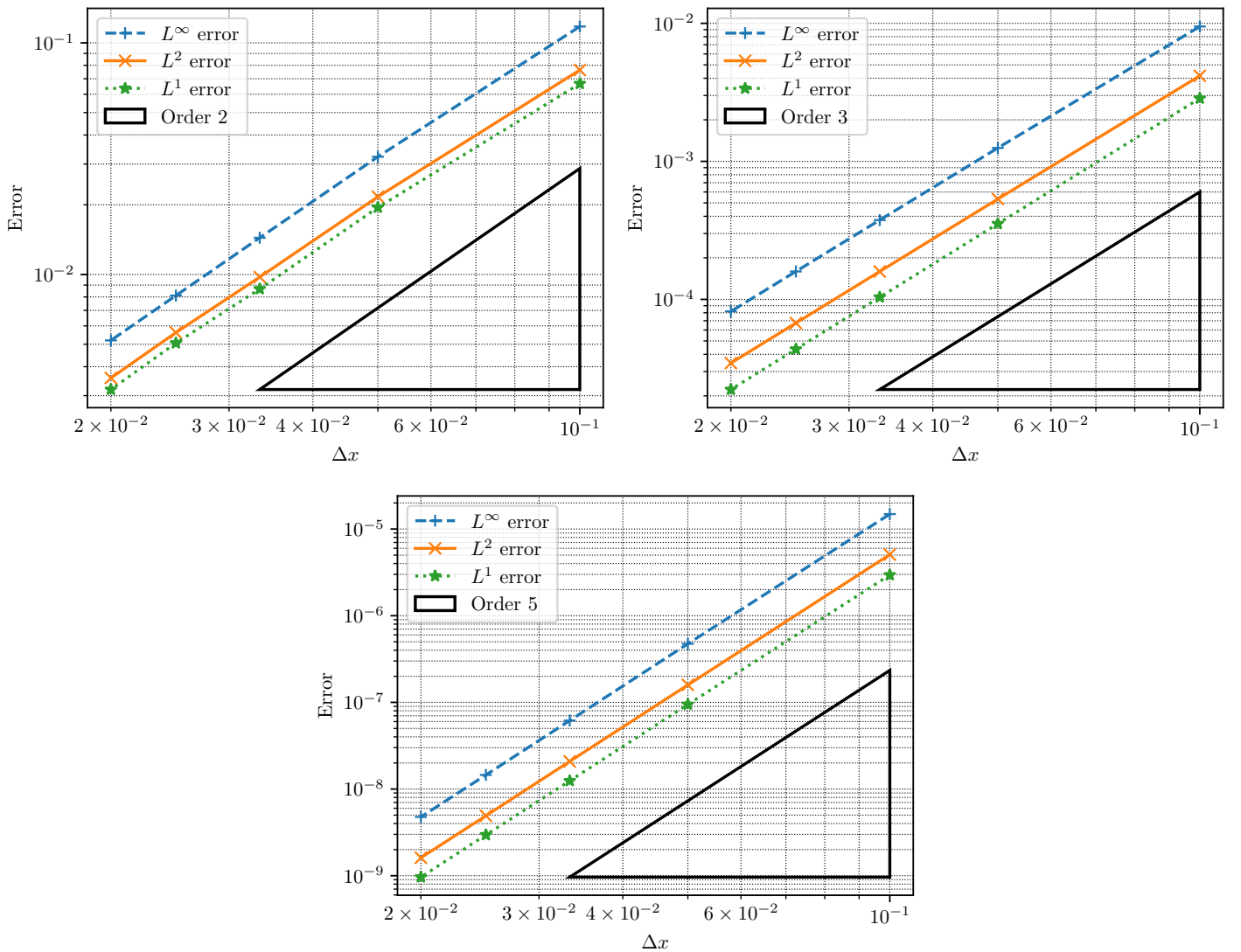


Figure 4.2: Convergence test on smooth advection equation for P^1 , P^2 and P^4 elements, without artificial viscosity.

Chapter 4. Numerical results and discussions

The scheme converges as expected in all norms. Indeed, no artificial viscosity has been added yet so we do not expect any limitation in convergence

Dilation based viscosity The results computed with dilation based artificial viscosity are presented in Table 4.4, Table 4.5, Table 4.6 and in Figure 4.3. The coefficients for the artificial viscosity are fixed at $c = 1$ and $c_{\max} = 0.5$. As before, the time integration is of order 3, therefore $\Delta t = C(\Delta x)^{(k+1)/3}$, with $C = 0.1$.

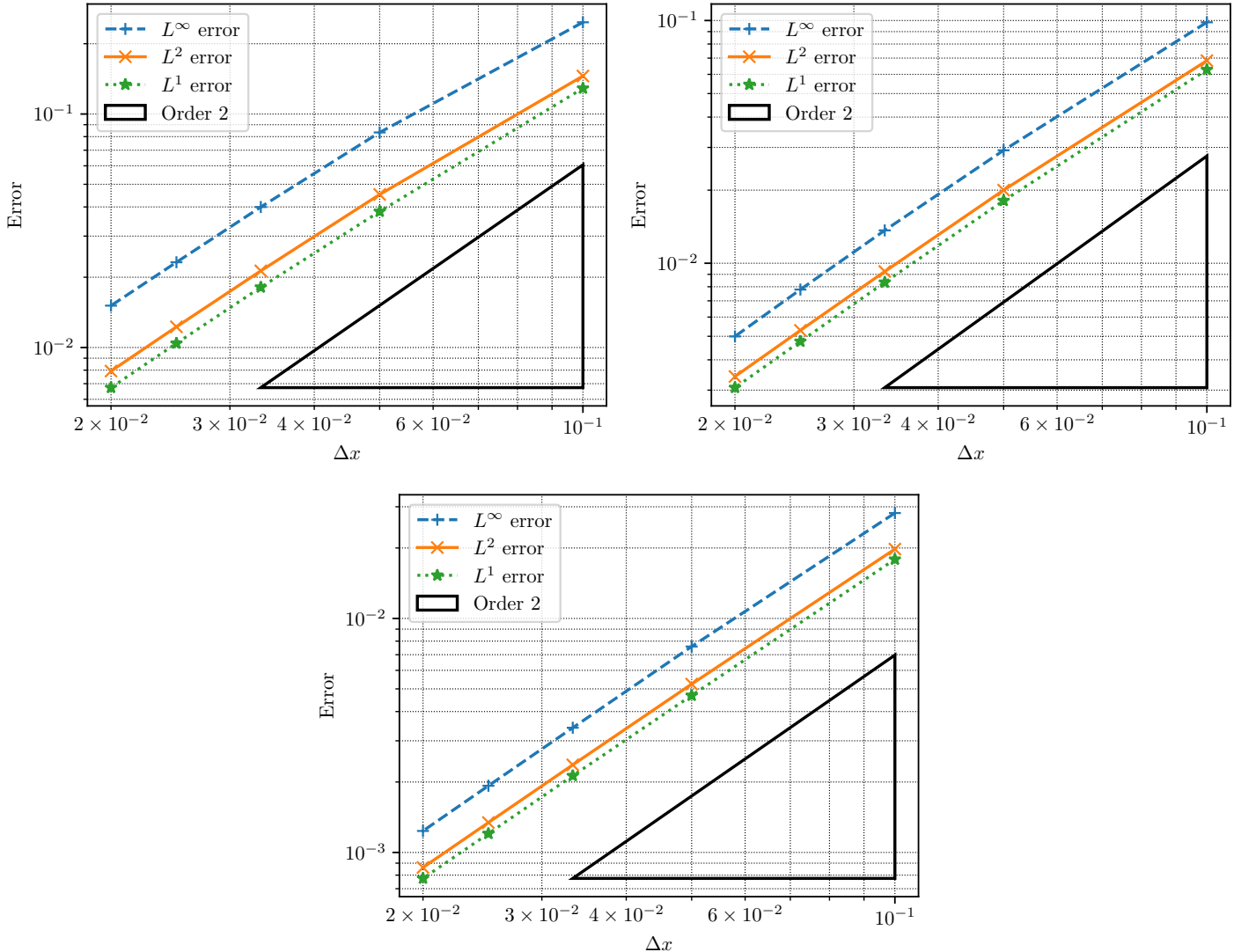


Figure 4.3: Convergence test on smooth advection equation for P^1 , P^2 and P^4 elements, with dilation based artificial viscosity.

4.1 1D advection equation

N	L^1 error	order	L^2 error	order	L^∞ error	order
10	1.288e-01	-	1.455e-01	-	2.471e-01	-
20	3.824e-02	1.75	4.523e-02	1.69	8.339e-02	1.57
30	1.811e-02	1.84	2.129e-02	1.86	3.997e-02	1.81
40	1.042e-02	1.92	1.226e-02	1.92	2.318e-02	1.89
50	6.732e-03	1.96	7.927e-03	1.95	1.511e-02	1.92

Table 4.4: Convergence test on smooth advection equation for P^1 elements, with dilation based viscosity.

N	L^1 error	order	L^2 error	order	L^∞ error	order
10	6.271e-02	-	6.834e-02	-	9.834e-02	-
20	1.810e-02	1.79	2.001e-02	1.77	2.919e-02	1.75
30	8.339e-03	1.91	9.244e-03	1.90	1.366e-02	1.87
40	4.761e-03	1.95	5.288e-03	1.94	7.791e-03	1.95
50	3.072e-03	1.96	3.415e-03	1.96	4.994e-03	1.99

Table 4.5: Convergence test on smooth advection equation for P^2 elements, with dilation based viscosity.

N	L^1 error	order	L^2 error	order	L^∞ error	order
10	1.788e-02	-	1.978e-02	-	2.821e-02	-
20	4.685e-03	1.93	5.243e-03	1.92	7.585e-03	1.89
30	2.127e-03	1.95	2.368e-03	1.96	3.411e-03	1.97
40	1.204e-03	1.98	1.342e-03	1.97	1.927e-03	1.98
50	7.746e-04	1.98	8.625e-04	1.98	1.236e-03	1.99

Table 4.6: Convergence test on smooth advection equation for P^4 elements, with dilation based viscosity.

This time, the convergence rate of the scheme is limited to 2. This is expected since the dilation based viscosity term is second order accurate in space.

Entropy based viscosity The results computed with entropy based artificial viscosity are presented in Table 4.7, Table 4.8, Table 4.9 and in Figure 4.4. The coefficients for the artificial viscosity are fixed at $c = 1$ and $c_{\max} = 0.5$. Here, the scheme is only second order accurate in time, therefore $\Delta t = C(\Delta x)^{(k+1)/2}$, with $C = 0.1$.

Chapter 4. Numerical results and discussions

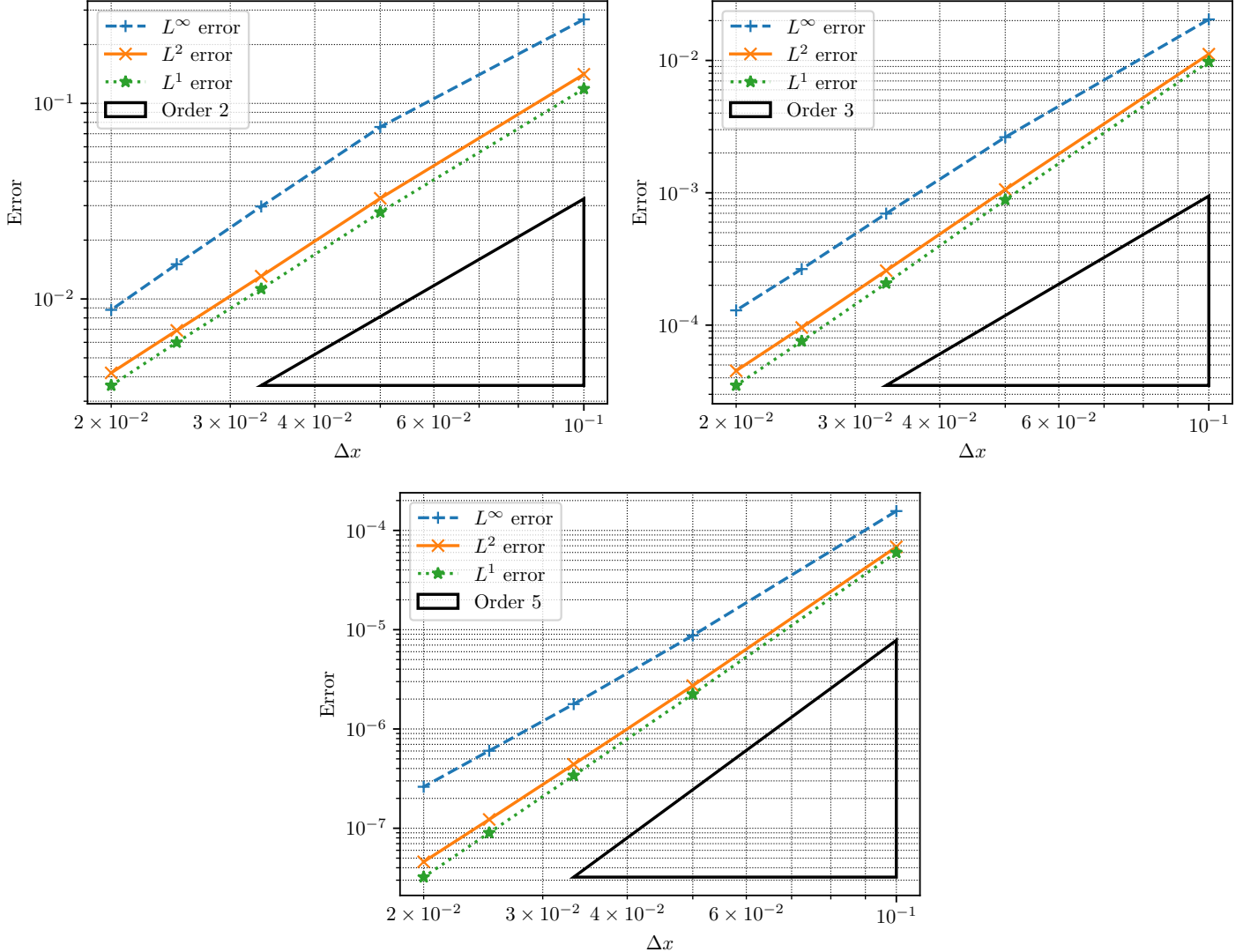


Figure 4.4: Convergence test on smooth advection equation for P^1 , P^2 and P^4 elements, with entropy based artificial viscosity.

N	L^1 error	order	L^2 error	order	L^∞ error	order
10	1.187e-01	-	1.409e-01	-	2.689e-01	-
20	2.776e-02	2.10	3.271e-02	2.11	7.578e-02	1.83
30	1.126e-02	2.23	1.307e-02	2.26	2.971e-02	2.31
40	5.997e-03	2.19	6.903e-03	2.22	1.506e-02	2.36
50	3.612e-03	2.27	4.188e-03	2.24	8.796e-03	2.41

Table 4.7: Convergence test on smooth advection equation for P^1 elements, with entropy based viscosity.

N	L^1 error	order	L^2 error	order	L^∞ error	order
10	9.773e-03	-	1.116e-02	-	2.042e-02	-
20	8.844e-04	3.47	1.058e-03	3.40	2.631e-03	2.96
30	2.071e-04	3.58	2.579e-04	3.48	6.96e-04	3.28
40	7.56e-05	3.50	9.592e-05	3.44	2.652e-04	3.35
50	3.501e-05	3.45	4.519e-05	3.37	1.293e-04	3.22

Table 4.8: Convergence test on smooth advection equation for P^2 elements, with entropy based viscosity.

N	L^1 error	order	L^2 error	order	L^∞ error	order
10	5.976e-05	-	6.829e-05	-	1.566e-04	-
20	2.238e-06	4.74	2.732e-06	4.64	8.752e-06	4.16
30	3.398e-07	4.65	4.403e-07	4.50	1.781e-06	3.93
40	8.996e-08	4.62	1.226e-07	4.44	6.034e-07	3.76
50	3.22e-08	4.60	4.596e-08	4.40	2.618e-07	3.74

Table 4.9: Convergence test on smooth advection equation for P^4 elements, with entropy based viscosity.

The scheme converges as expected for P^1 and P^2 elements but EB viscosity seems to significantly reduce the convergence with the P^4 elements.

4.2 1D Burgers' equation

Burgers' equation is a minimal example in which discontinuities can emerge from smooth initial data. It is therefore a good starting point to test the scheme's ability to capture shocks. The initial condition is set to $u_0(x) = \sin(2\pi x)$. The number of cell is fixed at $N = 20$ for all the tests and the final time is $t_{\text{fin}} = 0.4$. The numerical solution is compared with the reference solution computed by the ES WENO scheme. The coefficients for the artificial viscosity are fixed at $c = 1$ and $c_{\text{max}} = 0.5$ and the CFL number is set to $\text{CFL} = 0.1$ for all tests.

P^1 elements The results obtained without artificial viscosity, with dilation based and with entropy based viscosity for P^1 elements are shown in Figure 4.5, Figure 4.6 and Figure 4.7 respectively. The evolution of both artificial viscosities is plotted in Figure 4.8.

Chapter 4. Numerical results and discussions

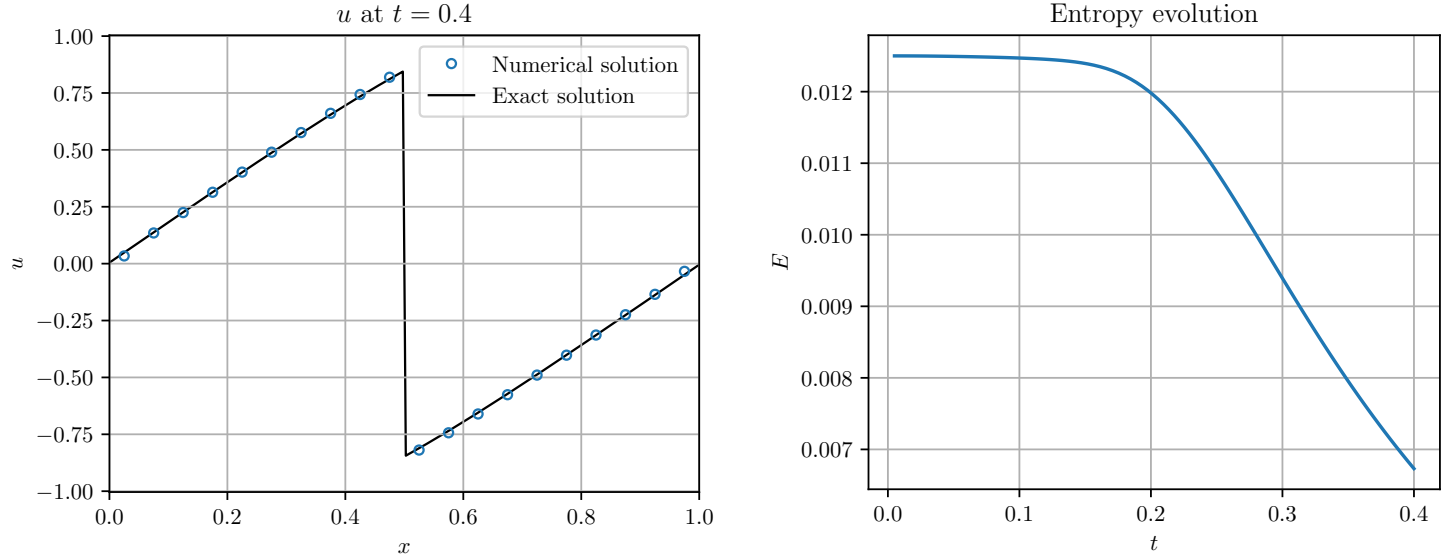


Figure 4.5: Solution (left) and entropy evolution (right) for Burgers' equation using P^1 and no artificial viscosity.

These results prove that the scheme is indeed able to capture shocks in a simple situation. As expected, the entropy is essentially constant at the beginning and starts to decrease when the shock appears. This shows that the entropy is indeed dissipated when necessary. In this specific example, the shock is actually static i.e. the discontinuity stays at $x = 0.5$.

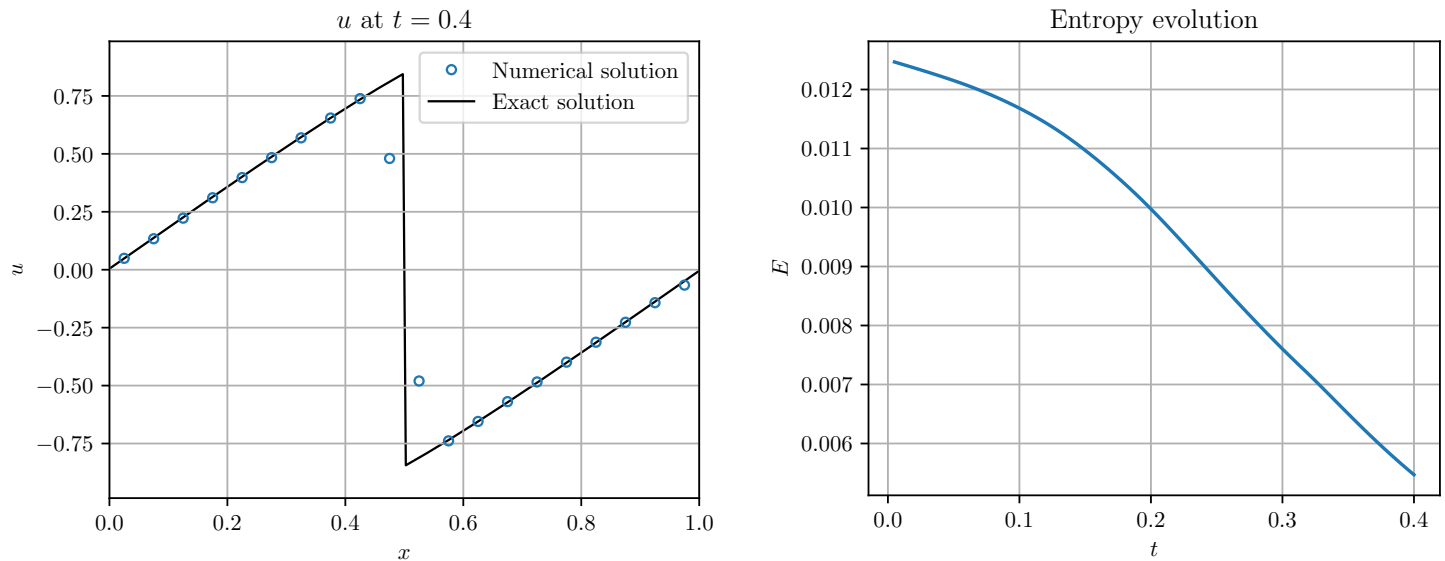


Figure 4.6: Solution (left) and entropy evolution (right) for Burgers' equation using P^1 and dilation based viscosity.

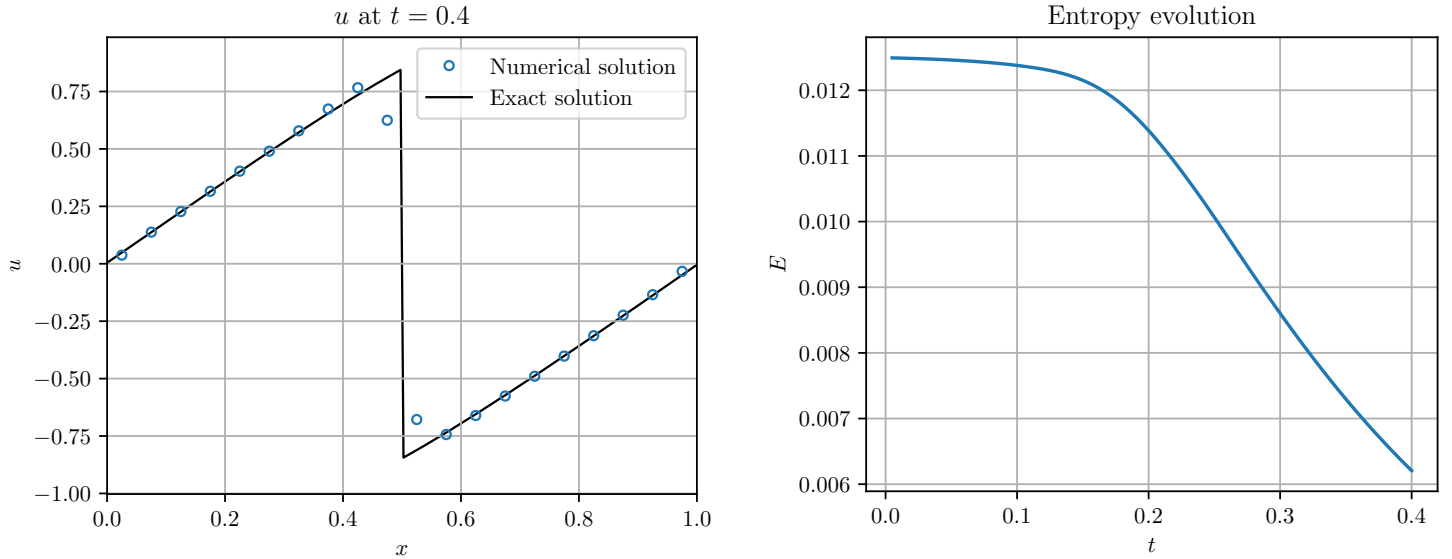


Figure 4.7: Solution (left) and entropy evolution (right) for Burgers' equation using P^1 and entropy based viscosity.

The effect of artificial viscosity is quite visible: the solution is smoothed at the discontinuity. The solutions obtained with artificial viscosity are therefore slightly worse than the original one. Again, this is specific to this situation and the advantage of artificial viscosity will become clearer in following tests. It is interesting to see that DB viscosity term dissipates entropy from the beginning of the simulation where the evolution of the entropy with EB viscosity is similar to the one without artificial viscosity. This is because EB viscosity increases only when entropy gets dissipated.

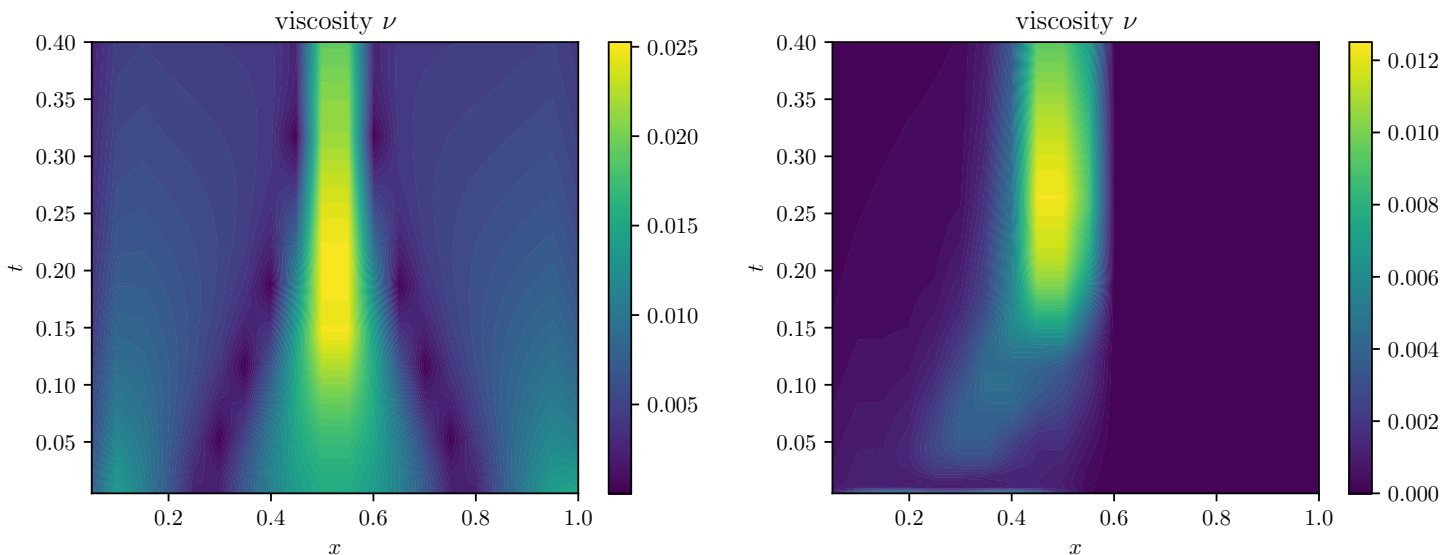


Figure 4.8: Dilation based (left) and entropy based (right) viscosity for Burgers' equation using P^1 elements.

Chapter 4. Numerical results and discussions

The artificial viscosity behaves as expected. Indeed, the solution is initially smooth until $t \sim 0.15$, where a shock forms. The dilation based viscosity seems to be less refined than the entropy based one. Indeed, even a slightly high derivative (not a shock) is enough to increase the DB viscosity. The magnitude of EB viscosity is also significantly lower. Interestingly, EB viscosity has a slight asymmetry whereas DB viscosity is almost perfectly symmetric.

P^2 elements The results obtained without artificial viscosity, with dilation based and with entropy based viscosity for P^2 elements are shown in Figure 4.9, Figure 4.10 and Figure 4.11 respectively. The evolution of both artificial viscosities is plotted in Figure 4.12.

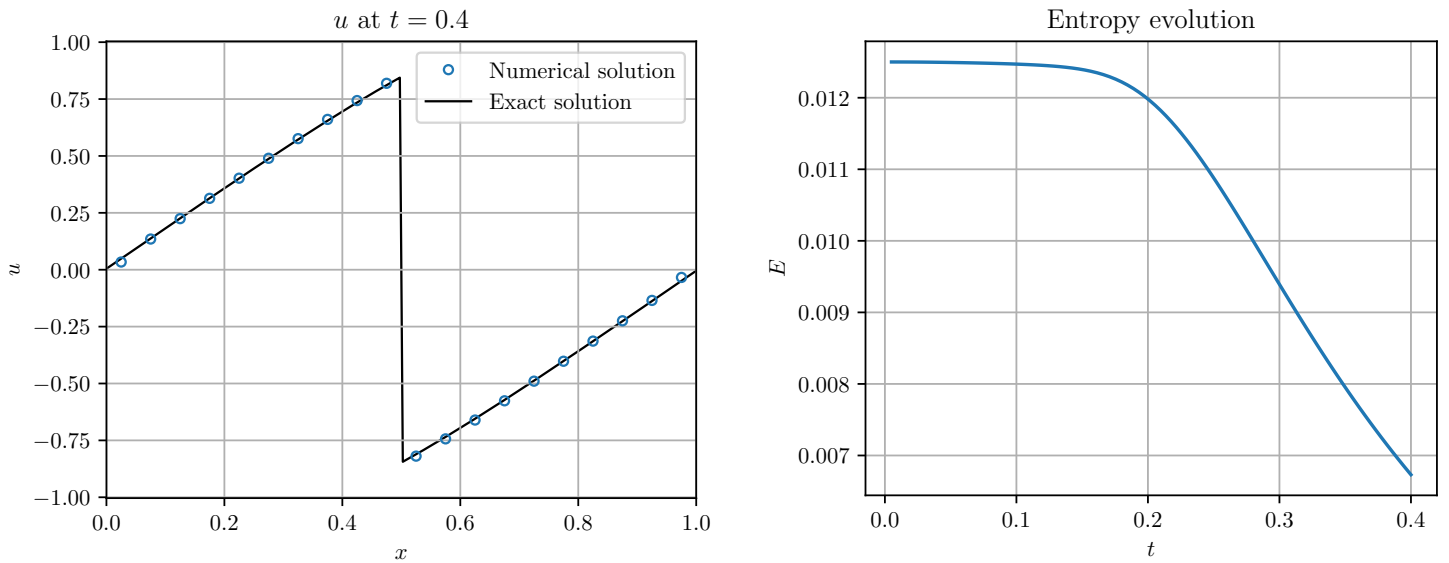


Figure 4.9: Solution (left) and entropy evolution (right) for Burgers' equation using P^2 and no artificial viscosity.

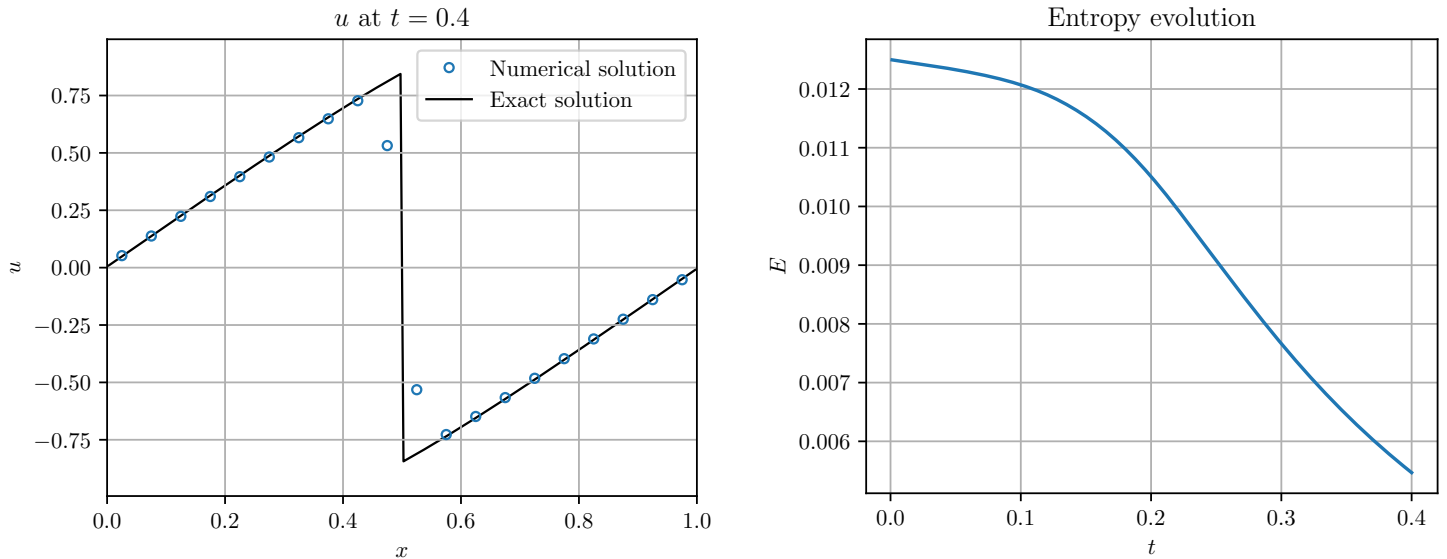


Figure 4.10: Solution (left) and entropy evolution (right) for Burgers' equation using P^2 and dilation based viscosity.

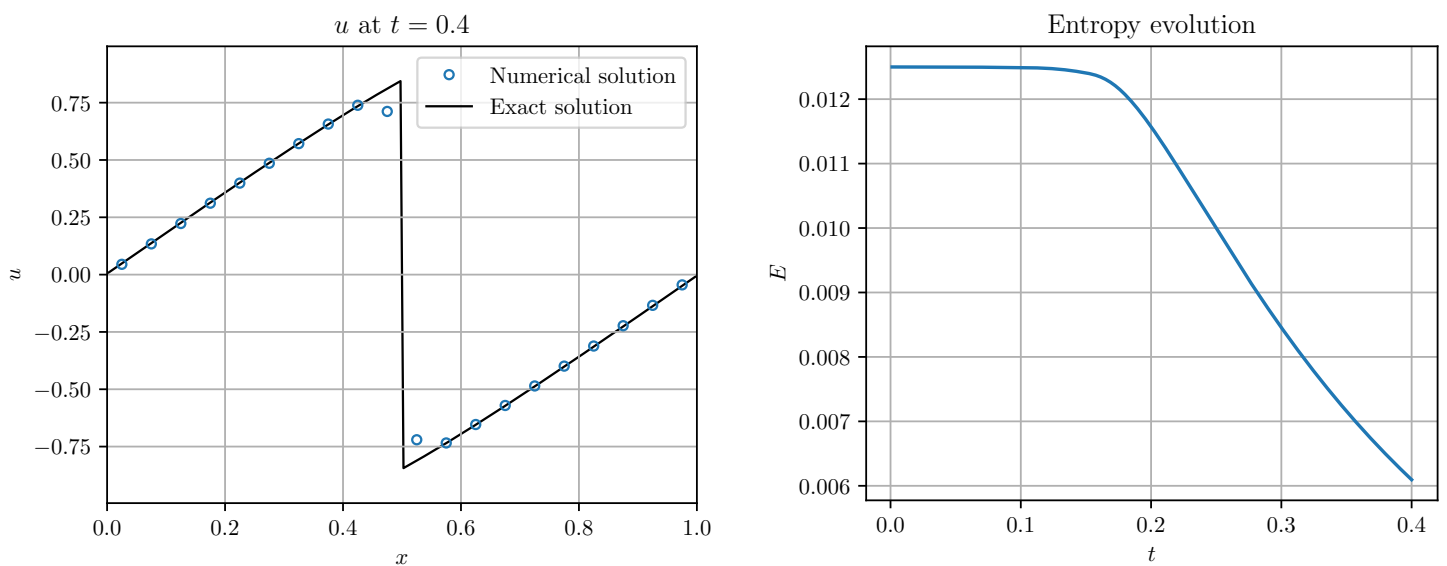


Figure 4.11: Solution (left) and entropy evolution (right) for Burgers' equation using P^2 and entropy based viscosity.

Chapter 4. Numerical results and discussions

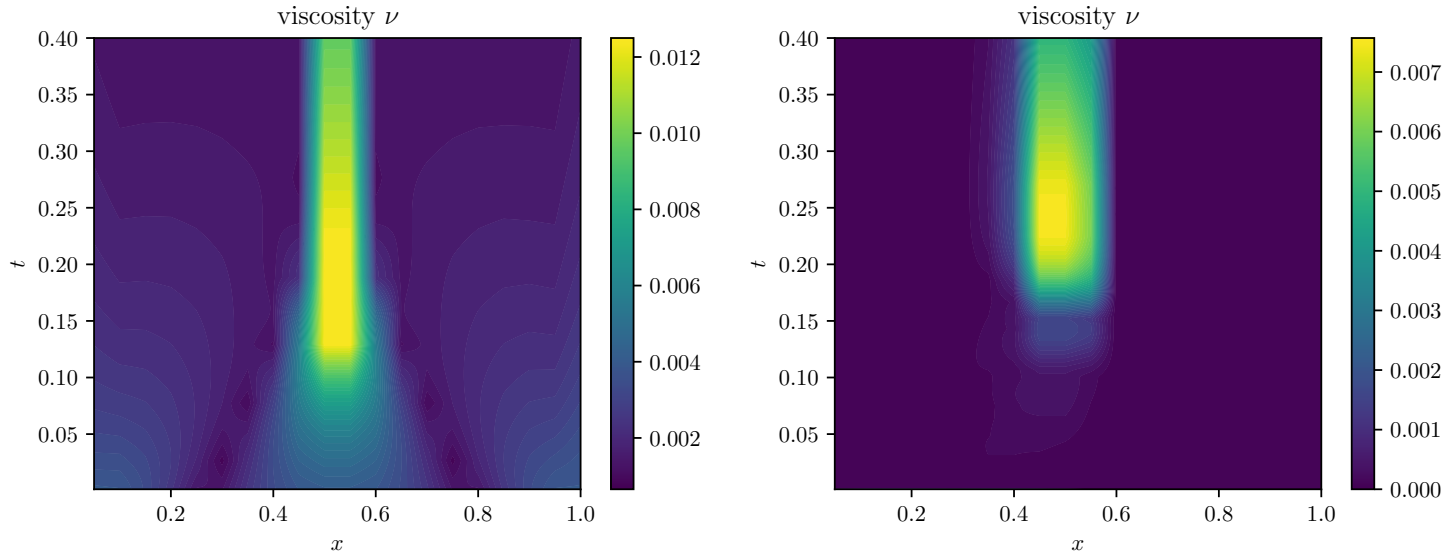


Figure 4.12: Dilation based (left) and entropy based (right) viscosity for Burger's equation using P^2 elements.

The results are very similar to the ones obtained with P^1 elements. Higher order elements seem to make both viscosity models slightly finer.

P^4 elements The results obtained without artificial viscosity, with dilation based and with entropy based viscosity for P^4 elements are shown in Figure 4.13, Figure 4.14 and Figure 4.15 respectively. The evolution of both artificial viscosities is plotted in Figure 4.16.

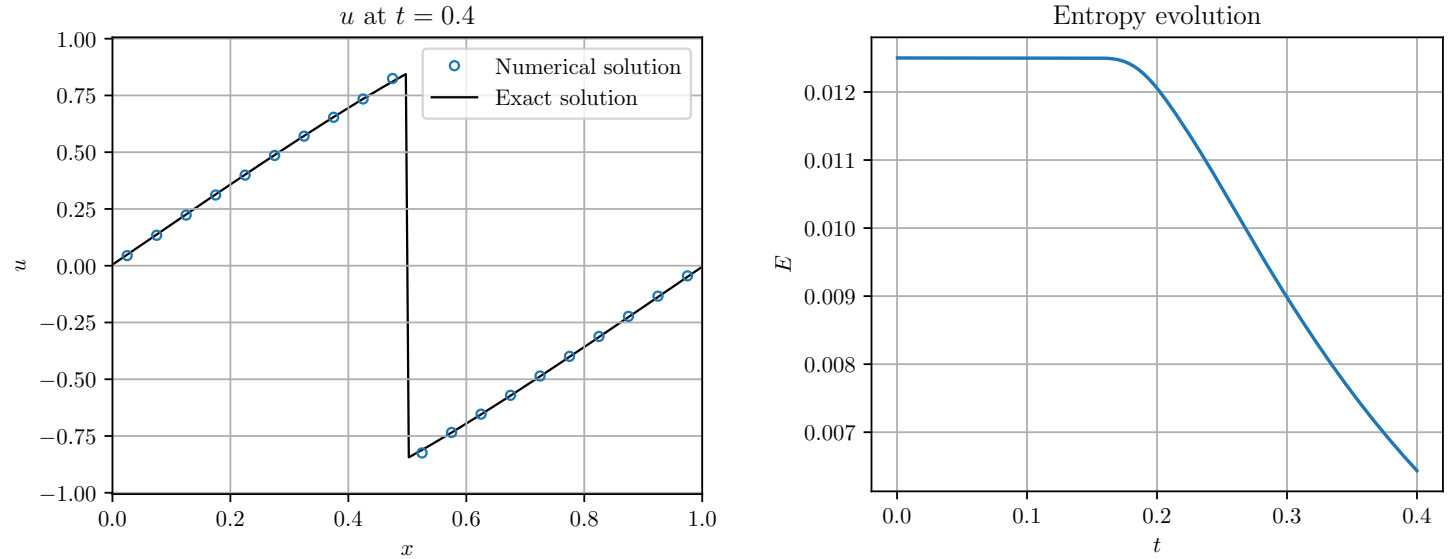


Figure 4.13: Solution (left) and entropy evolution (right) for Burgers' equation using P^4 and no artificial viscosity.

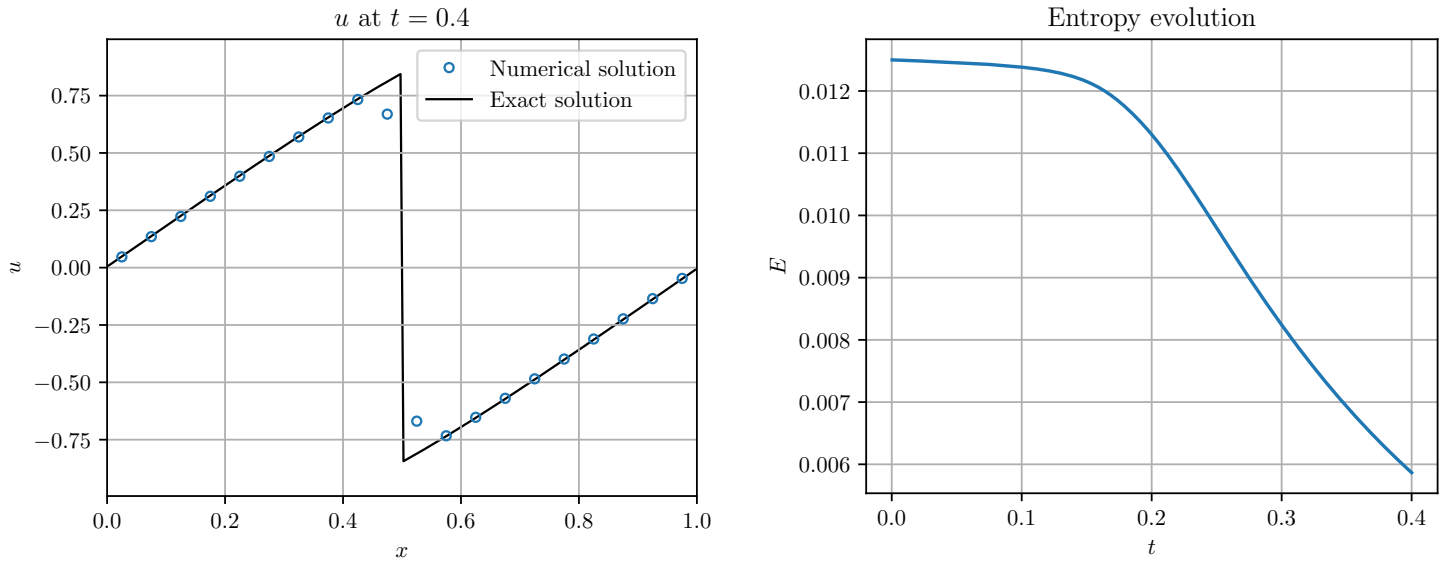


Figure 4.14: Solution (left) and entropy evolution (right) for Burgers' equation using P^4 and dilation based viscosity.

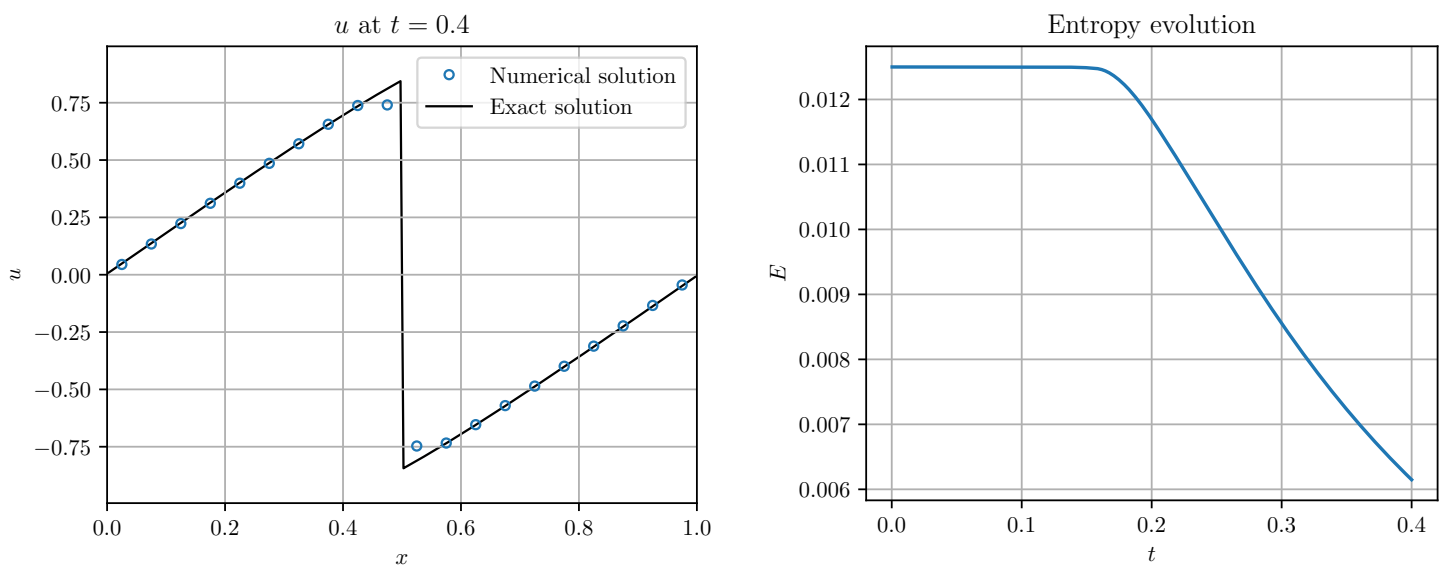


Figure 4.15: Solution (left) and entropy evolution (right) for Burgers' equation using P^4 and entropy based viscosity.

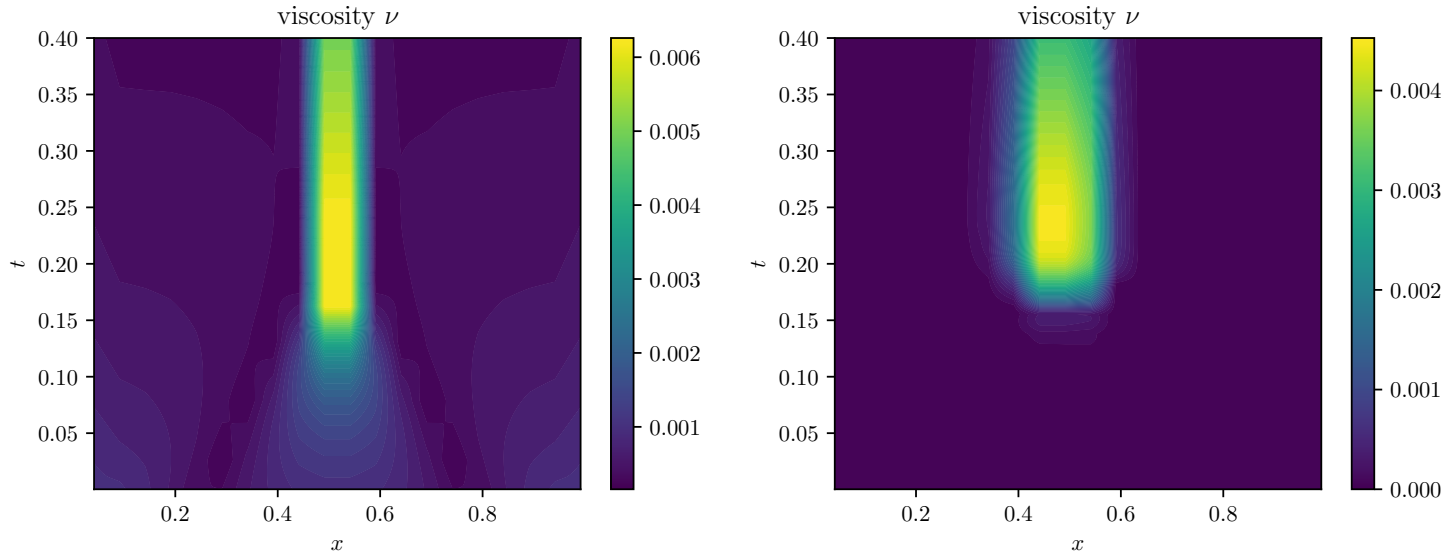


Figure 4.16: Dilation based (left) and entropy based (right) viscosity for Burger's equation using P^4 elements.

Again, the results are similar and the two viscosity models are even more refined, confirming the trend observed before. Higher order elements also seem to better conserve entropy when the solution is still smooth.

4.3 1D Euler equations

The scheme is now tested on the Euler equations, which is commonly used in the gas dynamics.

4.3.1 Sod's shock tube

The Sod shock tube is a typical test for shock capturing schemes. The initial condition is described by a left and a right state: $(\rho_L, P_L, v_L) = (1.0, 1.0, 0.0)$ and $(\rho_R, P_R, v_R) = (0.125, 0.1, 0.0)$. The reference solution is computed with a 5th-order entropy stable finite difference WENO scheme. The solutions are computed with $N = 70$ cells and compared with the reference solution at the final time $t_{fin} = 0.2$. The CFL number is fixed at $CFL = 0.1$ for all tests.

P^1 elements The results obtained without viscosity, with DB viscosity and with EB viscosity for P^1 elements are shown in Figure 4.17, Figure 4.18 and Figure 4.19 respectively. The evolution of the DB and EB viscosities can be seen in Figure 4.20.

4.3 1D Euler equations

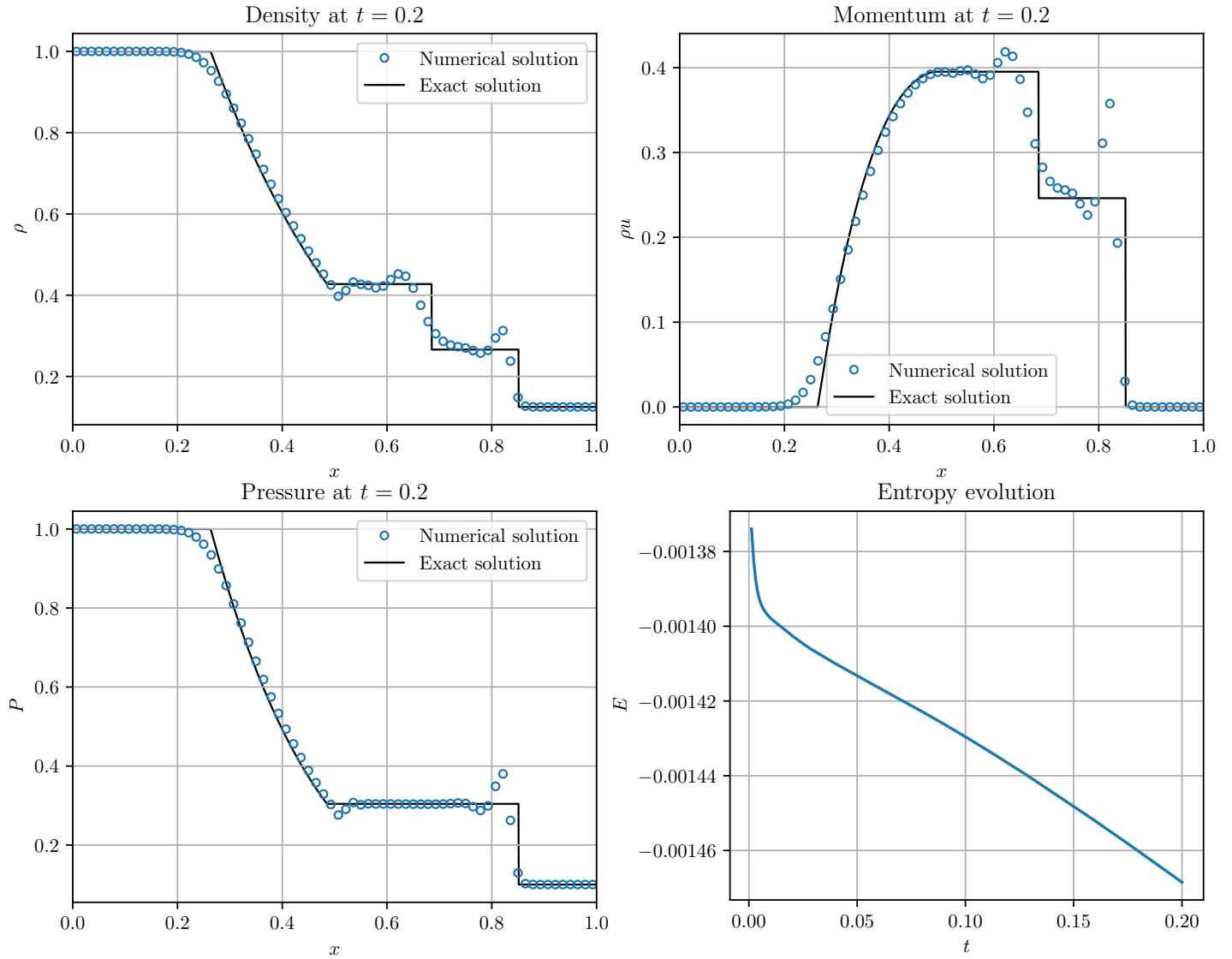


Figure 4.17: Solutions of ρ , ρu , P and entropy evolution for Euler equations using P^1 elements and no viscosity.

Chapter 4. Numerical results and discussions

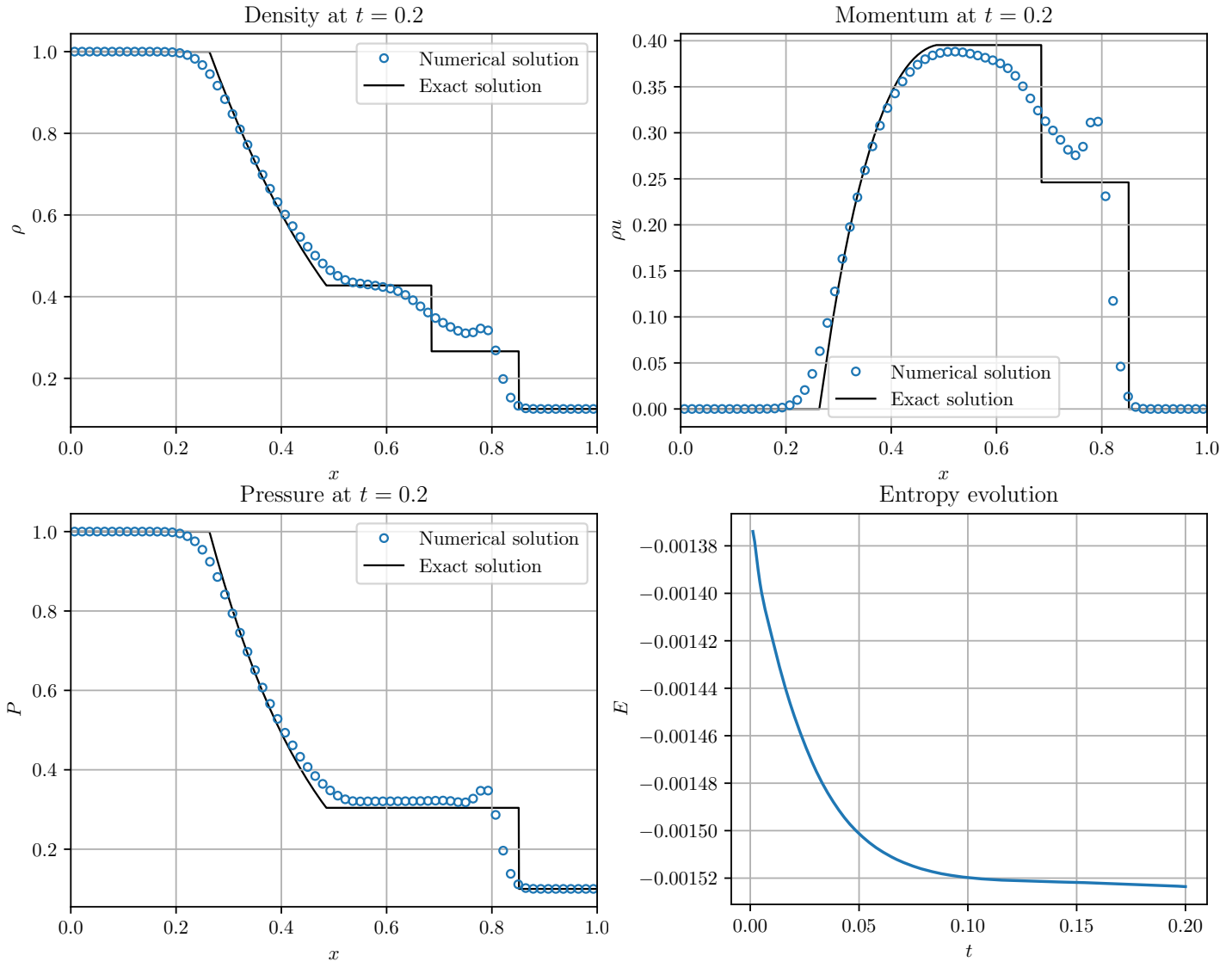


Figure 4.18: Solutions of ρ , ρu , P and entropy evolution for Euler equations using P^1 elements and with DB viscosity.

4.3 1D Euler equations

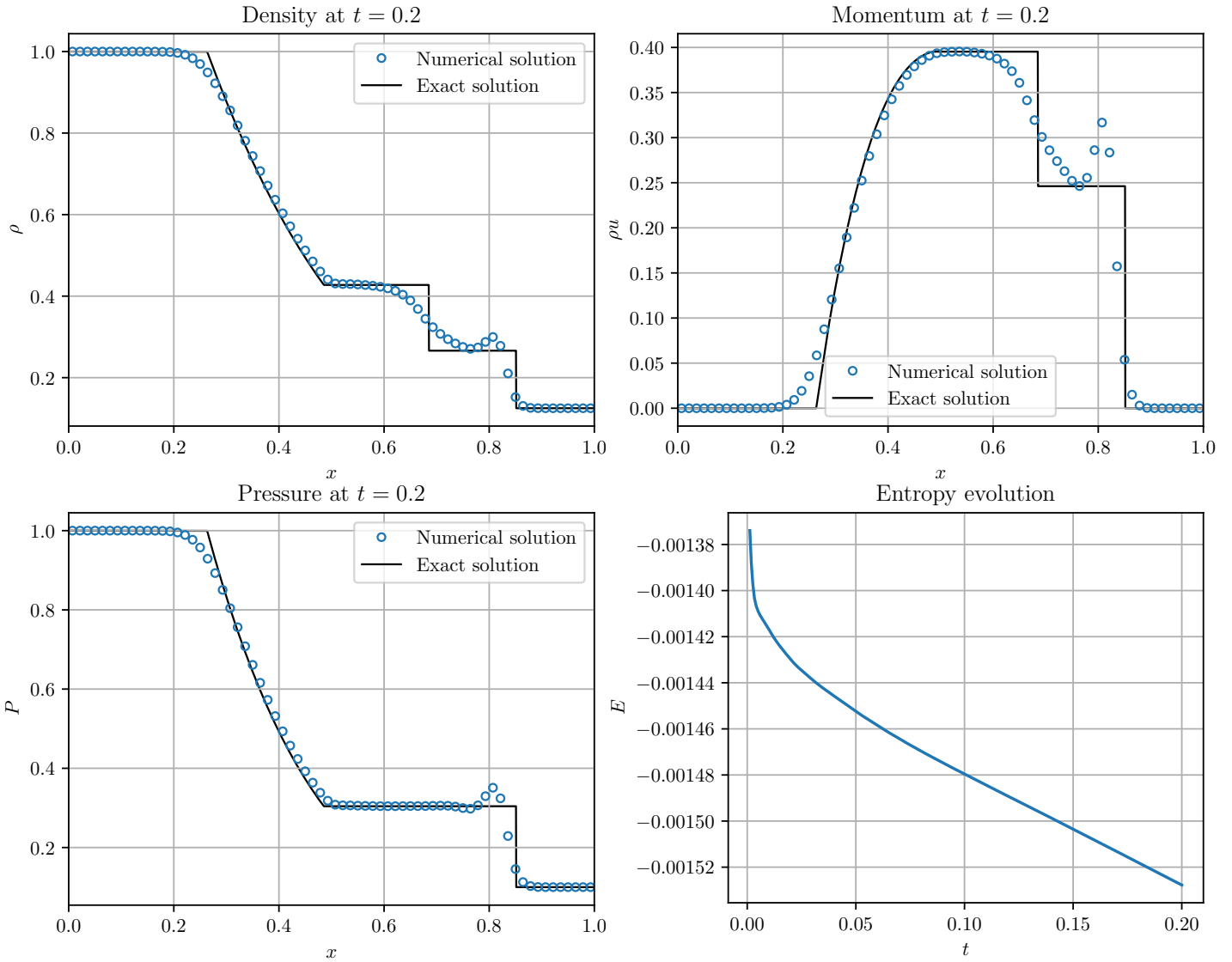


Figure 4.19: Solutions of ρ , ρu , P and entropy evolution for Euler equations using P^1 elements and EB viscosity.

The P^1 elements show a clear limitation in precision. Indeed, the difference between the reference and the computed solutions is relatively high, in particular at discontinuities. Although one should consider the limited amount of cells used in this example. Increasing the number of cell would certainly improve the results. The DB viscosity smoothes the solution more than the EB one, although this could be tuned with the parameters c and c_{\max} . This also leads to smaller overshoots for the DB model.

Chapter 4. Numerical results and discussions

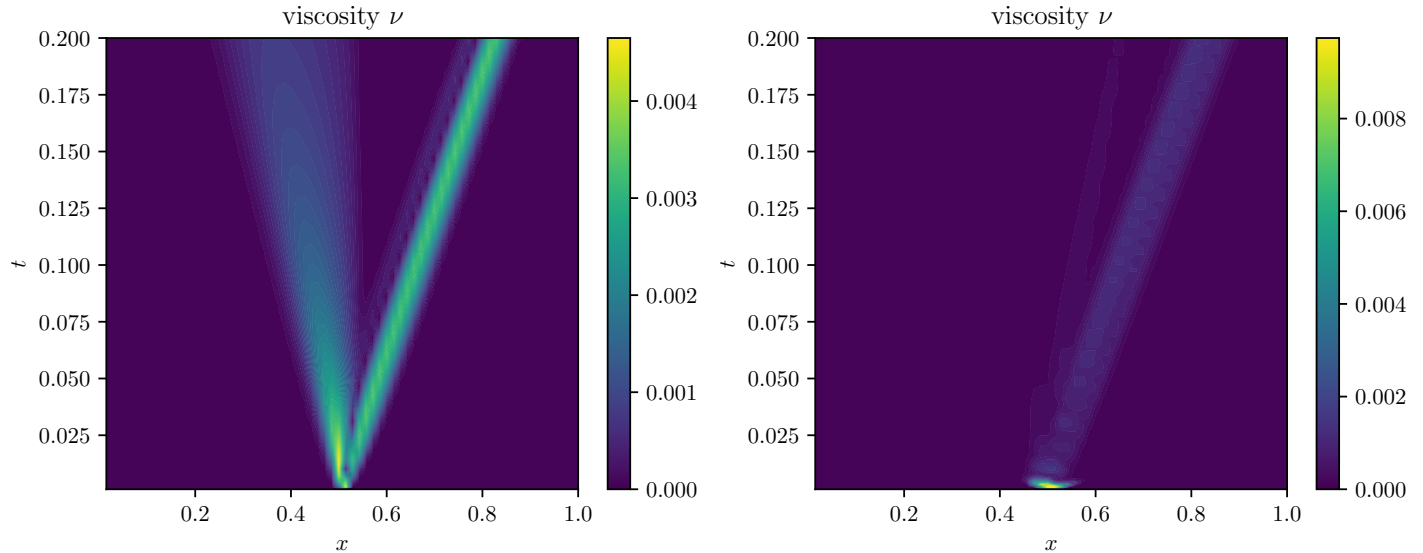


Figure 4.20: DB (left) and EB (right) viscosity for Sod's test using P^1 elements.

Both viscosity models show the expected behavior. Indeed, the viscosity appears at the beginning of the simulation since a shock is present in the initial condition. The viscosity then "follows" the shock moving to the right. The EB model produces a very high viscosity followed quickly by a drastic decrease. This effect is reflected in the entropy evolution graph in Figure 4.19. Indeed, the entropy drops very quickly at the beginning and then slowly tends to a slower steady decline. The maximal value is about two times higher for the EB viscosity.

P^2 elements The results obtained without viscosity, with DB viscosity and with EB viscosity for P^2 elements are shown in Figure 4.21, Figure 4.22 and Figure 4.23 respectively. The evolution of the DB and EB viscosities can be seen in Figure 4.24.

4.3 1D Euler equations

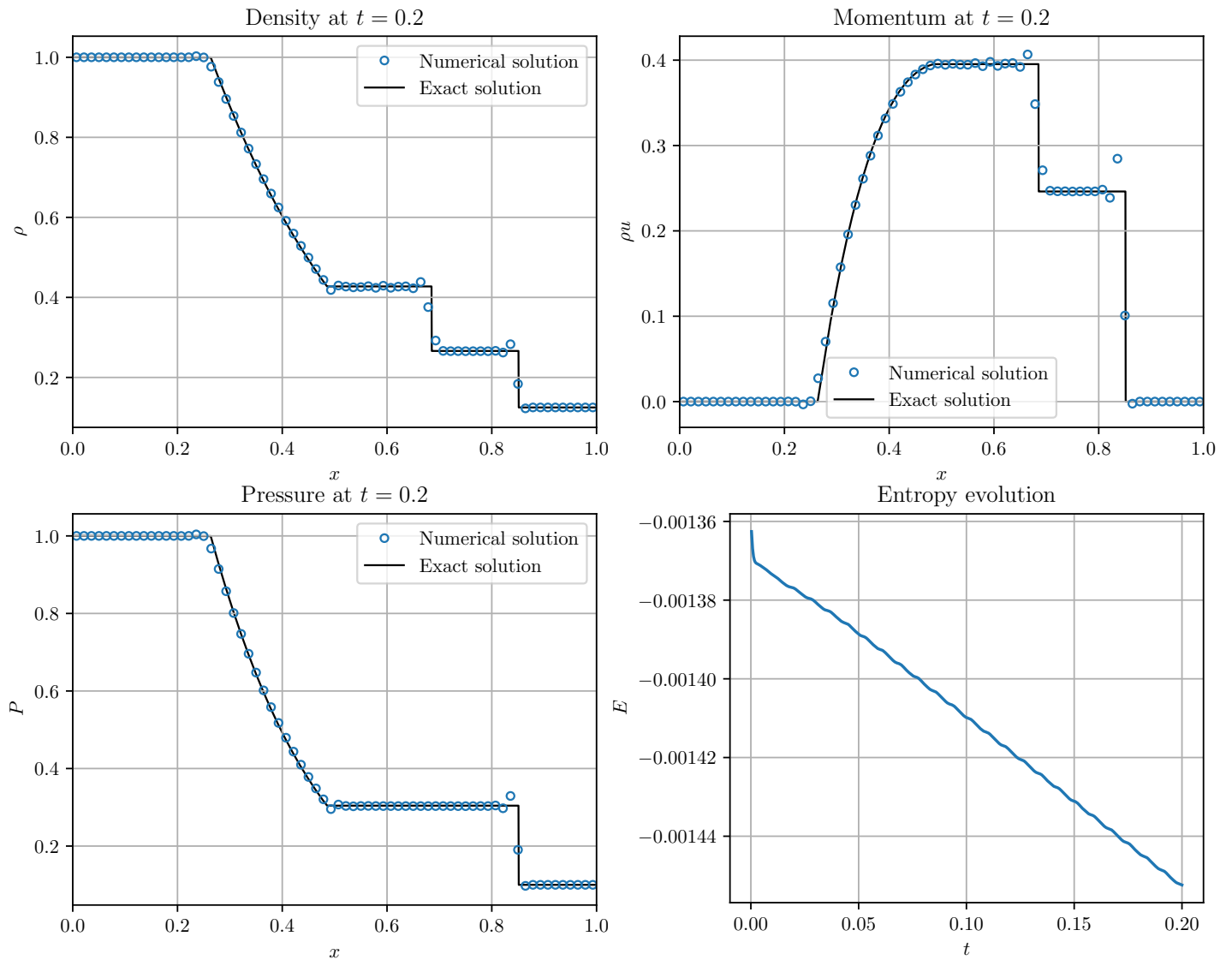


Figure 4.21: Solutions of ρ , ρu , P and entropy evolution for Euler equations using P^2 elements and no viscosity.

Chapter 4. Numerical results and discussions

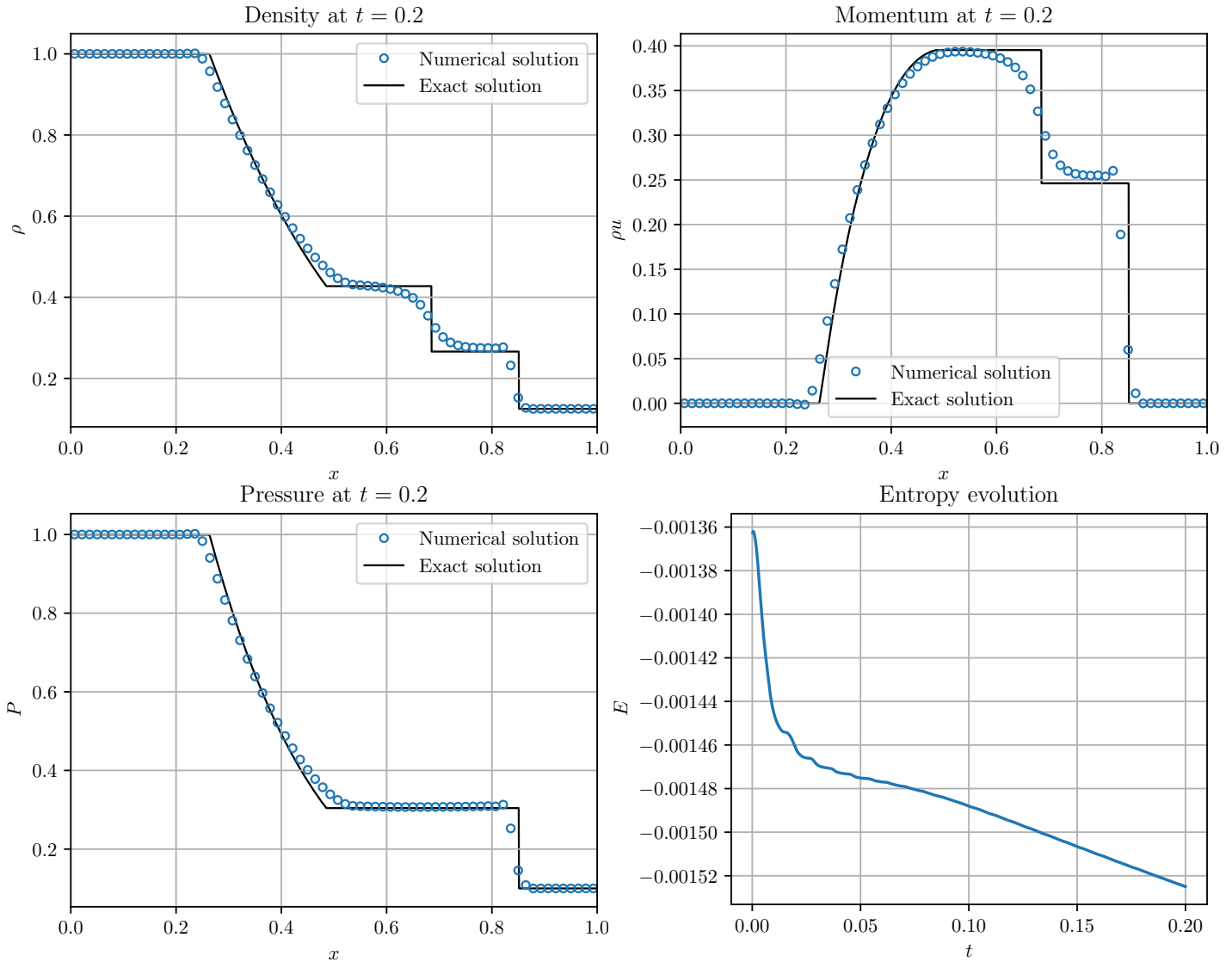


Figure 4.22: Solutions of ρ , ρu , P and entropy evolution for Euler equations using P^2 elements and with DB viscosity.

4.3 1D Euler equations

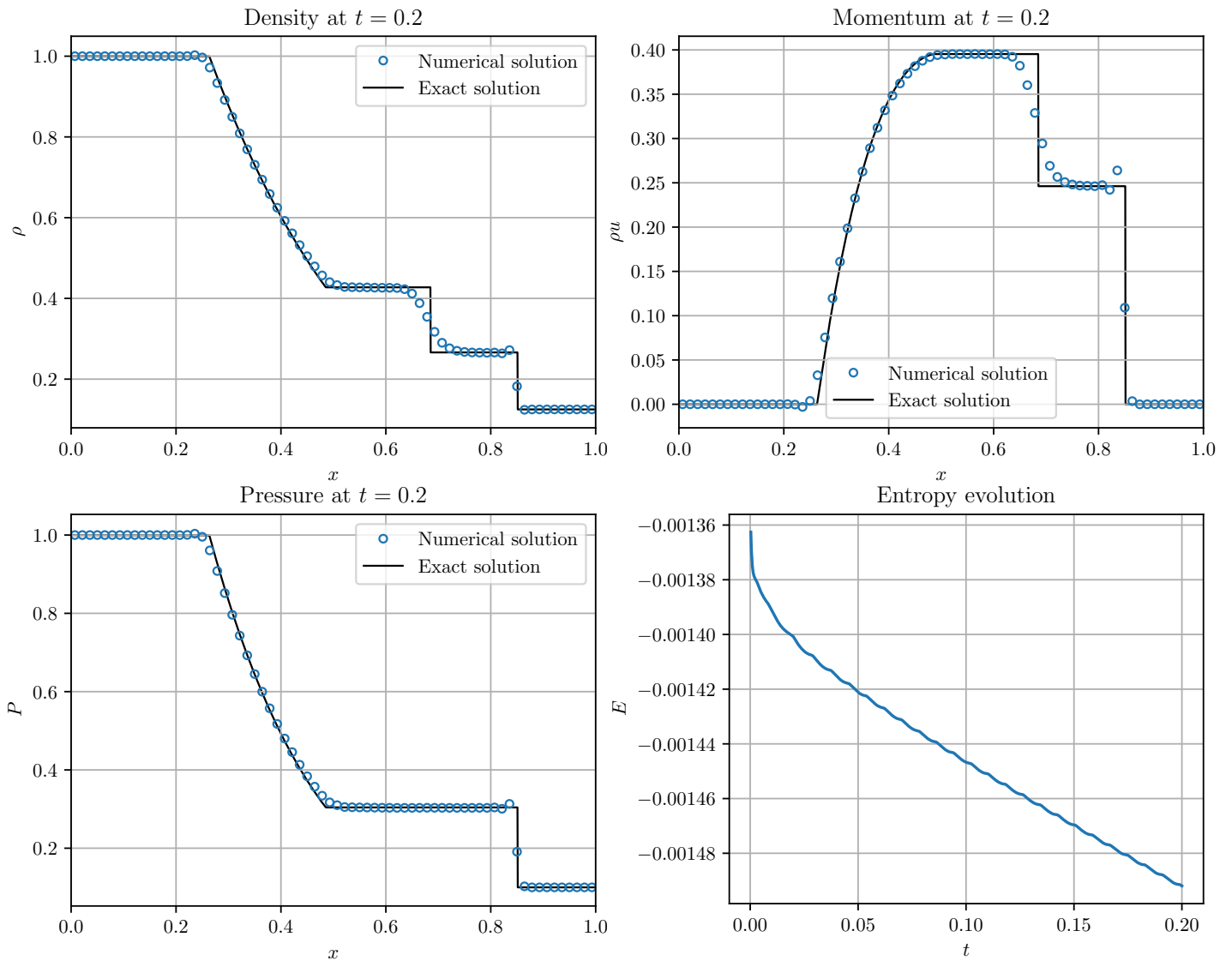


Figure 4.23: Solutions of ρ , ρu , P and entropy evolution for Euler equations using P^2 elements and EB viscosity.

Chapter 4. Numerical results and discussions

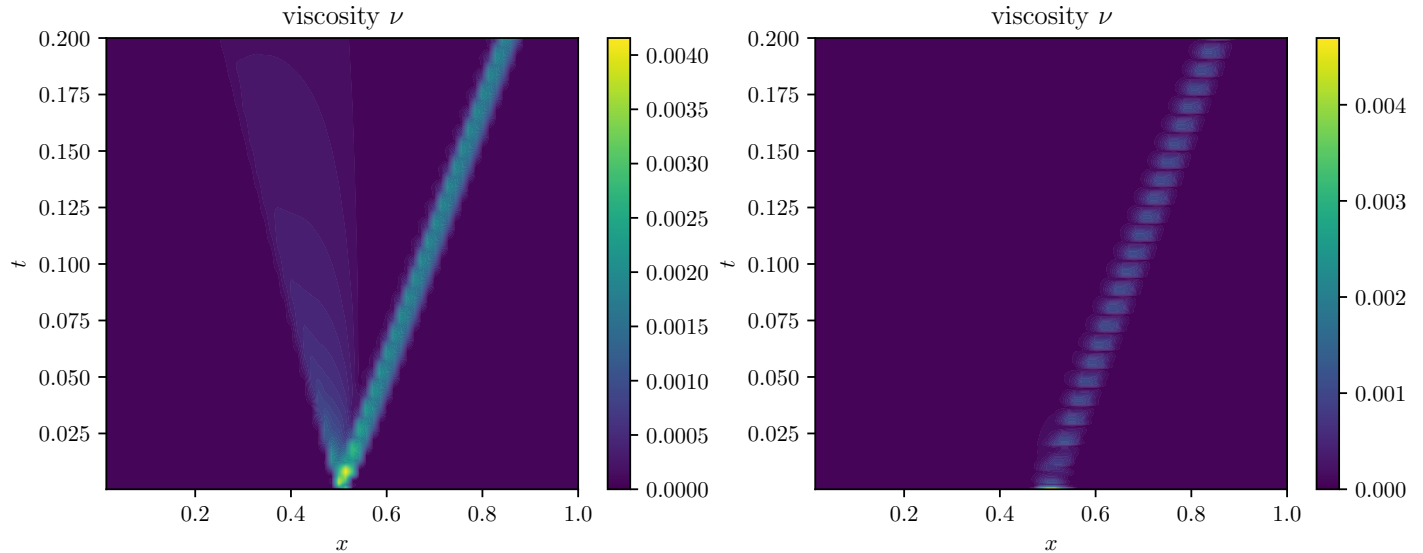


Figure 4.24: DB (left) and EB (right) viscosity for Sod's test using P^2 elements.

Using P^2 elements already lead to a great improvement in comparison to P^1 elements. The numerical solution is much closer to the reference one, although a slight overshoot is still presented at the shocks. Higher order schemes seem to reduce entropy dissipation. The artificial viscosity reduce the overshoot significantly which is the desired behavior. As expected shocks are also smoothed by the viscosity term. The EV viscosity seems to have less impact on the solutions than the DB one, though this could be tweaked with the coefficients c and c_{\max} .

Again, both viscosity models are able to follow the moving shock. This time, the scale is comparable between the two models.

P^4 elements The results obtained without viscosity, with DB viscosity and with EB viscosity for P^4 elements are shown in Figure 4.25, Figure 4.26 and Figure 4.27 respectively. The evolution of the DB and EB viscosities can be seen in Figure 4.28.

4.3 1D Euler equations

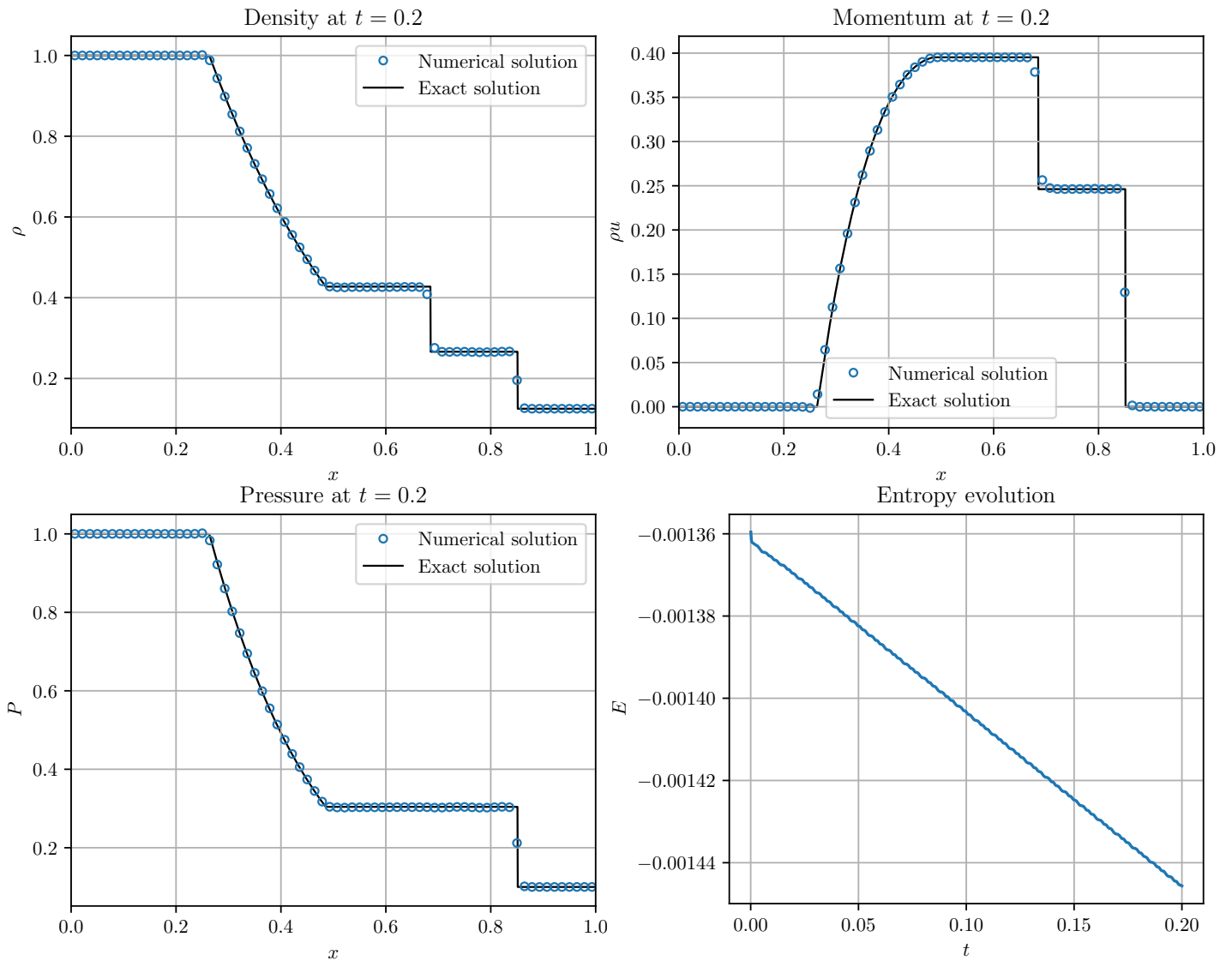


Figure 4.25: Solutions of ρ , ρu , P and entropy evolution for Euler equations using P^4 elements and no viscosity.

Chapter 4. Numerical results and discussions

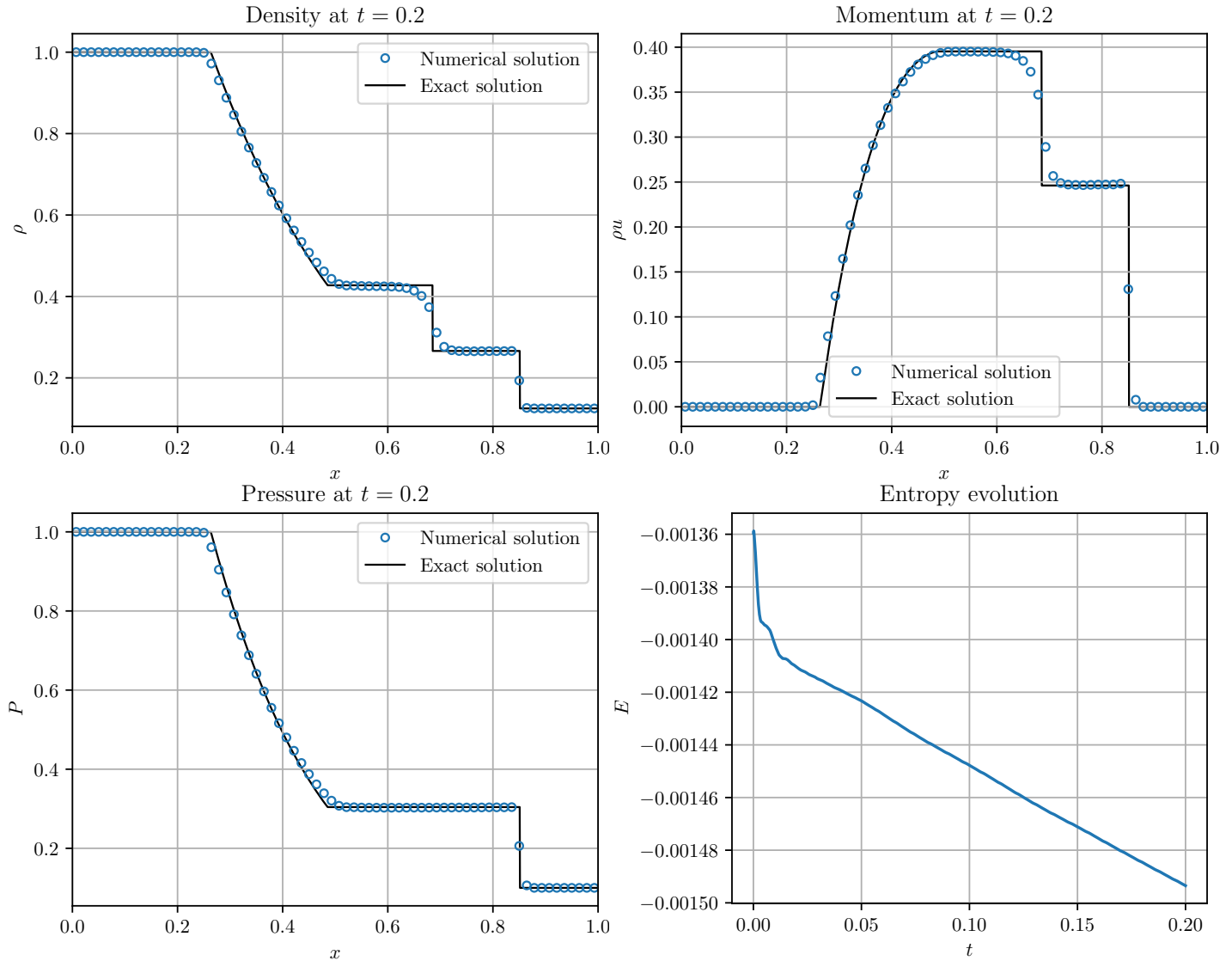


Figure 4.26: Solutions of ρ , ρu , P and entropy evolution for Euler equations using P^4 elements and with DB viscosity.

4.3 1D Euler equations

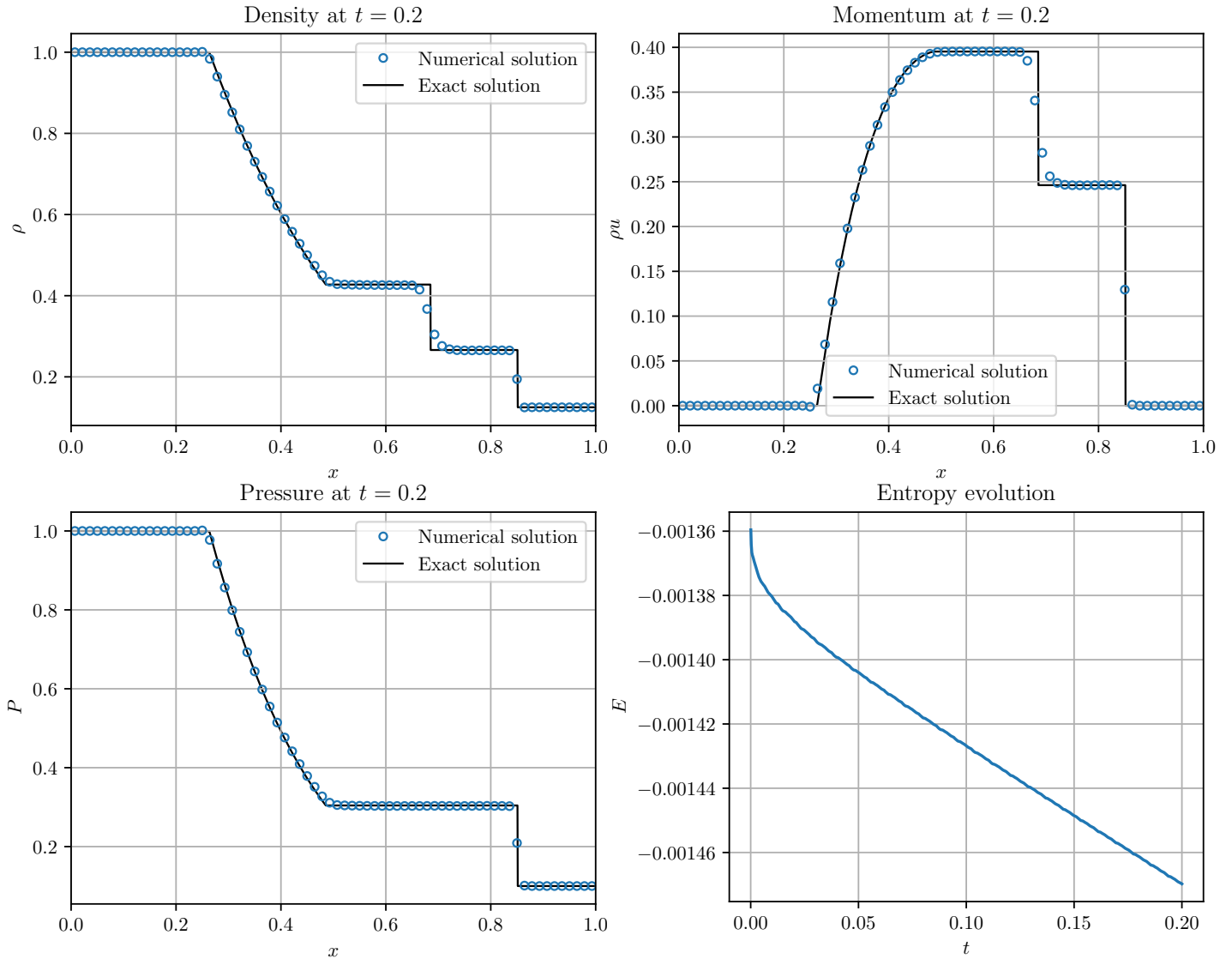
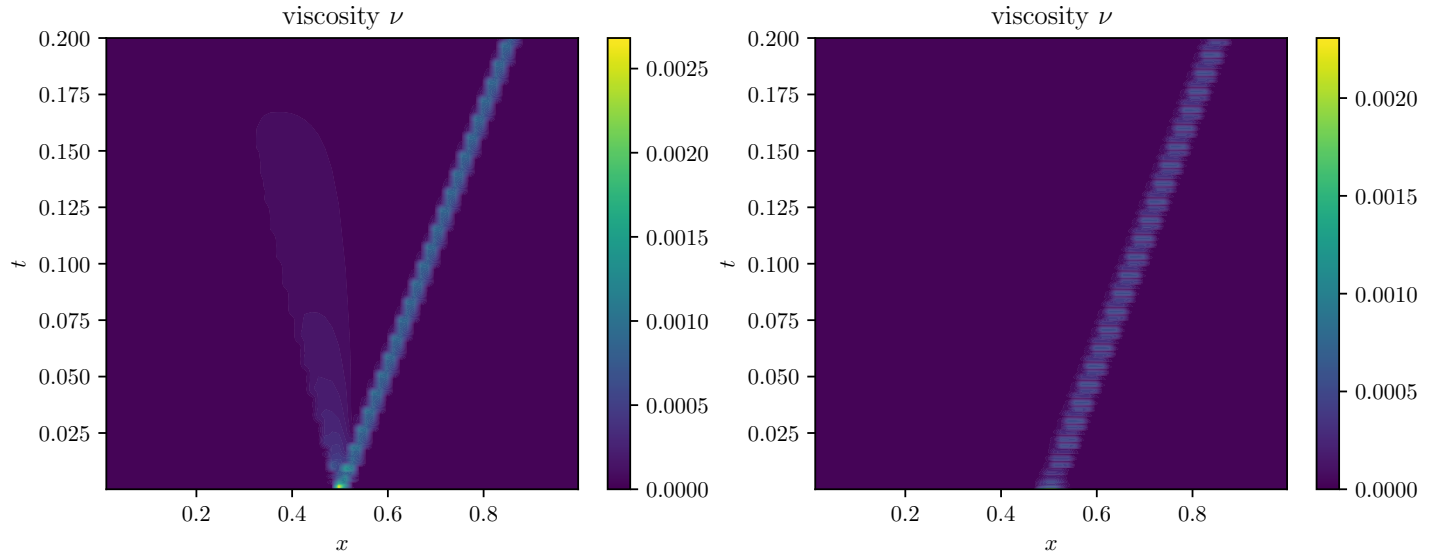


Figure 4.27: Solutions of ρ , ρu , P and entropy evolution for Euler equations using P^4 elements and EB viscosity.


 Figure 4.28: DB (left) and EB (right) viscosity for Sod's test using P^4 elements.

Without viscosity, P^4 elements give a solution that is essentially indistinguishable from the reference one, even with the limited number of cell. This means that modifying the scheme with artificial viscosity could worsen the solution, unless the viscosity term is really low. Indeed, Figure 4.26 and Figure 4.27 show that the shocks are slightly smoothed and the solution is not as good, though the difference is quite low.

Again, both viscosity models are able to follow the moving shock. The scale is about two times lower than with P^2 elements, for both models.

4.4 2D Euler equations

4.4.1 Isentropic vortex convection

The smooth isentropic vortex convection test allows to verify the convergence of the 2D scheme using Euler equations. The initial condition is given by

$$\begin{cases} \rho = T^{\frac{1}{\gamma-1}}, & P = \rho^\gamma \\ v_1 = 1 - \frac{5}{2\pi} \exp\left(\frac{1-r^2}{2}\right)(y - y_0), & v_2 = 1 + \frac{5}{2\pi} \exp\left(\frac{1-r^2}{2}\right)(x - x_0) \\ T = 1 - \frac{25(\gamma-1)}{8\gamma\pi^2} \exp(1-r^2), & r = \sqrt{(x-x_0)^2 + (y-y_0)^2} \end{cases} \quad (4.2)$$

where $(x_0, y_0) = (-5, -5)$. The domain is $[-10, 10]^2$ and the final time is $t = 10$. The solution at the final time is given by Equation (4.2) with $(x_0, y_0) = (5, 5)$. The initial condition and the final value of the density are shown in Figure 4.29.

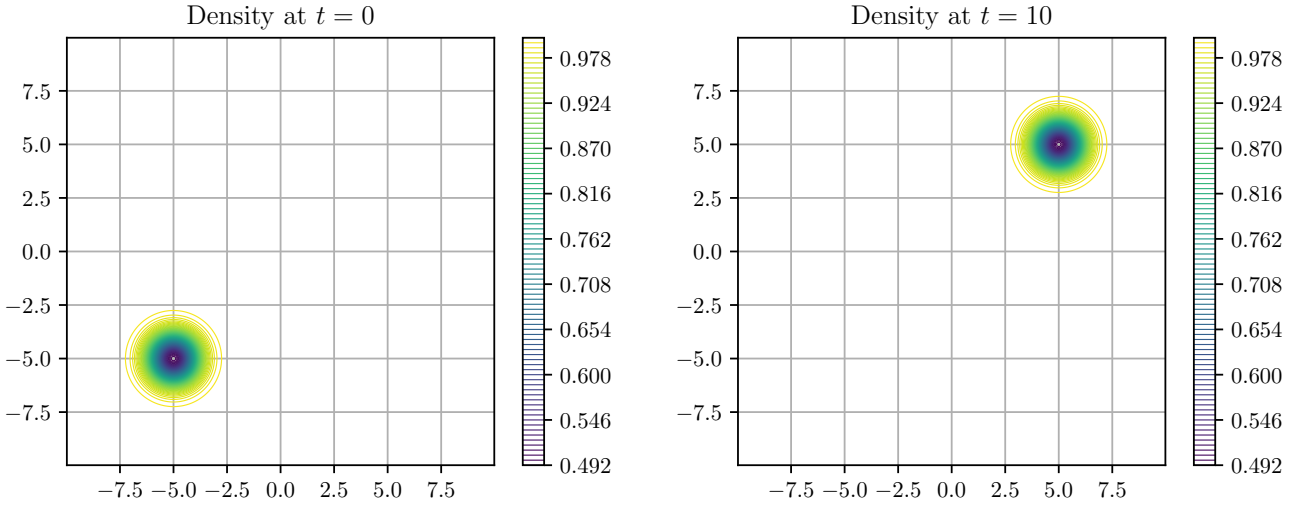


Figure 4.29: Density at the initial (left) and final (right) time for the isentropic vortex test.

The error ϵ is computed on the density only using the following three norms:

- $L^1 : \epsilon = \frac{\Delta x \Delta y}{(k+1)^2} \left(\sum_{i=1}^{N_x} \sum_{j=1}^{N_y} \sum_{l=0}^k \sum_{m=0}^k |\rho_{i,j}^{l,m} - \rho(x_{i,j}^{l,m})| \right)$
- $L^2 : \epsilon = \left(\frac{\Delta x \Delta y}{(k+1)^2} \sum_{i=1}^{N_x} \sum_{j=1}^{N_y} \sum_{l=0}^k \sum_{m=0}^k (\rho_{i,j}^{l,m} - \rho(x_{i,j}^{l,m}))^2 \right)^{1/2}$
- $L^\infty : \epsilon = \max_{1 \leq i,j \leq N} \max_{0 \leq l,m \leq k} |\rho_{i,j}^{l,m} - \rho(x_{i,j}^{l,m})|$

P^1 elements The number of cell in both direction is equal ($N_x = N = N_y$) and varied between $N = 110$ and $N = 150$. The results are shown in Figure 4.30, Table 4.10 and Table 4.10. The time integration is of order 3, therefore $\Delta t = C(\Delta x)^{(k+1)/3}$, with $C = 0.05$.

N	L^1 error	order	L^2 error	order	L^∞ error	order
110	1.077e-03	-	5.915e-03	-	9.459e-02	-
120	9.121e-04	1.91	5.020e-03	1.89	7.940e-02	2.01
130	7.815e-04	1.93	4.307e-03	1.92	6.796e-02	1.94
140	6.767e-04	1.94	3.731e-03	1.94	5.834e-02	2.06
150	5.914e-04	1.95	3.260e-03	1.95	5.071e-02	2.03

 Table 4.10: Convergence test on the isentropic vortex for P^1 elements, without artificial viscosity.

Chapter 4. Numerical results and discussions

N	L^1 error	order	L^2 error	order	L^∞ error	order
110	1.988e-03	-	6.763e-03	-	1.247e-01	-
120	1.646e-03	2.17	5.736e-03	1.89	1.06e-01	1.87
130	1.38e-03	2.20	4.905e-03	1.96	9.123e-02	1.87
140	1.169e-03	2.24	4.224e-03	2.02	7.968e-02	1.83
150	1.000e-03	2.26	3.664e-03	2.06	6.935e-02	2.01

Table 4.11: Convergence test on the isentropic vortex for P^1 elements, with dilation based viscosity.

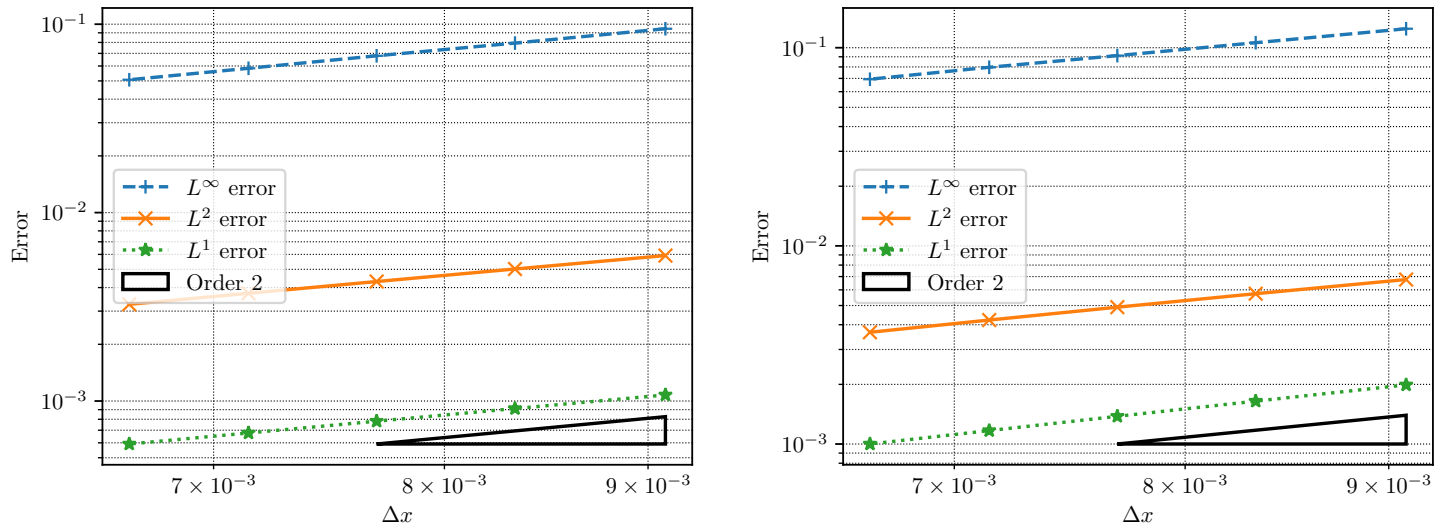


Figure 4.30: Convergence test on the isentropic vortex for P^1 elements. Left: without artificial viscosity. Right: with dilation based viscosity.

The 2D scheme converges with the expected rate both without and with dilation based viscosity. Note that the absolute errors are higher with artificial viscosity. This is because the solution is smooth which means artificial viscosity is unnecessarily added, leading to slightly worse solution.

P^2 elements The number of cell in both direction is equal ($N_x = N = N_y$) and varied between $N = 30$ and $N = 70$. The results are shown in Figure 4.31, Table 4.12 and Table 4.12. Again, the time integration is of order 3, therefore $\Delta t = C(\Delta x)^{(k+1)/3}$, with $C = 0.05$.

N	L^1 error	order	L^2 error	order	L^∞ error	order
30	5.709e-04	-	1.804e-03	-	2.95e-02	-
40	2.273e-04	3.20	7.36e-04	3.12	1.327e-02	2.78
50	1.087e-04	3.31	3.671e-04	3.12	6.931e-03	2.91
60	6.157e-05	3.12	2.137e-04	2.97	3.837e-03	3.24
70	3.861e-05	3.03	1.373e-04	2.87	2.330e-03	3.23

Table 4.12: Convergence test on the isentropic vortex for P^2 elements, without artificial viscosity.

N	L^1 error	order	L^2 error	order	L^∞ error	order
30	2.425e-03	-	9.691e-03	-	1.71e-01	-
40	1.453e-03	1.78	5.122e-03	2.22	9.7e-02	1.97
50	7.424e-04	3.01	2.824e-03	2.67	5.708e-02	2.38
60	4.756e-04	2.44	1.646e-03	2.96	3.414e-02	2.82
70	3.011e-04	2.96	1.016e-03	3.13	2.074e-02	3.23

Table 4.13: Convergence test on the isentropic vortex for P^2 elements, with dilation based viscosity.

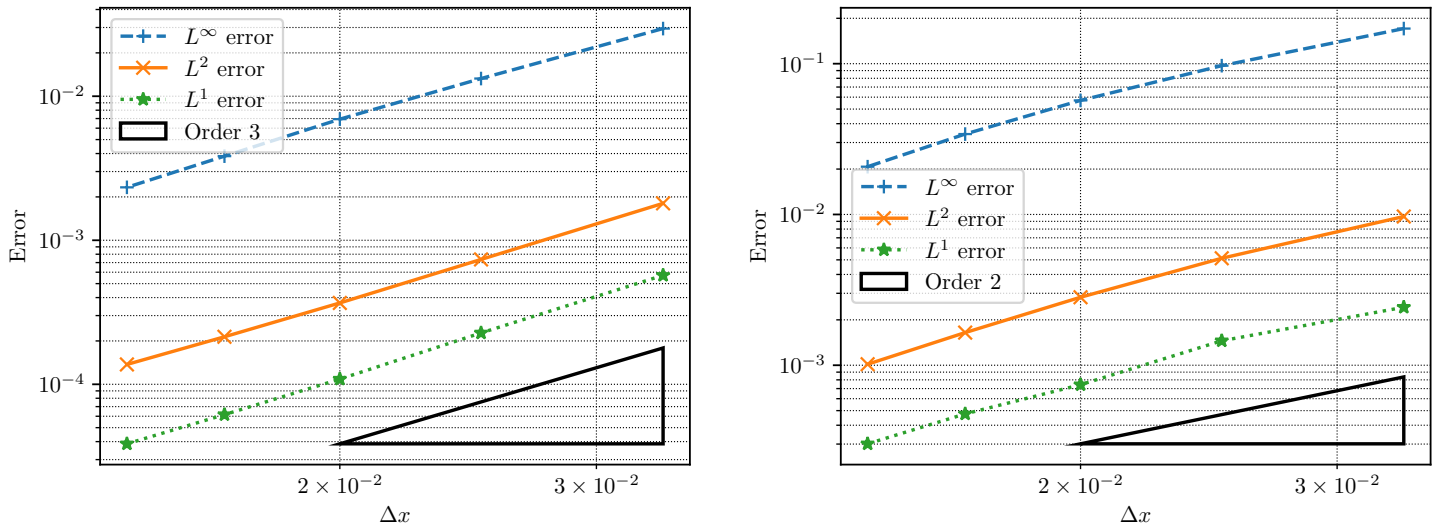


Figure 4.31: Convergence test on the isentropic vortex for P^2 elements. Left: without artificial viscosity. Right: with dilation based viscosity.

Again, the scheme converges as expected. Interestingly, the convergence rate is 3 with the DB viscosity, even though it should be limited to 2. This is probably due to the fact that the speed is essentially constant. The term $|\nabla \cdot \mathbf{s}|$ is therefore almost 0 and the viscosity is consequently also 0.

Chapter 4. Numerical results and discussions

P^4 elements The number of cell in both direction is equal ($N_x = N = N_y$) and varied between $N = 10$ and $N = 50$. The results are shown in Figure 4.32, Table 4.14 and Table 4.14. Once again, the time integration is of order 3, therefore $\Delta t = C(\Delta x)^{(k+1)/3}$, with $C = 0.05$.

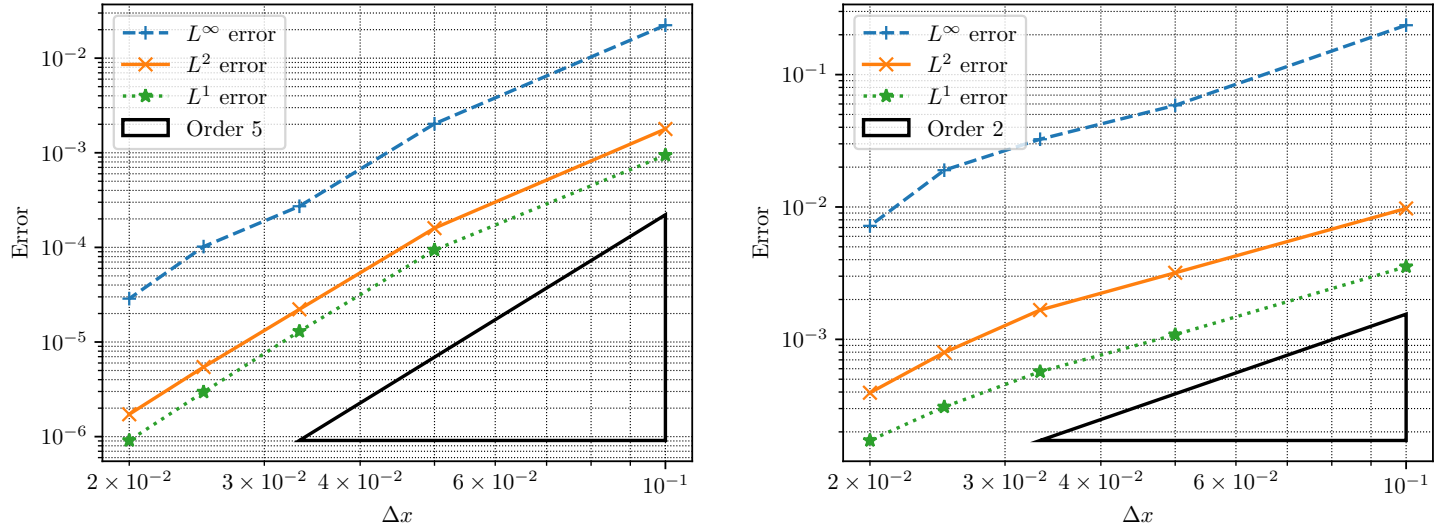


Figure 4.32: Convergence test on the isentropic vortex for P^4 elements. Left: without artificial viscosity. Right: with dilation based viscosity.

N	L^1 error	order	L^2 error	order	L^∞ error	order
10	9.418e-04	-	1.782e-03	-	2.229e-02	-
20	9.376e-05	3.33	1.597e-04	3.48	2.024e-03	3.46
30	1.296e-05	4.88	2.215e-05	4.87	2.721e-04	4.95
40	2.959e-06	5.13	5.436e-06	4.88	1.02e-04	3.41
50	9.105e-07	5.28	1.722e-06	5.15	2.872e-05	5.68

Table 4.14: Convergence test on the isentropic vortex for P^4 elements, without artificial viscosity.

N	L^1 error	order	L^2 error	order	L^∞ error	order
10	3.538e-03	-	9.748e-03	-	2.361e-01	-
20	1.084e-03	1.71	3.183e-03	1.61	5.858e-02	2.01
30	5.701e-04	1.58	1.666e-03	1.60	3.250e-02	1.45
40	3.088e-04	2.13	7.956e-04	2.57	1.897e-02	1.87
50	1.722e-04	2.62	3.950e-04	3.14	7.202e-03	4.34

Table 4.15: Convergence test on the isentropic vortex for P^4 elements, with dilation based viscosity.

Without viscosity, the scheme converges as expected. This time the DB viscosity seems to limit the convergence as predicted.

4.4.2 2D Riemann problem 1

This problem is described by the following initial condition

$$(\rho, v_1, v_2, P) = \begin{cases} (1.0, 0.7276, 0.0, 1.0) & x < 0.5, y > 0.5 \\ (0.5313, 0.0, 0.0, 0.4) & x > 0.5, y > 0.5 \\ (0.8, 0.0, 0.0, 1.0) & x < 0.5, y < 0.5 \\ (1.0, 0.0, 0.7276, 1.0) & x > 0.5, y < 0.5 \end{cases} \quad (4.3)$$

on the domain $[0, 1]^2$ and with a final time of $t_{fin} = 0.25$. The number of cell in both direction is fixed to $N_x = 200 = N_y$ and the CFL number is set at $\text{CFL} = 0.25$ for all tests.

The results obtained without viscosity for both P^1 and P^2 elements are shown in Figure 4.33.

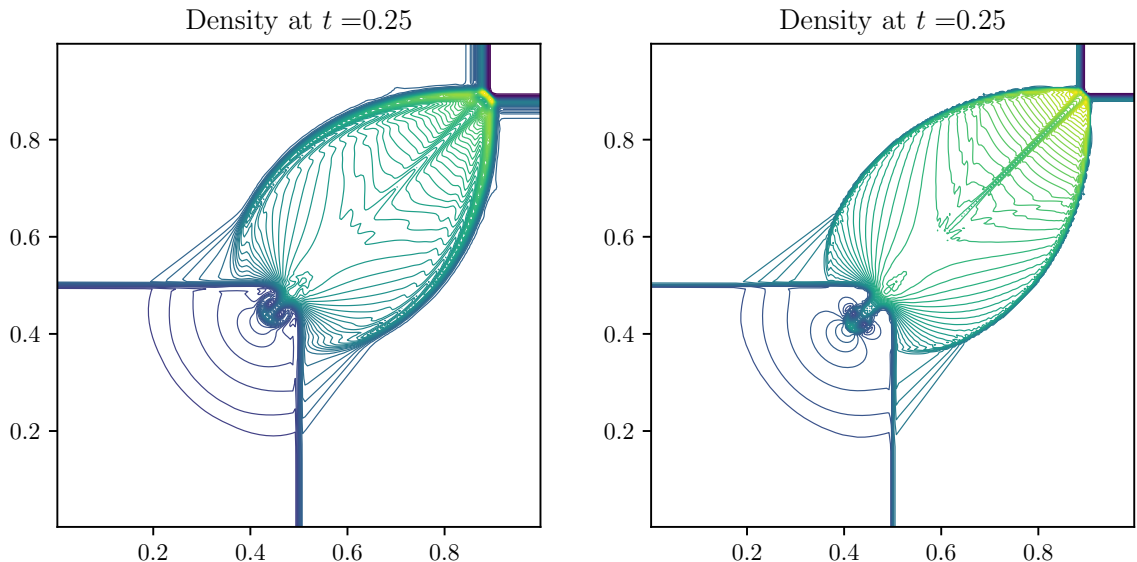


Figure 4.33: Results obtained without artificial viscosity, for P^1 (left) and P^2 (right) elements on the first 2D Riemann problem.

The results obtained with DB viscosity are shown in Figure 4.34 for P^1 elements and in Figure 4.35 for P^2 elements.

Chapter 4. Numerical results and discussions

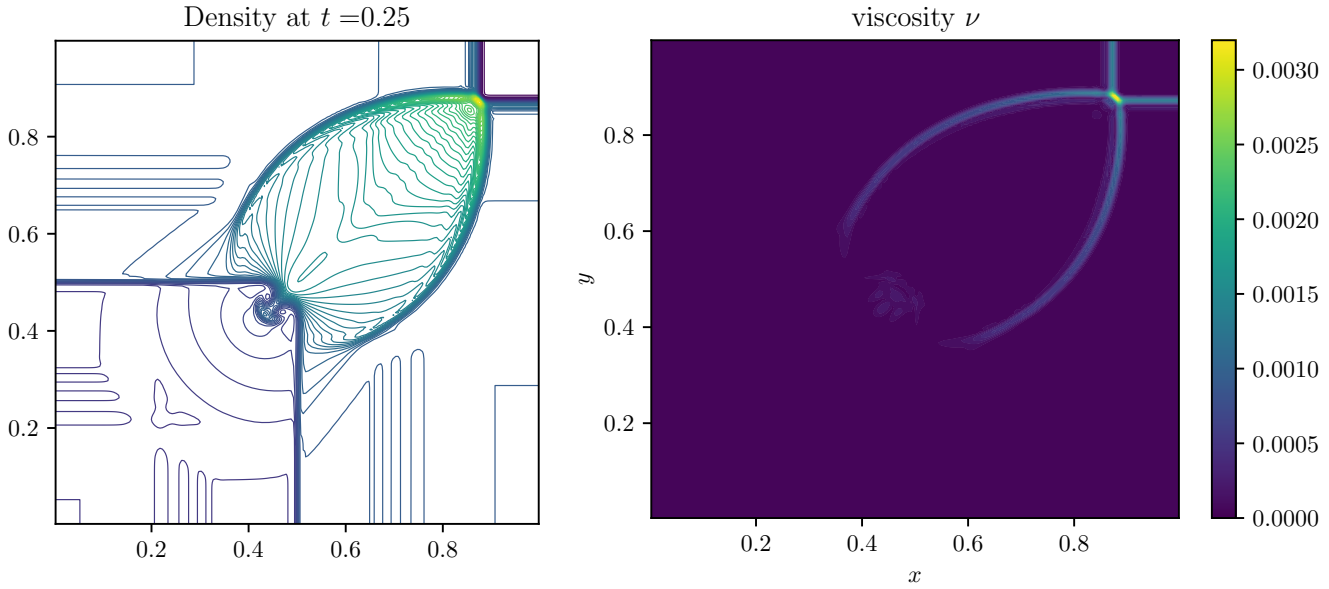


Figure 4.34: Results obtained with DB viscosity and P^1 elements on the first 2D Riemann problem. Density with dilation based viscosity and the corresponding artificial viscosity at the final time.

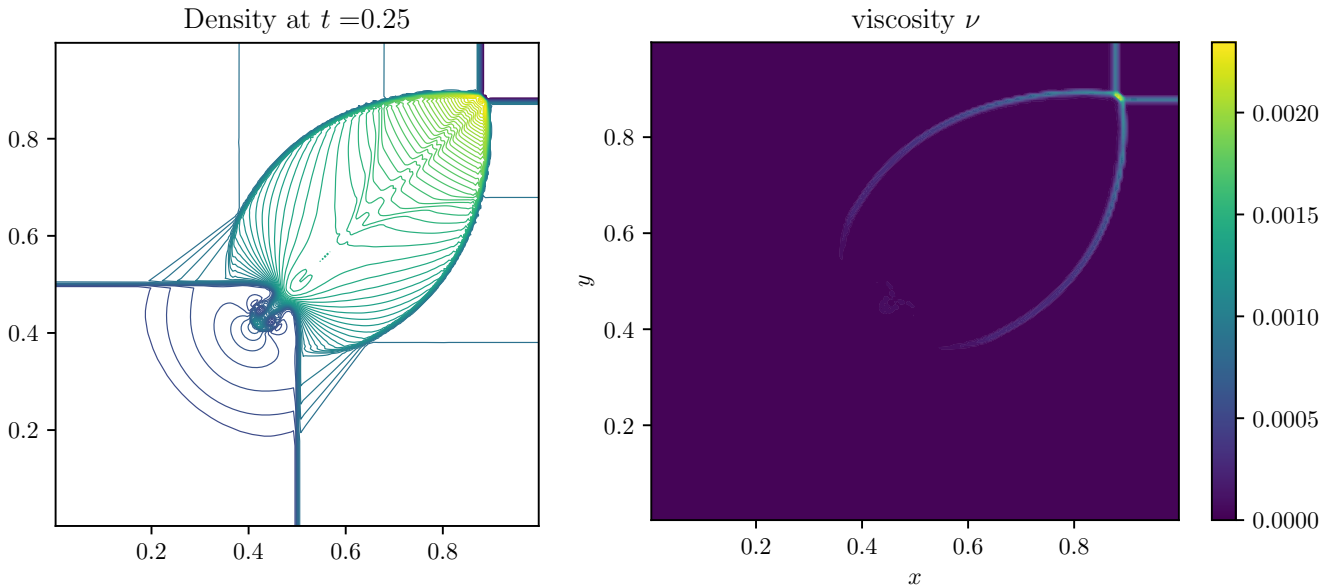


Figure 4.35: Results obtained with DB viscosity and P^2 elements on the first 2D Riemann problem. Density with dilation based viscosity and the corresponding artificial viscosity at the final time.

It is clear that P^2 elements give much sharper shocks in comparison to P^1 elements. The artificial viscosity helps smoothing oscillations but also decreases the sharpness of shocks at the same time. This is particularly visible on the diagonal between $(0, 0)$ and $(1, 1)$. As with the

1D scheme, the artificial viscosity is lower with higher order elements.

4.4.3 2D Riemann problem 2

The initial condition is given by

$$(\rho, v_1, v_2, P) = \begin{cases} (2.0, 0.75, 0.5, 1.0) & x < 0.5, y > 0.5 \\ (1.0, 0.75, 0.5, 1.0) & x > 0.5, y > 0.5 \\ (1.0, -0.75, 0.5, 1.0) & x < 0.5, y < 0.5 \\ (3.0, -0.75, -0.5, 1.0) & x > 0.5, y < 0.5 \end{cases} \quad (4.4)$$

on the domain $[0, 1]^2$ and with a final time of $t_{fin} = 0.3$. The number of cell in both direction is fixed to $N_x = 200 = N_y$ and the CFL number is set at $\text{CFL} = 0.25$ for all tests.

The results obtained without viscosity for both P^1 and P^2 elements are shown in Figure 4.36.

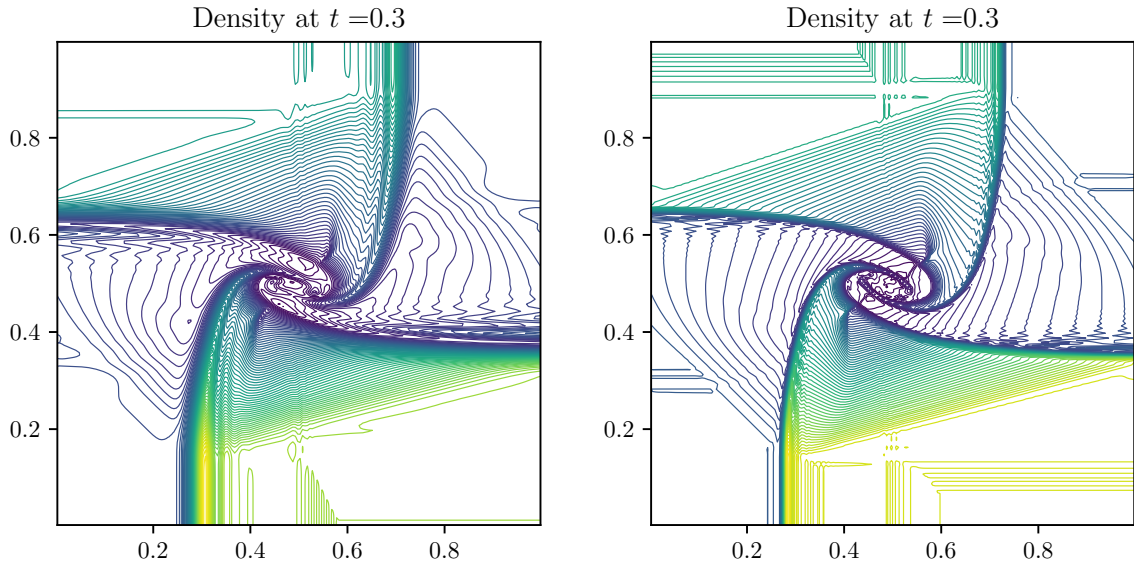


Figure 4.36: Results obtained without artificial viscosity, for P^1 (left) and P^2 (right) elements on the second 2D Riemann problem.

The results obtained with DB viscosity are shown in Figure 4.37 for P^1 elements and in Figure 4.38 for P^2 elements.

Chapter 4. Numerical results and discussions

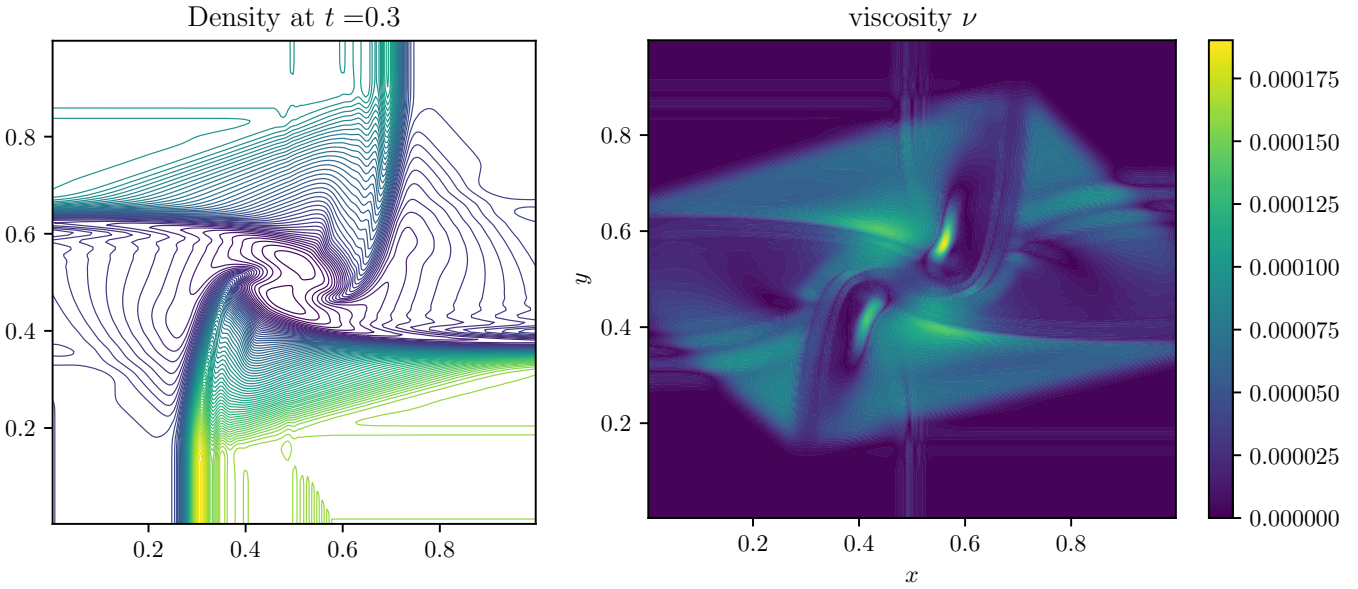


Figure 4.37: Results obtained with DB viscosity and P^1 elements on the second 2D Riemann problem. Density with dilation based viscosity and the corresponding artificial viscosity at the final time.

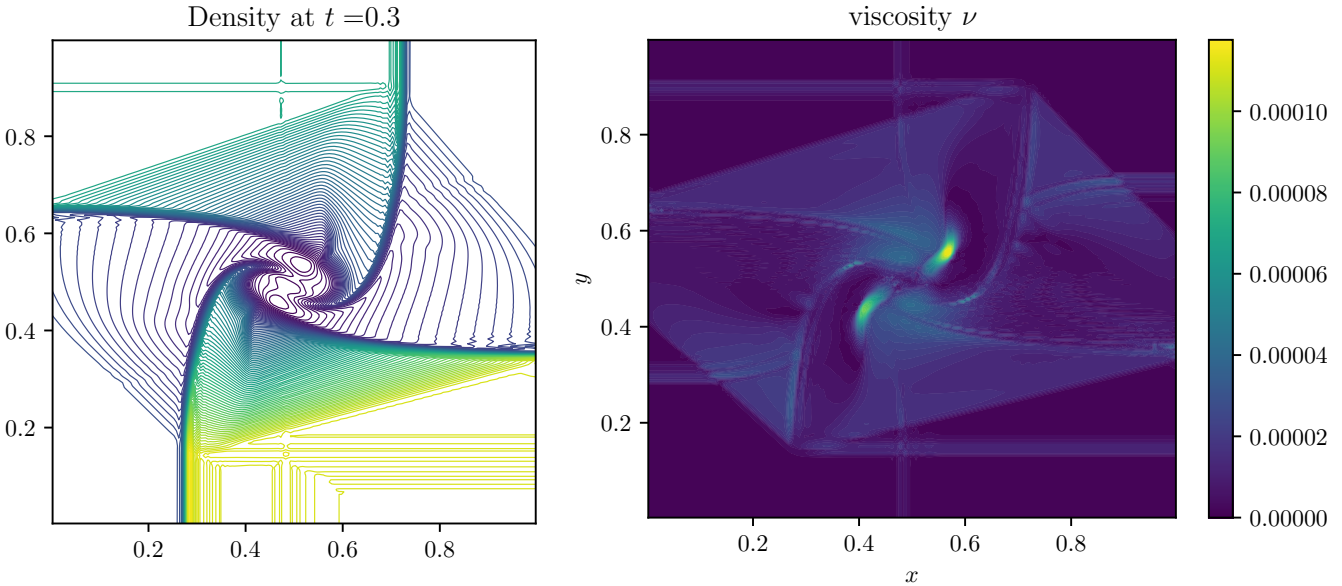


Figure 4.38: Results obtained with DB viscosity and P^2 elements on the second 2D Riemann problem. Density with dilation based viscosity and the corresponding artificial viscosity at the final time.

Again, P^2 elements are able to capture finer details in the solution. The viscosity efficiently suppress oscillations close to shocks e.g. around $(x, y) = (0.1, 0.6)$.

4.4.4 2D Riemann problem 3

The initial condition is given by

$$(\rho, v_1, v_2, P) = \begin{cases} (0.5065, 0.8939, 0.0, 0.35) & x < 0.5, y > 0.5 \\ (1.1, 0.0, 0.0, 1.1) & x > 0.5, y > 0.5 \\ (1.1, 0.8939, 0.8939, 1.1) & x < 0.5, y < 0.5 \\ (0.5065, 0.0, 0.8939, 0.35) & x > 0.5, y < 0.5 \end{cases} \quad (4.5)$$

on the domain $[0, 1]^2$ and with a final time of $t_{fin} = 0.15$. The number of cell in both direction is fixed to $N_x = 200 = N_y$ and the CFL number is set at $\text{CFL} = 0.25$ for all tests.

The results obtained without viscosity for both P^1 and P^2 elements are shown in Figure 4.39.

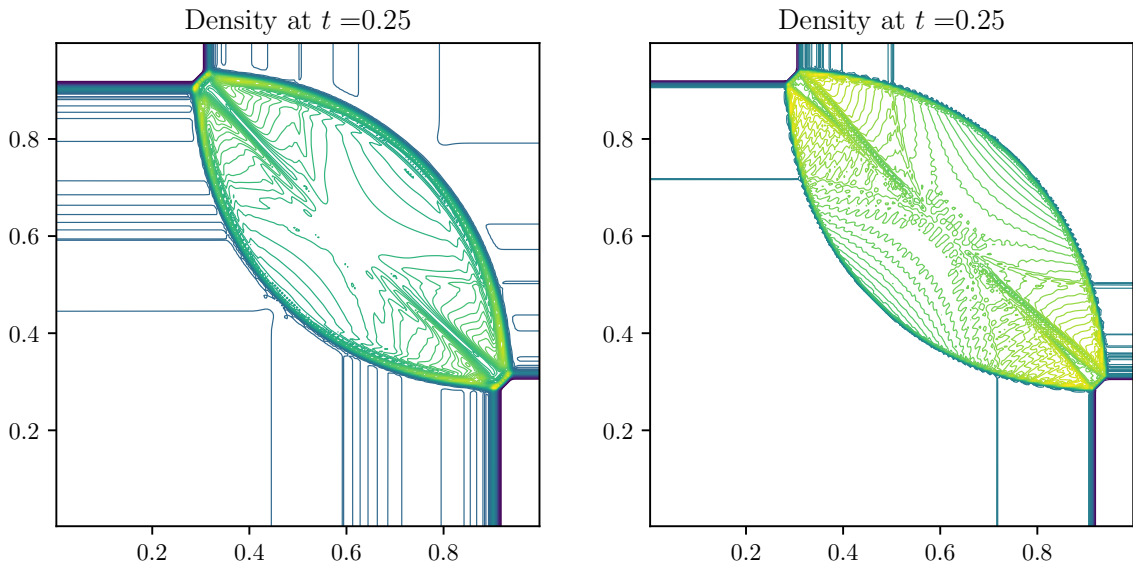


Figure 4.39: Results obtained without artificial viscosity, for P^1 (left) and P^2 (right) elements on the third 2D Riemann problem.

The results obtained with DB viscosity are shown in Figure 4.40 for P^1 elements and in Figure 4.41 for P^2 elements.

Chapter 4. Numerical results and discussions

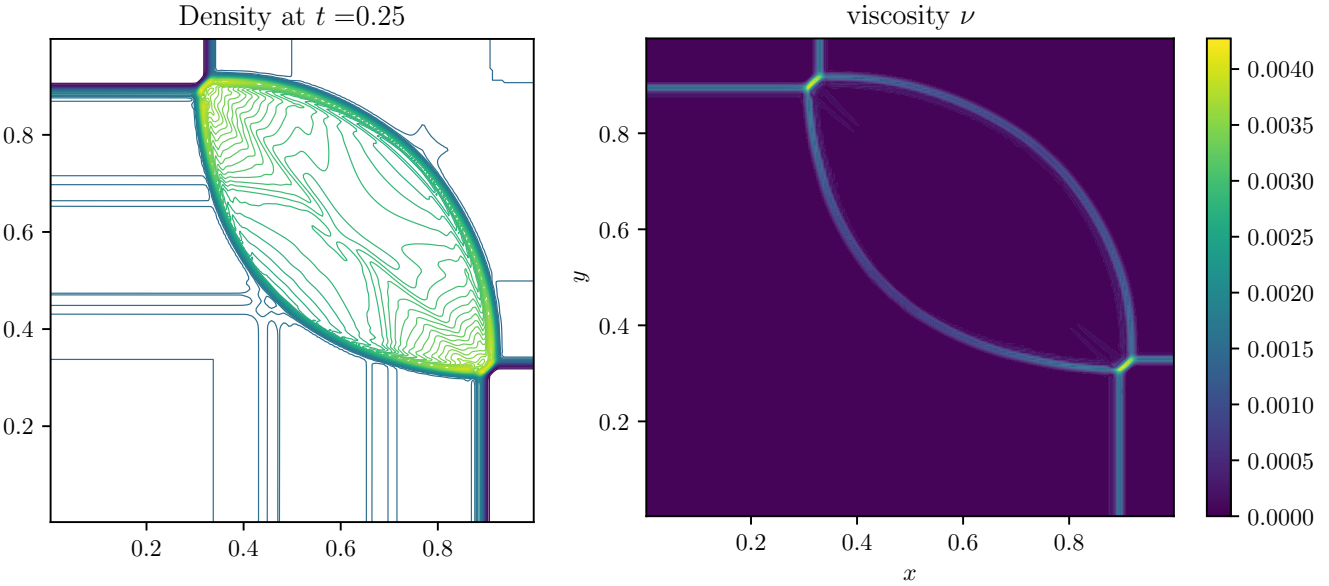


Figure 4.40: Results obtained with DB viscosity and P^1 elements on the third 2D Riemann problem. Density with dilation based viscosity and the corresponding artificial viscosity at the final time.

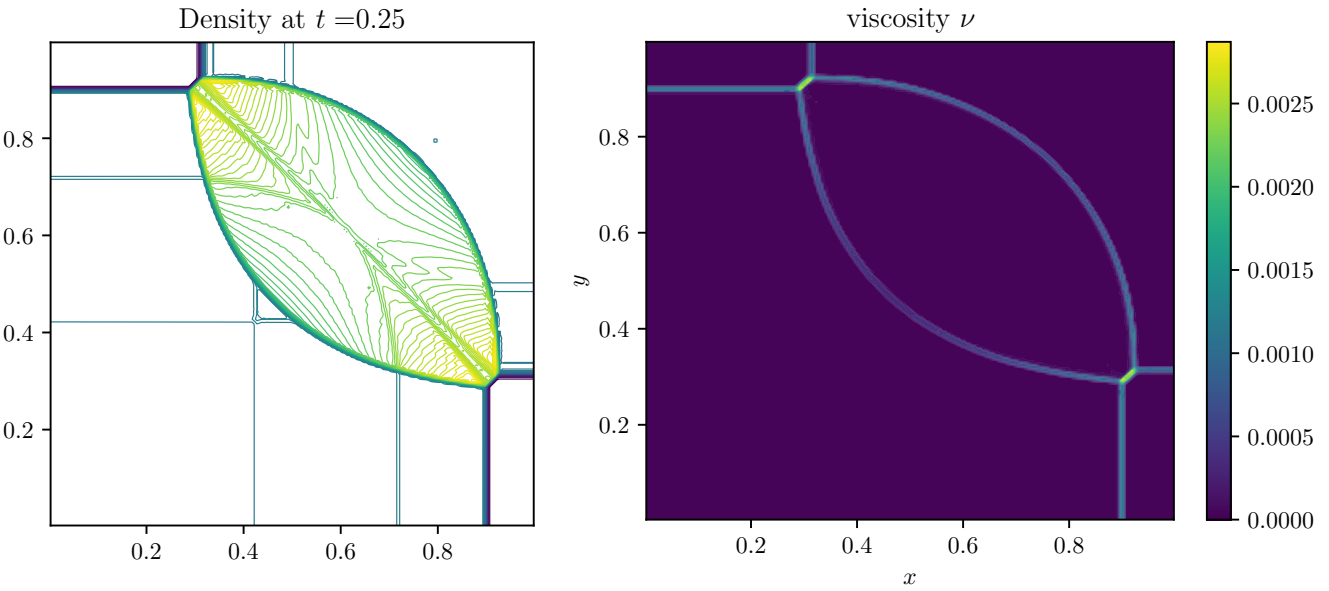


Figure 4.41: Results obtained with DB viscosity and P^2 elements on the third 2D Riemann problem. Density with dilation based viscosity and the corresponding artificial viscosity at the final time.

This example shows the artificial viscosity is useful. Indeed, many small oscillations are present inside the "leaf" shaped area when no viscosity is used. Artificial viscosity smoothes almost all of them while retaining shocks. The shock around the point $(x, y) = (0.5, 0.8)$ is arguably too smooth with viscosity.

5 Conclusion

Discontinuous Galerkin (DG) methods provide an elegant and parallel efficient way to get arbitrarily high-order numerical schemes for systems of conservation laws. To further improve the stability by incorporating the discrete entropy conditions, the last decade has seen the fast development of the entropy stable (ES) DG method. Although it is widely used in solving many different hyperbolic systems, the discrete entropy conditions are generally not enough to suppress unphysical oscillations near discontinuities. The motivation of this work is using artificial viscosity to further stabilize the ES DG schemes.

Chapter 1 gave a general description of CLs and entropy conditions together with a review of the literature on ES schemes.

Chapter 2 presented details about the time integration, FVM, the DG methods and ES DG methods. We added an artificial viscosity term to the ES DG schemes which helps to reduce spurious oscillations around discontinuities. The artificial viscosity term was built on the entropy variables so that the overall schemes still satisfied the discrete entropy conditions. Two different artificial viscosity models were implemented, namely the dilation based and the entropy based viscosity models.

Our ES DG method with artificial viscosity was implemented in both 1D and 2D. The schemes were tested on multiple problems, described in Chapter 3, including advection equation, Burgers' equations, and the Euler equations.

Chapter 4 presented our numerical results on different test cases. The theoretical convergence rates have been verified and the schemes were successfully tested in several benchmarks. The results showed that the artificial viscosity term can stabilize the ES DG schemes, reduce oscillations near discontinuities, and prevent the blow up of the code, although the coefficient in the artificial viscosity should be carefully chosen to avoid over amount of numerical dissipation which may smooth the discontinuity too much.

Further works include detailed study of the choice of the viscosity at each quadrature point inside one cell and further improve the resolution near the discontinuities.

Bibliography

- Carpenter, M. H., Fisher, T. C., Nielsen, E. J., and Frankel, S. H. (2014). Entropy stable spectral collocation schemes for the navier–stokes equations: Discontinuous interfaces. *SIAM Journal on Scientific Computing*, 36(5):B835–B867.
- Chen, T. and Shu, C.-W. (2017). Entropy stable high order discontinuous galerkin methods with suitable quadrature rules for hyperbolic conservation laws. *Journal of Computational Physics*, 345:427–461.
- Ciarlet, P., Lions, J., and Glowinski, R. (1990). *Handbook of Numerical Analysis*. Number Bd. 9 in Handbook of Numerical Analysis. North-Holland.
- Fjordholm, U. S., Mishra, S., and Tadmor, E. (2012). Arbitrarily high-order accurate entropy stable essentially nonoscillatory schemes for systems of conservation laws. *SIAM Journal on Numerical Analysis*, 50(2):544–573.
- Gassner, G. J. (2013). A skew-symmetric discontinuous galerkin spectral element discretization and its relation to sbp-sat finite difference methods. *SIAM Journal on Scientific Computing*, 35(3):A1233–A1253.
- Gassner, G. J. and Winters, A. R. (2021). A novel robust strategy for discontinuous galerkin methods in computational fluid mechanics: Why? when? what? where? *Frontiers in Physics*, 8.
- Hesthaven, J. S. (2018). *Numerical Methods for Conservation Laws*. Society for Industrial and Applied Mathematics, Philadelphia, PA.
- Johansson, F. and Mezzarobba, M. (2018). Fast and rigorous arbitrary-precision computation of gauss-legendre quadrature nodes and weights.
- Shu, C.-W. (2020). Essentially non-oscillatory and weighted essentially non-oscillatory schemes. *Acta Numerica*, 29:701–762.
- Tadmor, E. (1987). Entropy functions for symmetric systems of conservation laws. *Journal of Mathematical Analysis and Applications*, 122(2):355–359.

Bibliography

- Winckel, G. v. (2004). Lgl quadrature points and weights. <https://www.mathworks.com/matlabcentral/fileexchange/4775-legende-gauss-lobatto-nodes-and-weights>. Accessed: January 20, 2023.
- Yu, J. and Hesthaven, J. S. (2020). A study of several artificial viscosity models within the discontinuous galerkin framework. *Communications in Computational Physics*, 27(5):1309–1343.
- Zingan, V., Guermond, J.-L., Morel, J., and Popov, B. (2013). Implementation of the entropy viscosity method with the discontinuous galerkin method. *Computer Methods in Applied Mechanics and Engineering*, 253:479–490.